Robust functionalization of graphene for organic electrode materials

March 2021

Rizwan Khan

Graduate School of Natural Science and Technology

(Doctor Course)

Okayama University

Two-dimensional nanocarbons, as represented by graphene, have been the subject of active research owing to their outstanding physical properties, such as toughness, high specific surface area, and high electrical and thermal conductivities. As the physical properties of graphene and its analogs have mostly been elucidated by intense research over more than 15 years, the development of functionalization methods to further enhance their physical/chemical properties is in great demand. Particularly, graphene oxide (GO) brings unique chemical reactivity. This is mainly due to the large amounts of reactive epoxy, hydroxyl, and carboxyl groups. These oxygenated groups provide the possibility of covalently grafting functional molecules onto GO sheets in high grafting density by using various organic reactions.

The present study aims to robust functionalization of graphene and their applications for organic electrodes. This thesis is divided into six chapters. The first two chapter is consisting of introduction.

Chapter 1 presents a comprehensive literature review of graphene is given. Initially, various graphene synthesis methods are introduced. Then the functionalization of graphene, GO, and reduced graphene oxide (RGO) and classification between covalent and non-covalent functionalization are explained. The covalent functionalization was discussed in detail.

Chapter 2 describes various functionalization routes of graphene with redox-active materials (small molecules and polymers) and their application for lithium-ion batteries (LIBs) and supercapacitors (SCs) were discussed.

The next three chapters of this thesis report major scientific advances achieved through this study; they all detail robust functionalization of graphene and applications for energy storage systems as given below.

In chapter 3, a new concept for graphene functionalization using brominated graphene has been developed, in which brominated graphene is successfully functionalized by heteroatom-containing molecules to form onium bonds, such as pyridinium or ammonium. The counterion bromide is replaced with other anions, such as sulfate, by treating with sulfuric

acid while retaining the molecules, which demonstrates the durable properties of onium bonding. To emphasize the advantages of this strategy for graphene functionalization, the performance for energy-related applications, such as biofuel cells, SCs, and LIBs, is evaluated after introducing redox-active moieties onto graphene through onium bonding. Among applications such as the LIBs, SCs, and biofuel cell, the SCs was found to be promising.

In chapter 4, a three-step reaction furnished a composite of graphene and a conductive polymer. In the first step, GO was modified with a diamine, which acted as a linker for polymer attachment. In the second step, an initiating site was attached to the free amine of the linker. Finally, a polymer was grown from the initiation site, and GO was reduced during polymer growth. The method does not require any catalyst, acid, or reducing agent, furnishing the graphene–polymer composite in a straightforward procedure. The electrical properties of the composite were evaluated to determine its suitability as an electrode material for a SCs. The covalent cross-linked polymer-graphene composite demonstrated a high capacitance and good cycling stability than non-crosslinked graphene–polymer mixture. This method of functionalization provides a guideline in the future for the preparation of another graphene–polymer-based composites.

In chapter 5, a series of organic molecules was functionalized on GO by using stepwise covalent double functionalization method. The first step consists of ring-opening reaction of epoxide group by amine compounds. The mono functionalized GO, containing more OH groups compared to pristine GO, was modified with α,β-unsaturated carbonyl compounds via Michael reaction. The role of double functionalization was studied in proton conductivity and SCs. The proton conductivity of double functionalized GO was improved by tuning the surface functional groups of GO. Similarly, the SCs performance of the double functionalized GO was improved by introducing redox-active molecules.

Chapter 6 present the final conclusion.

Contents

Chapter 1

Synthesis, functionalization and characterization of graphene, GO and RGO

1. Introduction

Carbon-based materials have extensively investigated due to their abundance, processability, stability, and relatively environmentally friendly characteristics.[1–3] Carbon-based materials exist in different allotropic form such as 0-D fullerenes, 1-D carbon nanotubes (single-walled carbon nanotubes (SWCNT), multi-walled carbon nanotubes (MWCNT), 1D), 2-D graphene, 3-D diamond and 3-D graphite, having different physical and chemical properties from each other. The advents of sp^2 and/or sp^3 hybridized structures, such as CNTs, conducting diamond and fullerenes offer a route for surface functionalization and are very promising for electrochemical research, especially electrocatalysis[4] and electrode materials.[5] Diamond and graphite have been known and extensively studied for centuries whereas nanotubes and fullerenes have been only discovered and investigated in the last two decades.[6,7] It is possible to think that graphite, nanotubes and fullerenes, as different structures built from the same hexagonal array of sp^2 carbon atoms, namely, graphene (Figure 1).[8] Among the other carbon-based materials , graphene emerged as an attractive candidate for variety of applications due to its unique structure and properties.[9] Surface modification of graphene result in variety of composites with unique properties.[10] Therefore, researchers have developed various covalent and noncovalent functionalization methods of graphene for variety of applications. Graphene is a one-atom-thick planar sheet of sp^2-bonded carbon atoms densely packed in a honeycomb crystal lattice. Naturally occurring graphite has been known as a mineral for nearly 500 years. Graphene, the building block of graphite, was theoretically established in 1940. Boehm and co-workers separated thin lamellae of carbon by heating and chemical reduction of graphite oxide in 1962.[11] However, until 2004, single-layer graphene was believed to be thermodynamically unstable under ambient conditions. Geim and co-workers first identified single layers of graphene in 2004.[12] This finding has provided a new dimension of research in the fields of chemistry, physics, biotechnology and materials science.

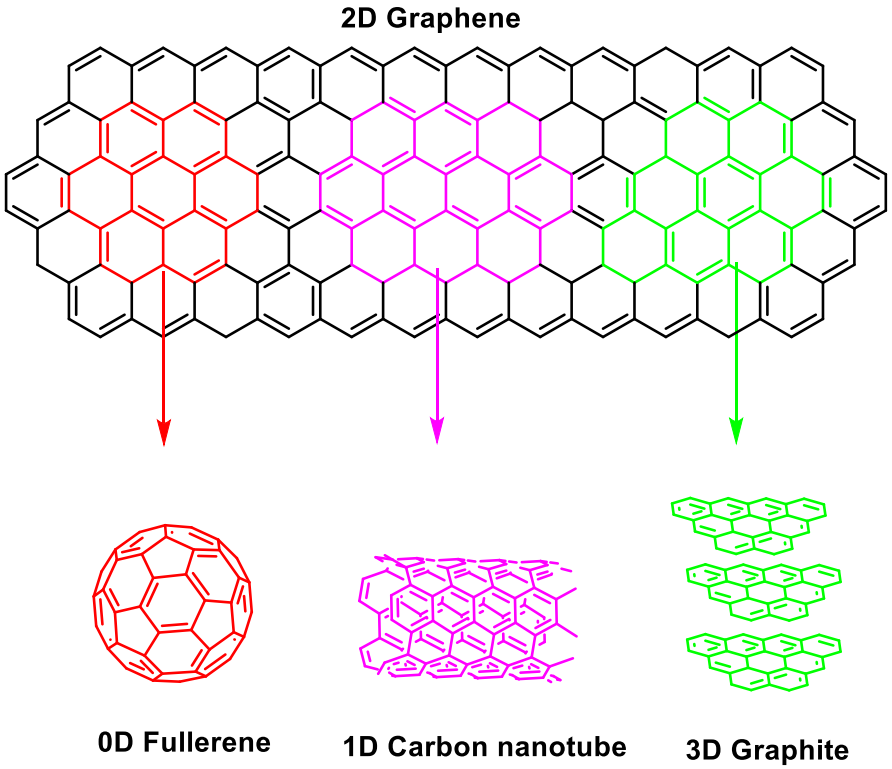

Figure 1: Different Carbon-based materials originate from graphene

The ‘‘thinnest’’ known material graphene shows excellent electrical conductivity, thermal conductivity, optical transparency, mechanical flexibility and low coefficient of thermal expansion behavior.[13] Graphene crystal, consisting of sp^2 carbon framework, exists in thin sheets. These carbon sheets can be produced in different forms such as monolayers, bilayers, or up to three layers of graphene or GO.

1.1. Synthesis of graphene

Several synthetic methods for graphene have been reported in the literature. These methods include exfoliation and cleavage of natural graphite, chemical vapor deposition (CVD), epitaxial growth on electrically insulating surfaces such as silicon carbide (SiC) and un-zipping of CNTs.

1.1.1. Mechanical exfoliation

In 2004, single layer graphene was isolated from few layered graphite through mechanical exfoliation. In this approach, bulk graphite was bonded onto borosilicate glass under a fixed condition and then remove leaving behind a single-layer or few-layer graphene sheets on the substrate (Figure 2). It is very difficult to scale up this process.[14]

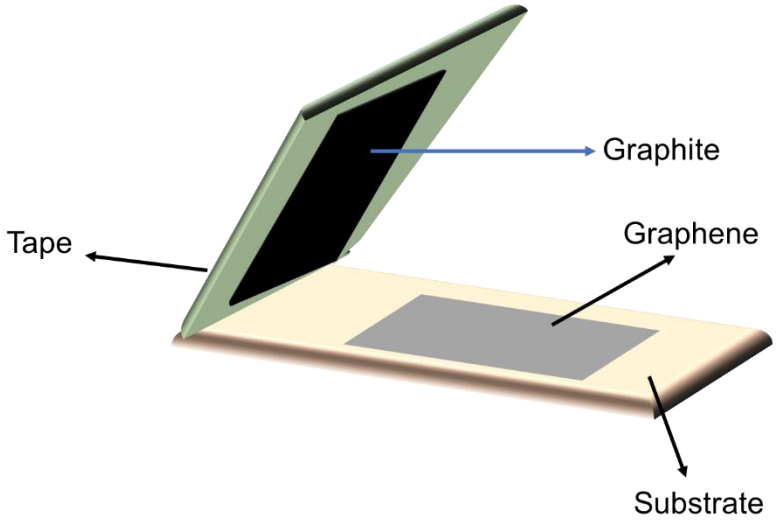

Figure 2: Synthesis of graphene through mechanical exploitation method

1.1.2. Ultrasonic cleavage

In this case graphene precursors are suspended in water or organic solvents, and then ultrasonicated to cleave the graphene precursors (Figure 3). The success of ultrasonic cleavage depends on the proper choice of solvents as well as the sonication time, frequency and amplitude.[15]

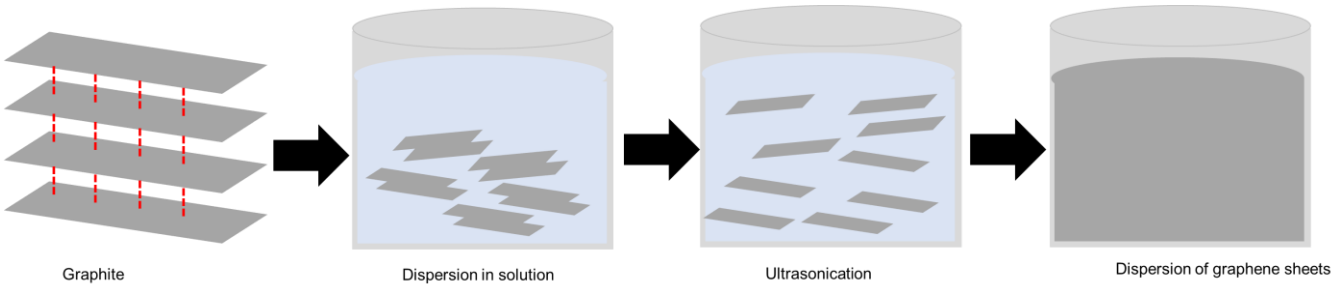

Figure 3: Synthesis of graphene through ultrasonic cleavage

1.1.3. CVD method

Graphene sheets can also be prepared on metallic surfaces including nickel, cobalt, platinum, iridium and copper. Generally, hydrocarbons used as a gas sources for this type of deposition such as acetylene, methane, or ethylene, which decompose when brought into contact with the surface of metals to form layers of graphene (Figure 4).[16] This method is cost effective and reproducible. However, the formation of toxic gases accompanying with this method.

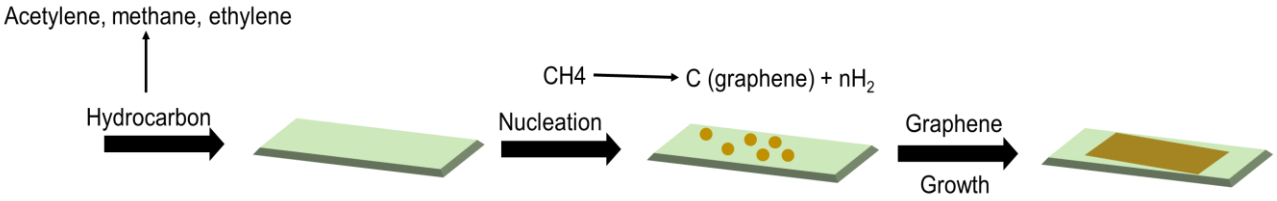

Figure 4: Synthesis of graphene through chemical vapor deposition method

1.1.4. Epitaxial growth on SiC

In this method, graphene is grown on the silicon carbide by thermal desorption of Si, which leaves behind a 2–3-layer thick graphene sheet (Figure 5). Unfortunately, this method is not adapted to prepare one atom thick graphene. Also, achieving large graphene domains with uniform thickness remains a challenge.

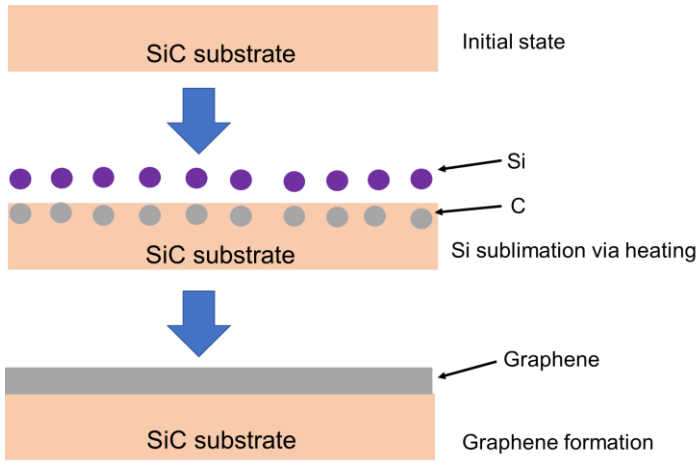

Figure 5: Synthesis of graphene through epitaxial growth on SiC

1.1.5. Unzipping of CNT

Graphene sheets can be prepared by unzipping of CNTs. In this process, NH_3-solvated Li^+ is simultaneous intercalated into MWCNTs, allowing unwrapping and exfoliation.[17] Another unzipping approach to use strong oxidizing agents.[18] Alternative safe method is the use of Ar plasma etching method to unzip MWCNTs (Figure 6).

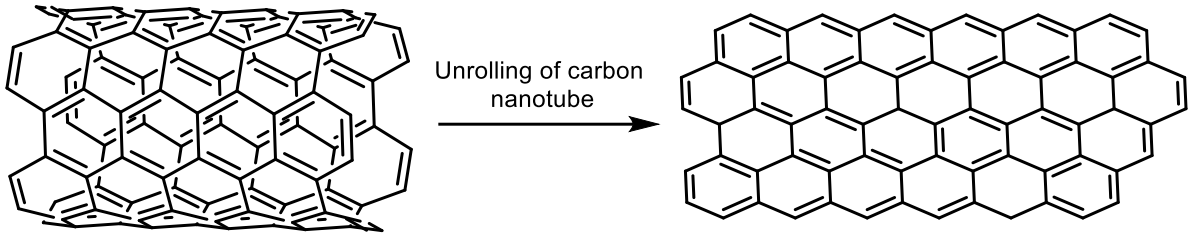

Figure 6: Synthesis of graphene through unzipping of CNT

1.2. Physical properties of graphene

Graphene is an allotrope of carbon in which each carbon atom is bonded with another carbon by sp^2 bonds. The carbon atoms are bonded in a honeycomb crystal lattice with a bond length of 0.14 nm.[19] Different research groups have measured the thickness of graphene from 0.35 nm to 1.00 nm.[20] Graphene displays high intrinsic strength (130 GPa) and Young's modulus (1.00 TPa), making it the strongest material. Further, it can be stretched to deformations well beyond the linear regime. The thermal conductivity of graphene at room temperature can reach 5000 W m^{-1} K^{-1}.[21] Graphene shows very high surface area of 2600 m^2 g^{-1}, much larger than the surface areas of graphite of 0.60 m^2 g^{-1} and CNTs of 1300 m^2 g^{-1}.[22] The physical properties is summarized in Table 1. These remarkable properties make graphene promising in applications such as polymer-composite materials, paper-like materials, photo-electronics, electromechanical systems, field effect transistors, sensors and electrochemical energy systems etc.[23]

Table 1: Physical properties of graphene as a material (experimental and theoretical)[21]

Bond length	0.14 nm
Thickness of single layer	0.35 nm to 1.00 nm
Intrinsic strength	130 GPa
Young's modulus	1.00 TPa
Thermal conductivity	5000 W m^{-1} K^{-1}
Surface area	2630 m^2 g^{-1}
Band gap	zero

1.3. Chemical functionalization methods of graphene

Graphene is aromatic in nature possessing highly electronic density both above and below the plane. The frontier molecular orbitals of organic molecules can easily interact with the p-electrons of graphene. Therefore, electrophilic substitution of graphene is much easier than nucleophilic substitution. The edges of graphene shows higher chemical reactivity than arm-chair edges; because the aromatic sextets are perturbed in the zig-zag edges, leading to thermodynamic instability.[24]

Graphene sheets can restack easily through π–π stacking and van der Waals interactions if the sheets are not well separated from each other. Chemical modification of graphene through covalent, non-covalent and ionic interaction avoids the aggregation of graphene sheets.[25] Further, organic functional groups introduce new properties that could be improve the properties of graphene. Therefore, the researcher has been focused on the development of new surface functionalization method of graphene, with aim of exploiting the most frequently proposed applications of graphene in the field of chemistry, physics and biology.

1.3.1. Functionalization through physical interaction

Graphene can be functionalized through physical interactions such as electrostatic interactions, hydrophobic and van der Waals interactions, without disturbing the electronic network in an easy and reversible way (Figure 7). The non-covalent functionalization is

playing a key role for the immobilization of organic molecules, particularly in electronic devices as a little modification in the electronic characteristics of the π system can lead to change the entire structure and properties of the system. The non-covalent interaction of graphene has been extensively investigated and classified in non-polar π–π, gas–π, H–π, anion–π and cation–π interaction.[26] The strength of these interactions is a combination of different forces that include electrostatic forces, inductive interactions, dispersive forces, and exchange repulsion as repulsive forces. Non-covalent interaction is simple and easy to prepared. However, these interactions are weak and molecular dissociation occurs easily.

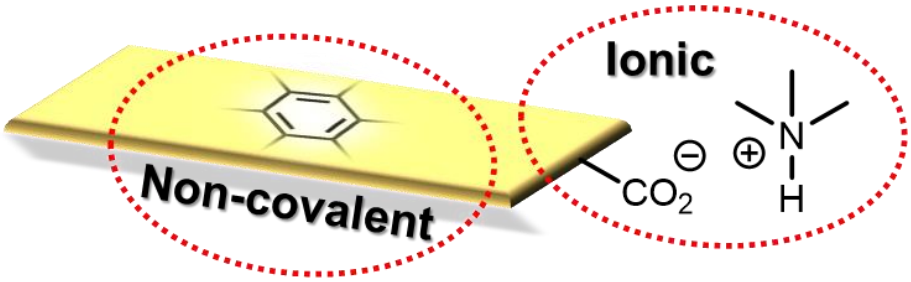

Figure 7: Functionalization of graphene through non-covalent and ionic bonding

1.3.2. Covalent functionalization reaction

In contrast to physical interaction, the covalent interaction is strong and stable. Covalent functionalization of graphene can be achieved through various organic reaction, which are given below.

1.3.2.1. Free Radical Addition Reactions

Free radicals are highly reactive organic species toward the aromatic structure of graphene to form covalent bonds. This functionalization has been achieved by chemical, thermal and photochemical treatments. Graphene has been functionalized through different free radical reaction such as aryl diazonium salts or peroxides such as Bergman cyclization and the Kolbe electrosynthesis.

1.3.2.1.1. Aryl diazonium salts

Surface modification of carbon-based materials with diazonium chemistry has been achieved initially by an isolated diazonium salt and later by *in situ*-generated one. Although diazonium salt is unstable, it can be easily synthesized with an amine and $NaNO_2$ in an acidic aqueous solution, *tert*-butyl nitrite, or $NOBF_4$. Diazonium salt generates a radical with the elimination of nitrogen, then covalently reacts with graphene (Figure 8). The radical formation can be initiated by electrochemical, thermal, or pH-dependent methods. Diazonium salts are important intermediates in organic chemistry, thus their derivatives are widely available.[27]

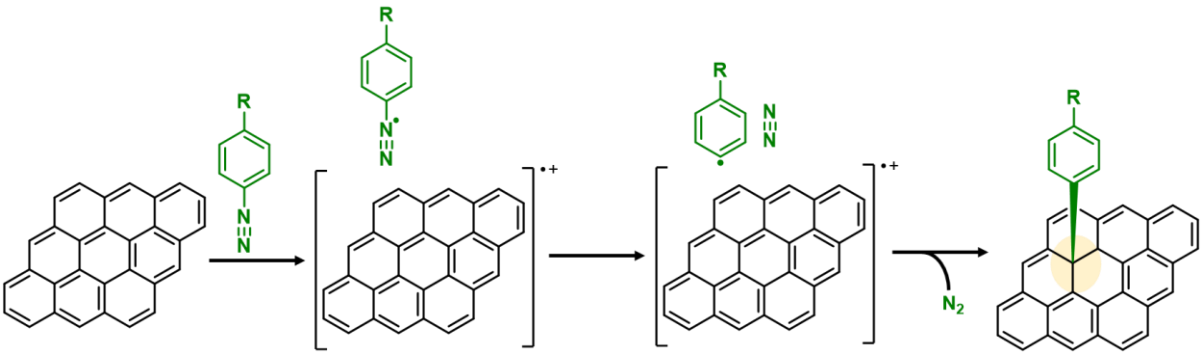

Figure 8: Functionalization of graphene through diazonium chemistry

1.3.2.1.2. Bergman cyclization.

The Bergman cyclization introduced six-member ring on sp^2 carbon network of graphene. The reaction proceeds through a radical mechanism. The starting materials consist of an ene-diyne moiety which undergoes cyclization at high temperature. The cyclization results in the formation of 1,4-bezenediyl biradical species. The highly reactive biradical species reacts with the graphene sp^2carbon network through one side of the biradical species. The other radical end could potentially available for other reaction such as hydrogen abstraction or polymerization (Figure 9). Ma and coworker functionalized graphene with polymer through Bergman cyclization.[28]

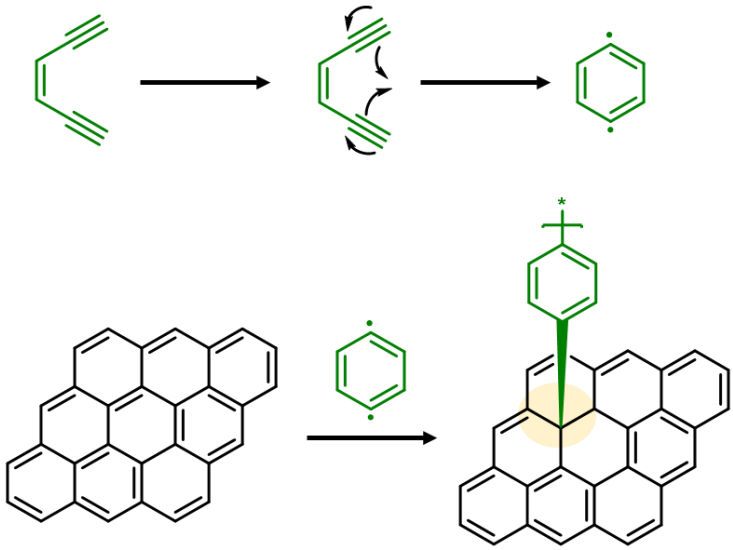

Figure 9: Functionalization of graphene through Bergman cyclization

1.3.2.1.3. Kolbe electrosynthesis.

The Kolbe reaction proceeds by means of the electrolysis of carboxylate ions to give radical species via a subsequent decarboxylation step. The direct radical species consist, most of the time, of only alkyl chains.[29] The alkyl radical then react with the sp^2 carbon network of graphene to form covalent bond (Figure 10).

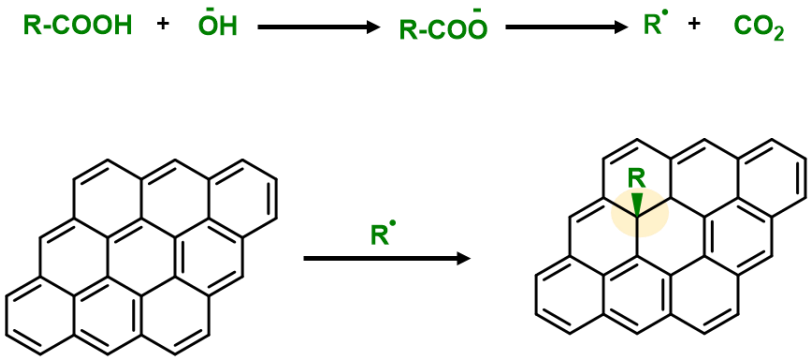

Figure 10: Functionalization of graphene through Kolbe electrosynthesis

1.3.2.2. Nucleophilic Addition Reactions

In a nucleophilic addition, graphene acts as an electron acceptor. The anionic moiety is formed by using a base, leading to the generation of nitrogen anions on carbazole. Subsequently, the anion reacts on the surface of graphene with the creation of a covalent bond (Figure 11). Xu et al. grafted polymer on graphene through nucleophilic addition reaction.[30]

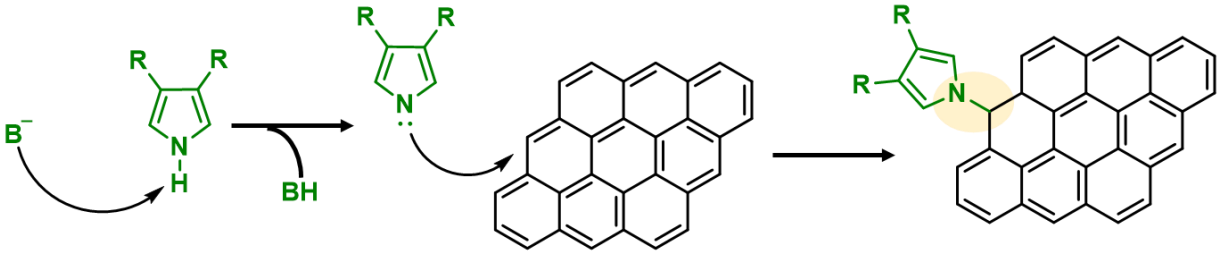

Figure 11: Functionalization of graphene through nucleophilic addition reaction

1.3.2.3. Reaction with Atomic Radicals

Graphene has been functionalized with atomic radicals such as hydrogen, fluorine and oxygen, with minimized possibility of side reactions. Atomic hydrogen reacts with graphene, lead to the formation of graphene (Figure 12a).[31] The total hydrogenated form of graphene is called graphane. The halogenation (F, Cl, Br, I) of graphene is similar to the hydrogenation (Figure 12b). Halogenated graphene allowing further transformation of graphene for variety of applications. Among the halogenated graphene, fluorinated graphene is extensively investigated for different applications. There are three main methods to produce it: (i) by etching using fluorinated compound (ii) by exposition to XeF2, and (iii) by liquid phase exfoliation of bulk graphite fluoride.[32] The common method for the oxidation of graphene is hummer method.[33] The oxygenation of graphene through this method is inhomogeneous. Oxygen radical lead to the formation of epoxide group on graphene (Figure 12c). The formation of epoxide groups has been obtained by exposing graphene at atomic oxygen beams and oxygen plasmas.

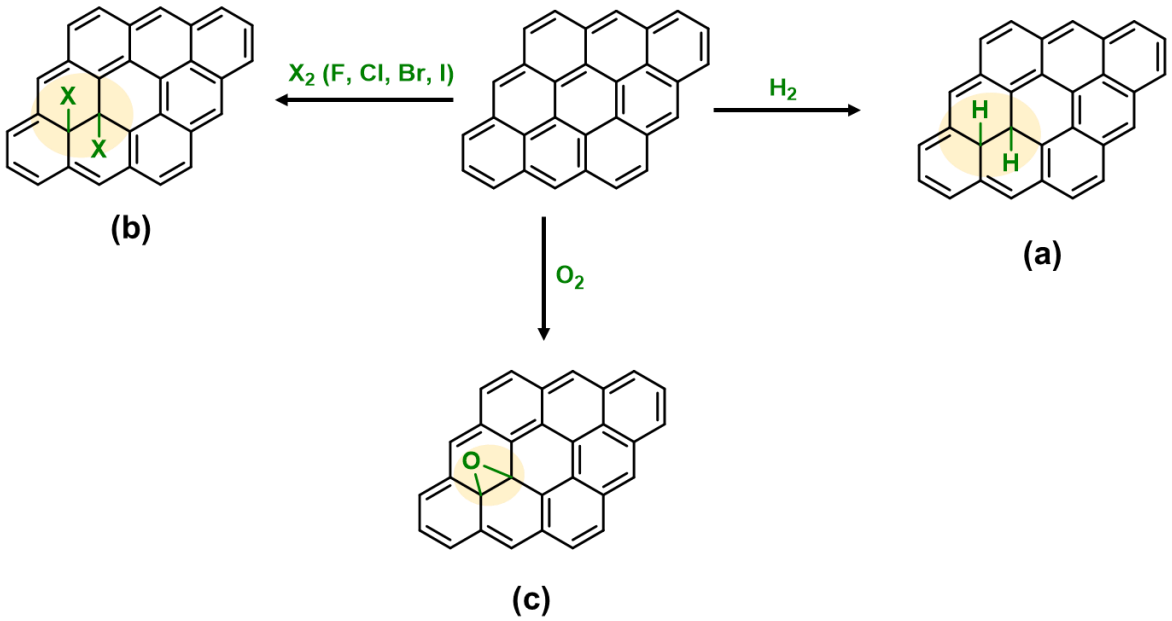

Figure 12: Functionalization of graphene through atomic radical

1.3.2.4. Electrophilic Substitution Reactions

Graphene can be functionalized by electrophilic substitution reaction due to its electron-rich nature. Examples of substitution reactions are the hydrogen–lithium exchange and Friedel–Crafts acylation. In hydrogen-lithium exchange reaction, first the carbometallation of graphene by butyl lithium, followed by the attachment of electrophile (Figure 13a).[34] The electrophile attach to the graphene by the elimination of lithium metal.The ketone moieties can be introduced to graphene by Friedel–Crafts acylation. The Lewis acid form the reactive intermediate (acyl cation), which proceed the reaction (Figure 13b).[35]

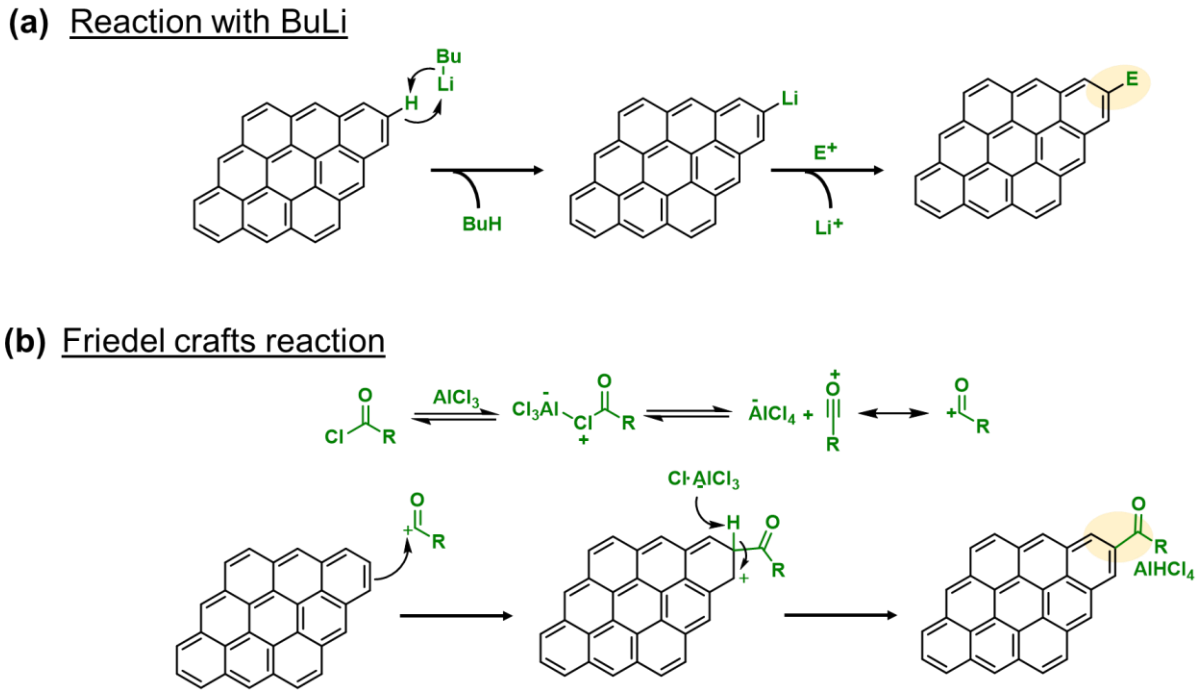

Figure 13: Functionalization of graphene through electrophilic substitution reactions

1.3.2.5. Cycloaddition Reactions

Four major types of cycloaddition introduced in the functionalization of graphene sp^2 carbon network: [2+1], [2+2], [3+2] and [4+2].

1.3.2.5.1. [2 + 1] cycloaddition.

This cycloaddition includes the Bingel reaction and reactions with nitrenes to form cyclopropane or aziridine adducts, respectively.

1.3.2.5.1.1. Bingel reaction.

This reaction can be performed in mild conditions. The base subtracts a proton, as a result the formation of enolate occurs, which attacks the C=C bond of graphene. The carbanion undergoes a nucleophilic substitution reaction with the elimination of the

halide to form a three-member ring on graphene (Figure 14). Single layer graphene has been functionalized through this reaction.[36]

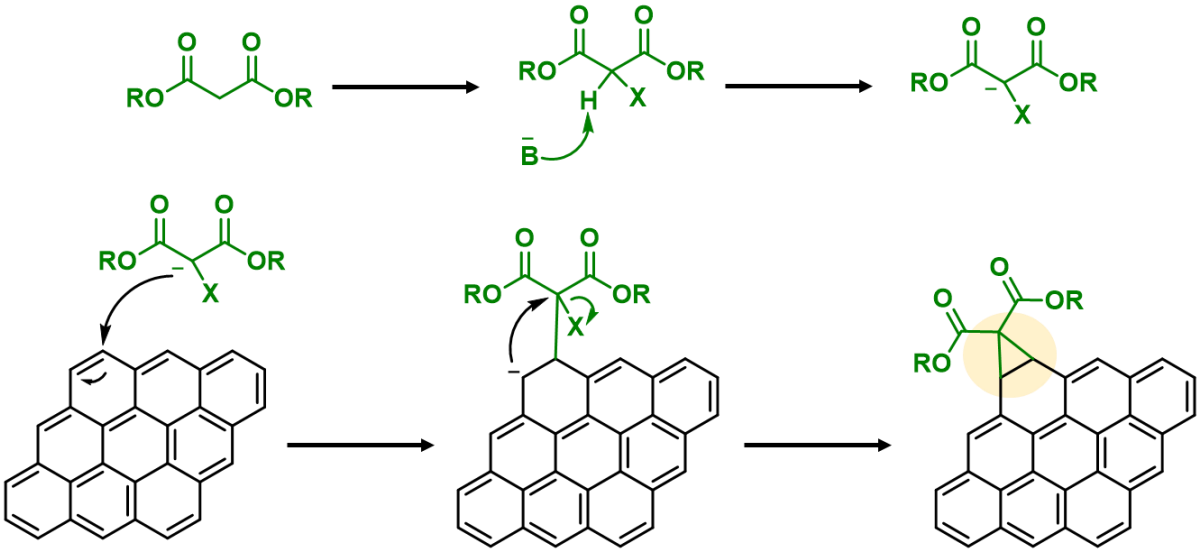

Figure 14: Functionalization of graphene through Bingel reactions

1.3.2.5.1.2. Aziridine adduct.

The introduction of aziridine adduct onto the graphene network is usually obtained via a nitrene intermediate. The nitrene intermediate is usually generated from a thermal- or photodecomposition of an azide group, in the form of gaseous nitrogen molecule, which is the most stable leaving group. This phenomenon generated highly reactive singlet nitrene which subsequently undergoes a cycloaddition reaction on the graphene sp^2 carbon network to provide an aziridine adduct (Figure 15).[37,38] Kim and co-workers were first to perform this reaction on graphene in 2009.

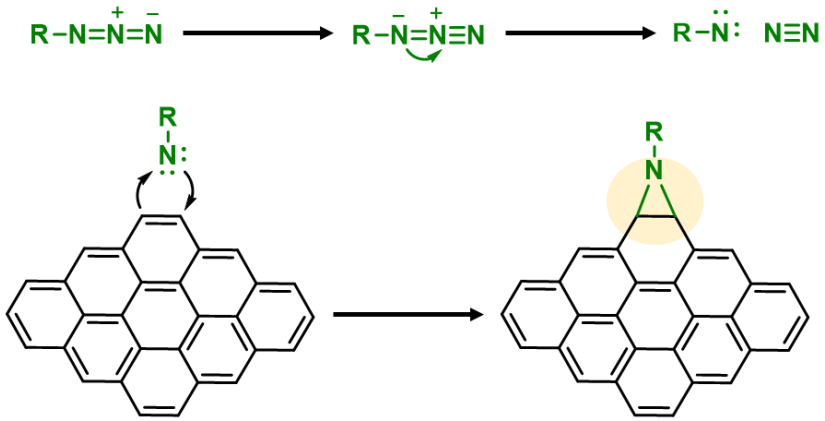

Figure 15: Functionalization of graphene through aziridine adduct

1.3.2.5.2. [2 + 2] cycloaddition.

The formation of four-member ring on graphene sp^2 carbon network goes through an aryne or benzyne intermediate via an elimination–addition mechanism. The presence of a fluoride ion induced a desilylation step to provide a carbanion with a filled sp^2 orbital in the plane of the ring. This proceeded by an elimination of the triflate group to give benzyne, which is electrophilic. Subsequent nucleophilic attack of benzyne on graphene carbon network resulted in a [2 + 2] cycloaddition (Figure 16).[39] The functionalization of graphene based on the benzyne cycloaddition method discussed above was demonstrated by Ma and co-worker.

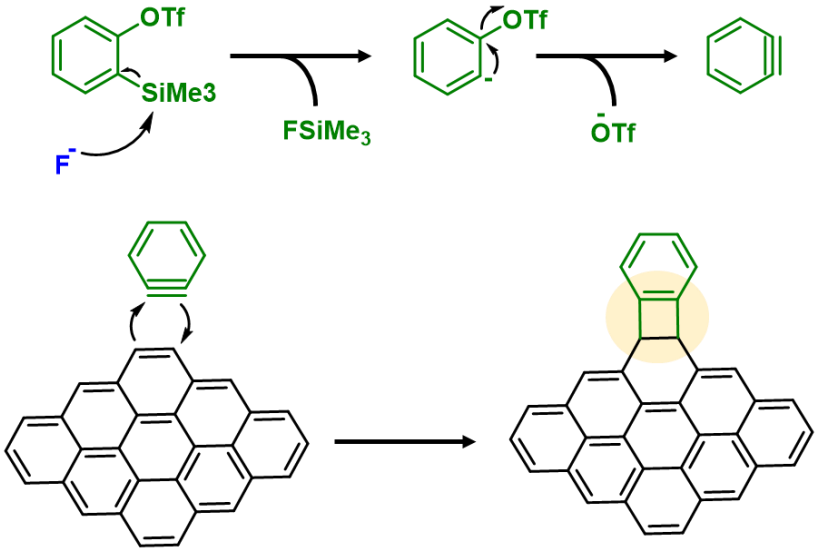

Figure 16: Functionalization of graphene through [2 + 2] cycloaddition reaction

1.3.2.5.3. [3 + 2] cycloaddition.

The introduction of five-membered ring on graphene can be achieved by the reaction of a 1,3-dipole and dipolarophile (graphene). The resulting [3 + 2] cycloaddition, also known as the 1,3-dipolar cycloaddition. This reaction can be also achieved by the reaction of azomethine ylide with graphene sp^2 carbon network (Figure 17).[40]

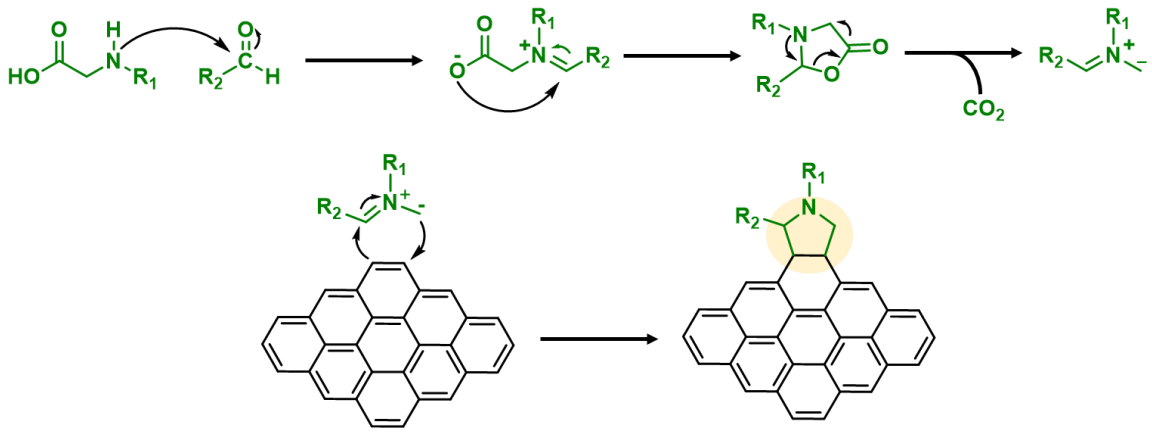

Figure 17: Functionalization of graphene through [3 + 2] cycloaddition reaction

1.3.2.5.4. [4 + 2] cycloaddition.

The [4 + 2] cycloaddition, is also known as the Diels–Alder cycloaddition, is the most famous pericyclic reaction in organic chemistry. The reaction proceeds in a single step via heat treatment to give a six-membered ring on graphene (Figure 18). The reaction involves the interaction between a conjugated diene (electron rich) and a dienophile (electron deficient). The reaction proceeds only when the diene is locked in an s-cis conformation. As for the dienophile, the reaction would proceed favorably in the presence of conjugation with an electron withdrawing group (phenyl group, chlorine atom etc.).[41]

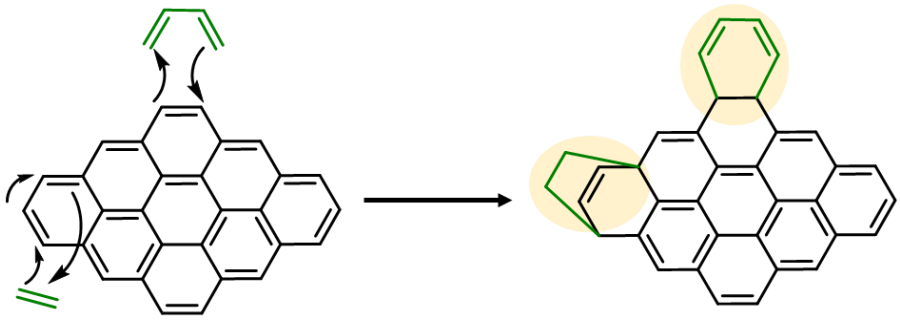

Figure 18: Functionalization of graphene through [4 + 2] cycloaddition reaction

1.4. Structure and properties of GO

GO is commonly obtained through an oxidative exfoliation of graphite. GO is made of a single layer graphitic with oxygenated and aromatic regions randomly distributed. Different oxygenated functional groups are present on GO such as such as epoxide groups and hydroxyl functions on the basal plane, while carboxyl, quinone, phenol and lactone groups are mainly present at the edges (Figure 19).[42] The surface composition of GO is strongly depending on the synthesis conditions. The presence of polar oxygenated functional group on GO makes it more hydrophilic than pristine graphene. GO has been used in different applications due to its hydrophilic nature. However, GO possesses large number of structural defects that can affect its physical properties. The presence of oxygen-containing groups allows further functionalization. The major issue with GO is the disordering of the π-network. A reduction of GO makes the removal of the oxygenated functional groups and partially

restoring aromaticity. GO has been often applied as a starting material for the synthesis of graphene. GO can be functionalized through covalent and non-covalent bond. Covalent functionalization can be performed on both oxygenated functional groups and aromatic region of GO while non-covalent functionalization can be achieved by taking advantage of the aromatic portions through hydrophobic weak interactions.

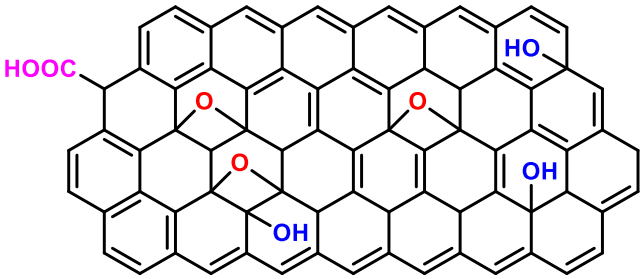

Figure 19: Schematic representation of GO

1.4.1. Synthesis of GO

Several methods have been applied for the synthesis of GO. Generally, the GO can be synthesized from graphite in two steps; (1) the first step is the oxidation of graphite to GO; (2) the second step is the removal of impurities (*e.g.* acids and manganese salts). Brodie's method, reported in 1859, where he performed the reaction in the presence of fuming HNO_3 to intercalate graphite while using $KClO_3$ as an oxidizer.[43] However, this process is time consuming and generate toxic gases during the reaction. In 1958, Hummers and Offeman developed alternative method. They perform the reaction with H_2SO_4 to intercalate graphite in the presence of $NaNO_3$, while $KMnO_4$ was used as oxidizer.[44] This method is presently the mostly employed way for the synthesis of GO. Tour *et al.* improved the Hummers method by performing the reaction in a 9 : 1 mixture of H_2SO_4/H_3PO_4.[45] The reaction performed in the absence of $NaNO_3$, while increasing the amount of $KMnO_4$. However, there are still several disadvantages of this method. To solve these problems, an improved Hummers method has recently been developed.

1.4.2. Covalent functionalization reactions of GO

GO contains different types of oxygenated groups such as hydroxyls, epoxides and carboxylic acids, these functional group can be functionalized by variety of organic reaction. The functionalization of GO has to be performed in mild conditions because of the instability of this material at high temperature.

1.4.2.1. Functionalization of GO through hydroxyl groups

The hydroxyl groups are mainly located on the basal plan of GO. They can undergo silanization and etherification reactions. The modified Claisen reaction allows to functionalize the hydroxyl groups of GO through ether bond. Only allylic alcohol of GO participates in this type of reaction. In this reaction, first the formation of ester, followed by the rearrangement, and then the formation of a C–C bond with the graphene (Figure 20).[46]

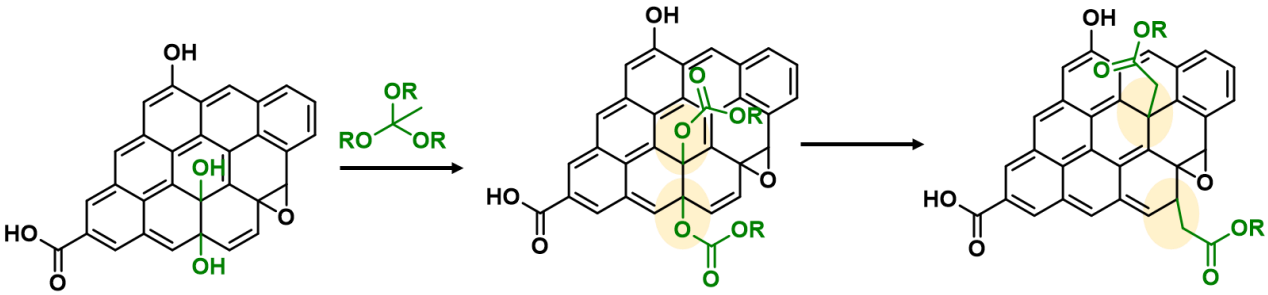

Figure 20: Functionalization of GO through modified Claisen reaction

The hydroxyl groups of the GO can be also functionalized through silanization reaction. Silanization is a two-step reaction. In the first step the hydrolysis of the trialkoxy groups of the silane and in the second step the reaction between the Si–OH groups and the hydroxyl groups of GO forming a Si–O–C bond (Figure 21). This reaction has been performed under mild conditions.[47]

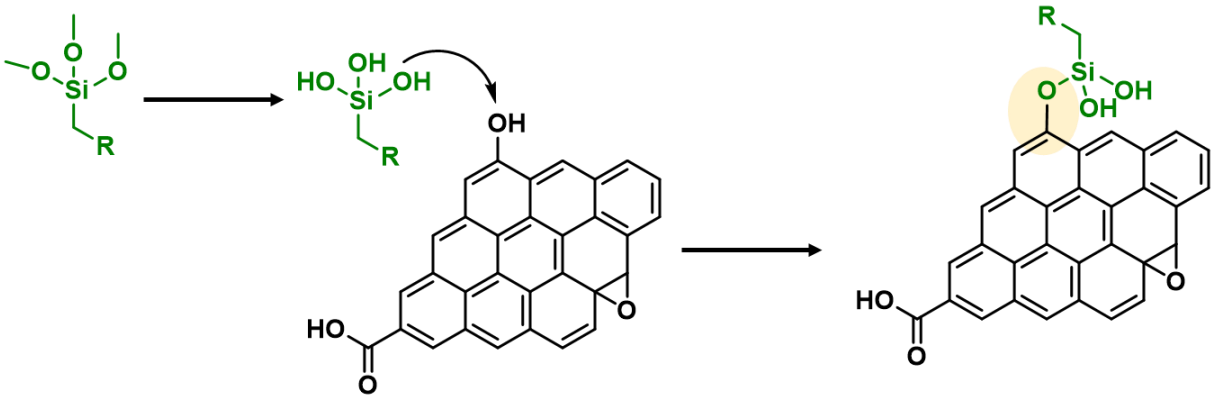

Figure 21: Functionalization of GO through silanization reaction

The hydroxyl group of GO can be derivatized by Williamson reaction under mild reaction conditions. The Williamson reaction allows the formation of an ether bond from an organohalide and a deprotonated alcohol (alkoxide ion) *via* a substitution reaction (Figure 22).[48]

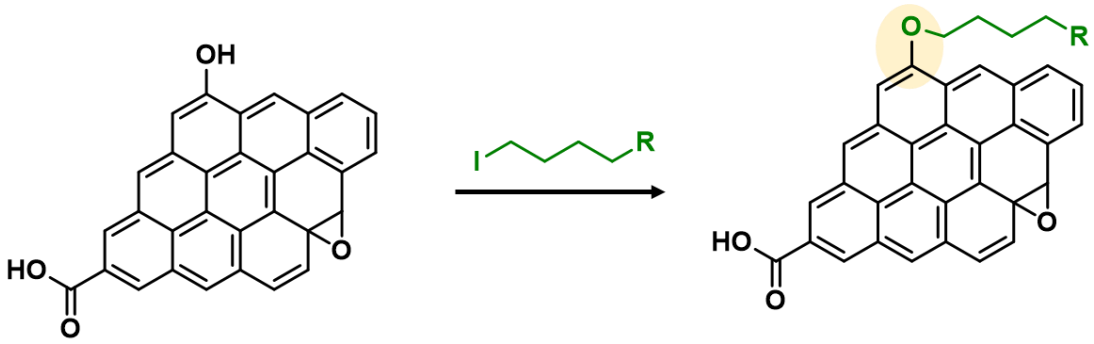

Figure 22: Functionalization of GO through Williamson reaction

Similarly, the hydroxyl group can be derivatize through esterification reaction using coupling agent (Figure 23).[49]

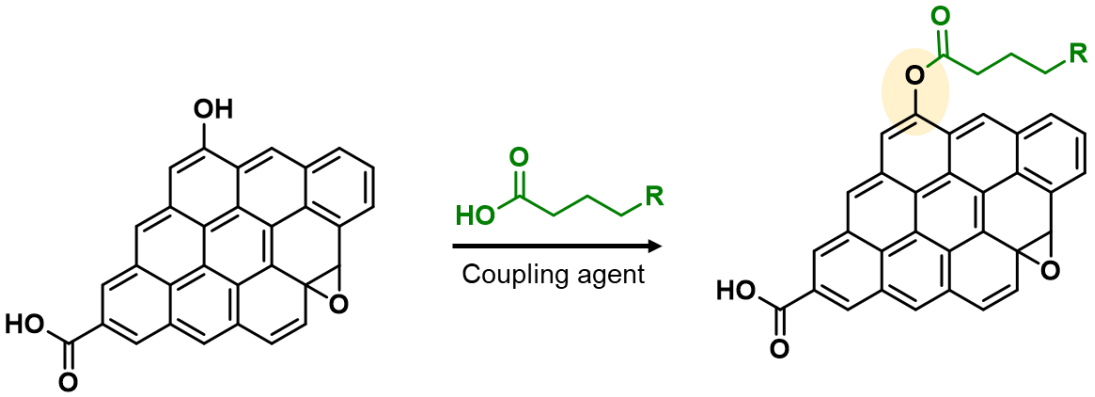

Figure 23: Functionalization of GO through esterification reaction

1.4.2.2. Functionalization of GO through carboxylic acids

The carboxylic acids mainly located at the edges of GO. Carboxylic acids of GO can react with amines or alcohol to form amides or esters. The amidation reaction can be performed in both mild or harsh conditions. In the first case, coupling agents are used to functionalize GO. In the second case, the carboxylic acid is activated to form an acyl chloride which are then reacted with amino compound to form amide bond (Figure 24a).[50] (Figure 24b).[51] The carboxyl group of GO can be also converted to amide bond by simple mixing and heating method (Figure 24c).

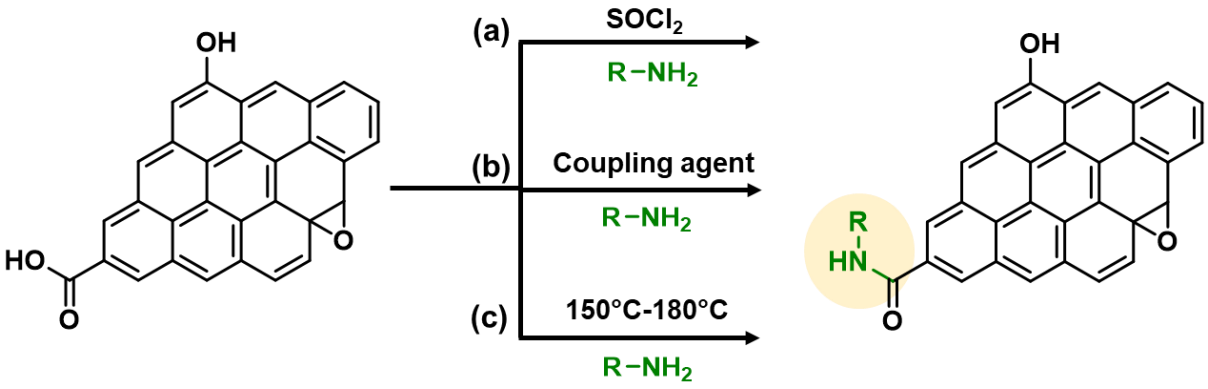

Figure 24: Functionalization of GO through carboxylic acid

1.4.2.3. Functionalization of GO through epoxides

The basal plane of GO mainly contains the epoxy groups. The epoxy goups can be functionalized through ring-opening reaction. The ring-opening reaction is mainly performed with amino and thiol compounds (Figure 25).[52,53]

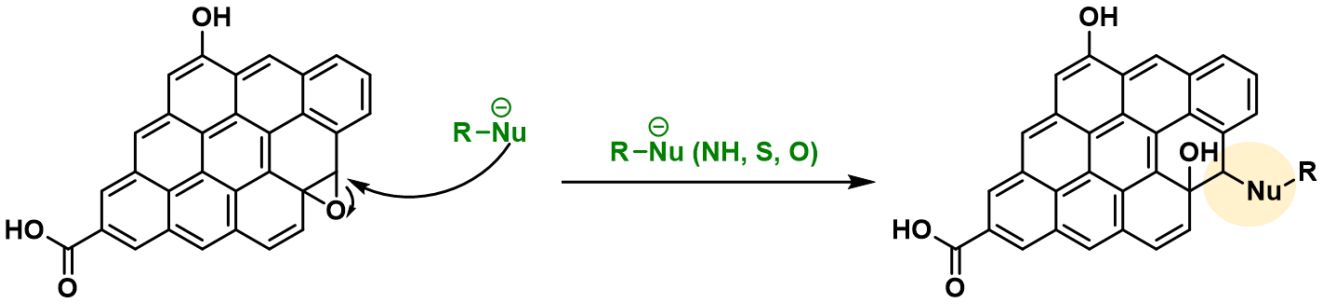

Figure 25: Functionalization of GO through epoxide group

1.4.3. Non-covalent functionalization reactions of GO

GO can be functionalized through non-covalent bond with small organic molecules and polymers. The non-covalent functionalization of GO occurs through π–π, H-bonding, van der Waals, H–π, electrostatic binding, cation–π and anion–π interactions. GO has been functionalized through non-covalent bond and applied for energy materials, biosensing, catalytic, and biomedical applications.[54]

1.5. Synthesis of RGO

The synthesis of graphene is expensive operation, graphene has the tendency to agglomerates and the mass production is low. Therefore, the researcher focused to developed new method to obtain cheaper graphene at the industrial scale. The easiest way to obtain graphene is through the oxidation and exfoliation of graphite to obtain GO, followed by the reduction. However, RGO is consist of graphene layers but it contains many defect sites in the basal plane as compared to graphene (Figure 26). A complete reduction of GO to graphene has not been achieved yet. Different methods have been used to synthesis this materials from GO such: (i) thermal reduction, (ii) chemical reduction, (iii) microwave reduction and (iv) electrochemical reduction.[55]

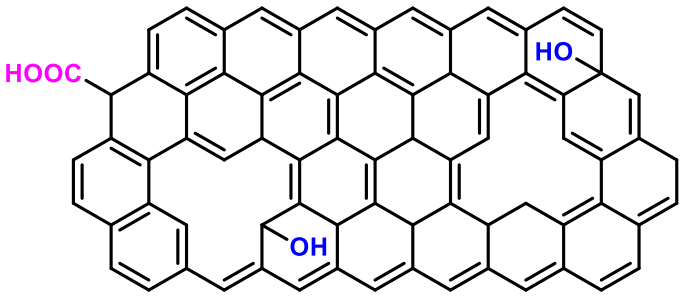

Figure 26: Schematic representation of RGO

1.5.1. Covalent functionalization of RGO

Covalent functionalization of RGO occurs both on oxygenated functional group and aromatic structure. Although, RGO possess limited amount of oxygenated functional group. The amount of oxygenated functional groups depends on the reduction method. Thus, it is important to assess which functions are present and to which extent. RGO is mainly functionalized on its aromatic domains. All covalent reactions already mentioned for graphene and GO, can be applied on RGO.

1.5.2. Non-covalent functionalization reactions of RGO

RGO can be functionalized with small organic molecules and polymer through non-covalent bond such as π–π stacking or van der Waals interactions.

1.6. Characterization

Different characterization techniques have been applied to confirm the structure of graphene, GO, RGO. In this section Fourier transform infrared (FT-IR) spectroscopy, Raman spectroscopy, X-ray photoelectron spectroscopy (XPS), thermogravimetric analysis (TGA), Scanning electron microscopy (SEM), and atomic force microscopy (AFM) will be discussed in detail.

1.6.1. Fourier transform infrared Spectroscopy

The FT-IR spectroscopy is used to identify the functional groups of a molecule. The FT-IR spectra of graphene showed no significant peak while for GO there are the characteristic peaks of the oxygenated functional groups. The FT-IR spectrum of GO include the presence of O–H (3435 cm^{-1}), C=O (1735 cm^{-1}), C=C (1615 cm^{-1}), and C–O (1052 cm^{-1}) functional groups (Figure 27). Besides from oxygenated functional group, GO also contains the adsorbed water, which give strong signal in the spectra. The removal of water content from GO is difficult because GO is thermally unstable.

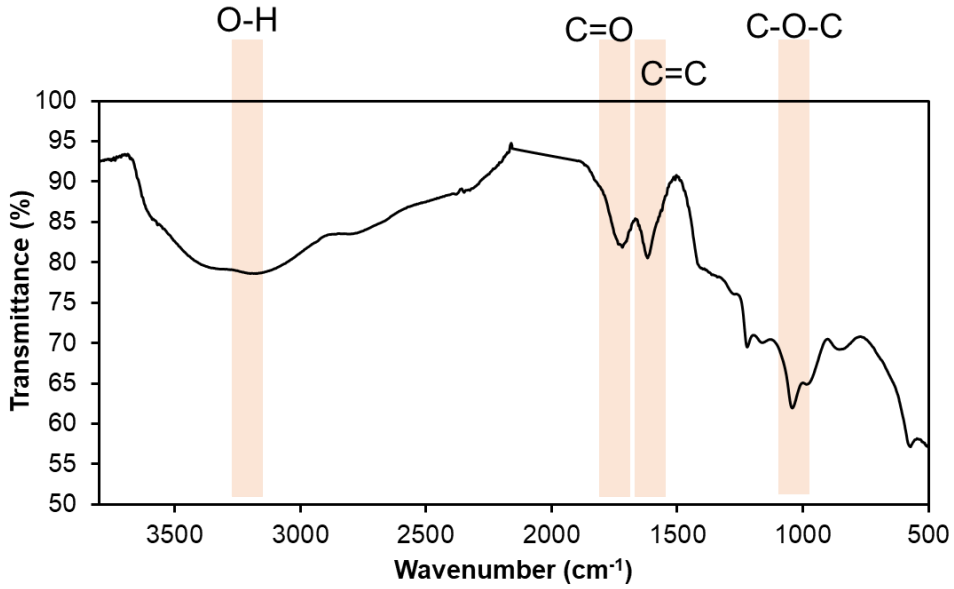

Figure 27: FT-IR spectra of GO

1.6.2. Raman spectroscopy

The Raman spectra of graphene and GO represents three main peaks. These peaks apeared at 1,350 cm^{-1} ,580 cm^{-1} and 2,700 cm^{-1}, related to D band, G band and 2D band, respectively (Figure 28). The G band is due to the sp^2 domains of carbon, the D band is due to the number of defects present in the material, and the 2D band gives information about the number of layers of the graphene material. In the case of single-layer graphene it is around 24 cm^{-1}, for graphite this band is around 45–60 cm^{-1}. In the case of single-layer graphene it is around 24 cm^{-1}, for graphite this band is around 45–60 cm^{-1}.

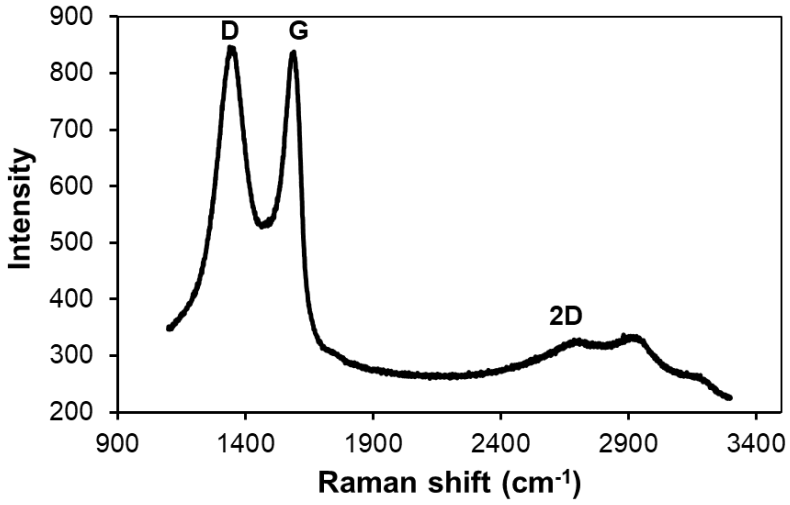

Figure 28: Raman spectra of GO

1.6.3. X-Ray photoelectron spectroscopy

XPS giving information on the elemental composition of the samples, chemical state, the empirical formula and the electronic state of the elements in a sample. The XPS spectra of graphene shows only one peak in C1s spectral region, at 284.5 eV relating to the sp^2 C=C. In GO we can find many peaks such as sp^2 and sp^3 carbon atoms, the epoxy, hydroxyl, carboxylic acid and carbonyl groups at 284.5, 285.2, 287.1, 286.4, 289.2 and 288.0 eV, respectively, in the C1s region (Figure 29).

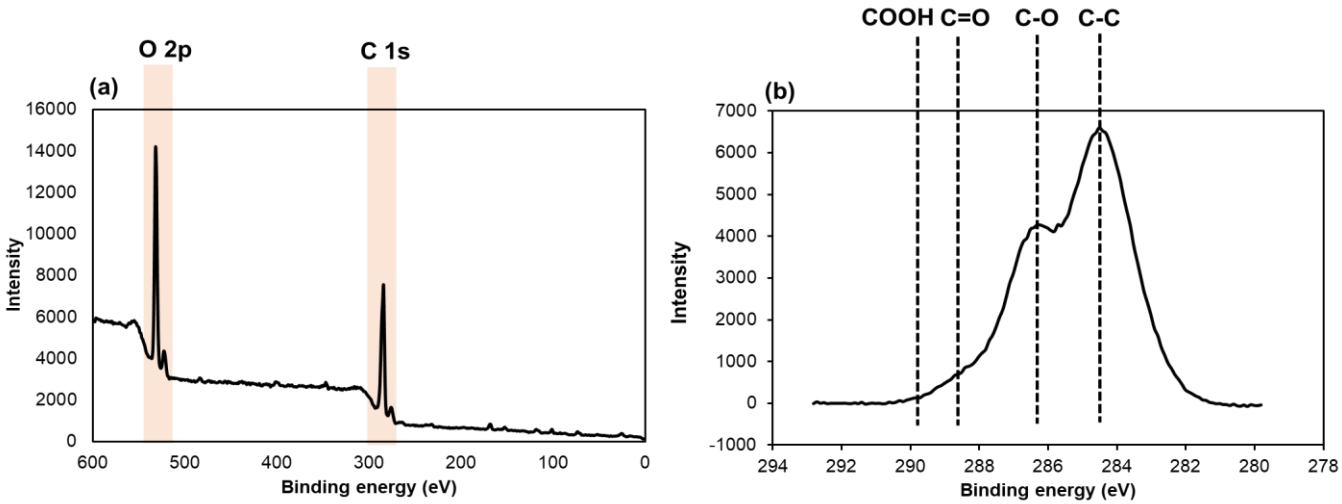

Figure 29: (a) Wide scan XPS spectra of GO, (b) high-resolution C 1s XPS spectra of GO

1.6.4. Thermogravimetric analysis

TGA giving information about the functional groups by calculating the weight loss as a function of increasing temperature. Graphene is stable at high temperatures. Functionalized graphene showed weight loss corresponding to the attached functional groups. The TGA curve of GO shows weight loss between 150 °C and 400 °C that can be assigned to the thermal decomposition of adsorbed water and oxygenated functional groups (Figure 30). Functionalized GO showed weight loss corresponding to oxygenated functional groups and the covalently attached molecules.

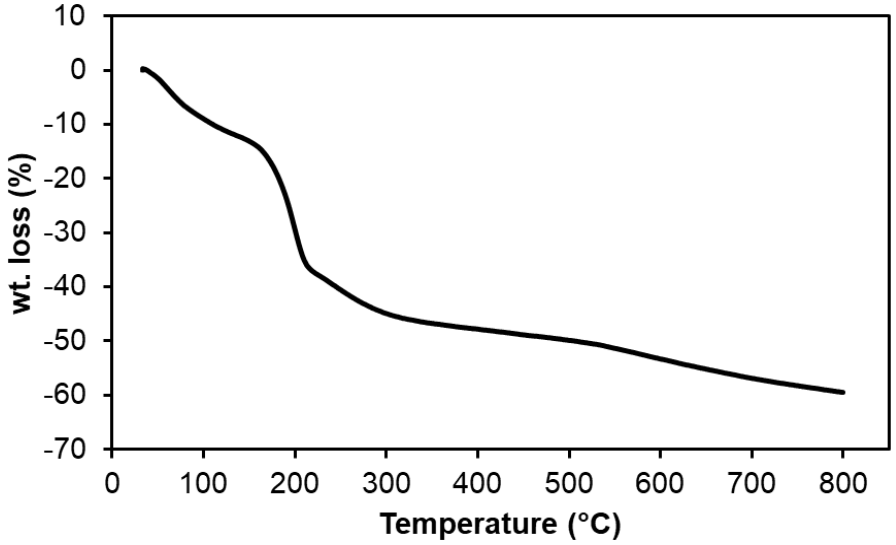

Figure 30: TGA analysis of GO

1.6.5. Scanning electron microscopy

SEM give information about the thickness, size and surface morphology of graphene and GO. Thicker graphene layers are seen as darker, bilayer graphene shows an intermediate contrast, whereas monolayer graphene film appeared as a slightly brighter contrast on silica substrate (Figure 31).

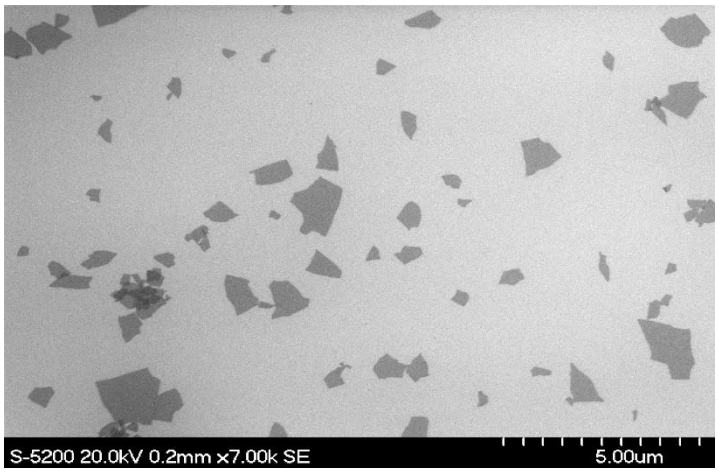

Figure 31: SEM image of GO

1.6.6. Atomic force Microscopy

AFM giving information about the surface morphology of GO and graphene at the nanometer scale. AFM determine the thickness, the number of layers and the lateral size of GO and graphene. The thickness of GO is 0.9 nm (Figure 32), due to the presence of oxygen groups, the distance between layers is increased to almost two times more compared to graphene.

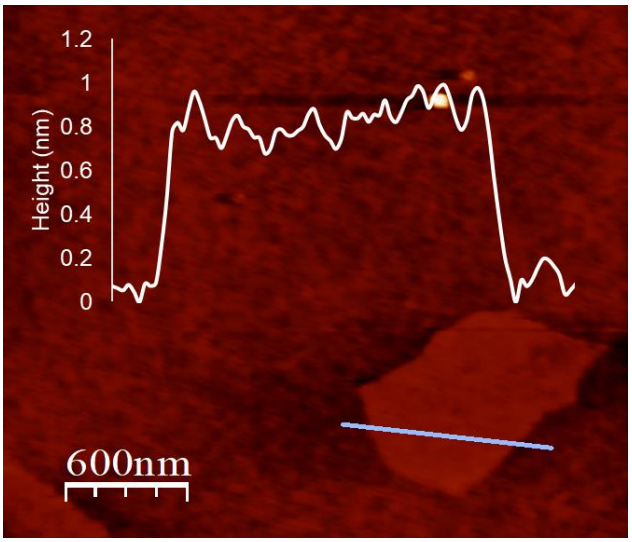

Figure 32: AFM image of GO

1.7. Conclusions

The various graphene synthesis methods are introduced mechanical exfoliation, ultrasonic cleavage, chemical vapor deposition, epitaxial growth on SiC, and unrolling of CNTs. GO is usually obtained by the oxidation of graphite. The RGO obtained as a result of reduction GO. Then the functionalization of graphene, GO and RGO are detailed and classified between covalent and non-covalent functionalization. Graphene can be functionalized through covalent bond using free radical addition, nucleophilic addition, atomic radical addition, electrophilic substitution reactions and cycloaddition. It can be also functionalized through physical interaction like non-covalent and ionic interaction. GO is

mainly covalently functionalized through their oxygenated functions such as carboxylic acids, hydroxyl groups and epoxides. It can be also functionalized through non-covalent interaction, ionic interaction and H-bonding. RGO is behave like graphene or GO, depending on the extent of reduction. However, the main difference between RGO and the graphene is the presence of defect in the former one. The choice of the materials (graphene, GO and RGO) depend on the purpose. For example, GO is suitable for biomedical applications, and graphene is more promising for electronic applications due to their excellent electrical conductivity. Graphene family member is investigated for only few years, therefore, there is still a lot to be discovered.

1.8. References:

1. G. Rajakumar, X.-H. Zhang, T. Gomathi, S.-F. Wang, M. Azam Ansari, G. Mydhili, G. Nirmala, M. A. Alzohairy and I.-M. Chung, *Processes*, 2020, **8**, 355.
2. S. Noamani, S. Niroomand, M. Rastgar and M. Sadrzadeh, *npj Clean Water*, 2019, **2**, 1–14.
3. M. S. Mauter and M. Elimelech, *Environ. Sci. Technol.*, 2008, **42**, 5843–5859.
4. C. Hu, Y. Xiao, Y. Zou and L. Dai, *Electrochem. Energ. Rev.*, 2018, **1**, 84–112.
5. U. Kamran, Y.-J. Heo, J. Lee and S.-J. Park, *Micromachines*, 2019, **10**, 234.
6. T. Evans, P. F. James and R. W. Ditchburn, *Math. Phys. Sci.*, 1964, **277**, 260–269.
7. M. Gokhale and R. Somani, *Mini Rev. Org. Chem.*, 2015, **12,** 355-366.
8. V. Georgakilas, J. A. Perman, J. Tucek, R. zboril, *Chem. Rev.*, 2015, **115**, 4744-4822.
9. X. Huang, Z. Yin, S. Wu, X. Qi, Q. He, Q. Zhang, Q. Yan, F. Boey and H. Zhang, *Small*, 2011, **7**, 1876–902.
10. J. Liu, J. Tang and J. Justin Gooding, *J. Mater. Chem.*, 2012, **22**, 12435–12452.
11. H. P. Boehm, A. Clauss, G. Fischer, U. Hofmann, Proceedings of the Fifth Conference on Carbon,, 1962, **1**, 73-80.
12. P. Avouris and C. Dimitrakopoulos, *Mater. Today*, 2012, **15**, 86–97.
13. Z. Zhen and H. Zhu, H. Zhu, Z. Xu, D. Xie and Y. Fang, Academic Press, 2018, 1–12.
14. M. Yi and Z. Shen, *J. Mater. Chem. A.*, 2015, **3**, 11700–11715.
15. C. Aksoy and D. Anakli, *Open Chemi.*, 2019, **17**, 581–586.
16. Y. I. Zhang, L. Zhang, C. Zhou., Acc. *Chem. Res.*, 2013, **46**, 2329-2339.
17. D. B. Shinde, J. Debgupta, A. Kushwaha, M. Aslam, V. Pillai, *J. Am. Chem. Soc*., 2011, **133**, 4168-4171.
18. A. C. Kleinschmidt, R. K. Donato, M. Perchacz, H. Beneš, V. Štengl, S. C. Amico and H. S. Schrekker, *RSC Adv.*, 2014, **4**, 43436–43443.
19. D.-M. Chen, P. Shenai and Y. Zhao, *Phys. chem. chem. phys.*, 2011, **13**, 1515–20.
20. Z. H. Ni, H. M. Wang, J. Kasim, H. M. Fan, T. Yu, Y. H. Wu, Z. H. Shen., *Nano Lett.*, 2007, **7**, 2758-2763.
21. S. Lee, H. Kim and B. Shim, *Carbon Lett.*, 2012, **62**, 1229.

22. H. J. Yun and S. Park, New Physics, 2012, 62,1229-1259
23. M. Coroş, F. Pogăcean, L. Măgeruşan, C. Socaci and S. Pruneanu, *Front. Mater. Sci.*, 2019, **13**, 23–32.
24. F. Perreault, A. F. de Faria and M. Elimelech, *Chem. Soc. Rev.*, 2015, **44**, 5861–5896.
25. T. Kuila, S. Bose, A. K. Mishra, P. Khanra, N. H. Kim and J. H. Lee, *Prog. Mater. Sci.*, 2012, **57**, 1061–1105.
26. I. A. Vacchi, C. Ménard-Moyon and A. Bianco, *Phys. Sci. Rev.*, 2017, **2**.
27. D. Hetemi, V. Noël and J. Pinson, *Biosensors*, 2020, **10**, 4.
28. X. Ma, F. Li, Y. Wang and A. Hu, *Chem. Asian J.*, 2012, **7**, 2547–2550.
29. C. K. Chua and M. Pumera, *Chem. Soc. Rev.*, 2013, **42**, 3222–3233.
30. X. Xu, P. Li, L. Zhang, X. Liu, H.-L. Zhang, Q. Shi, B. He, W. Zhang, Z. Qu and P. Liu, *Chem. Asian J.*, 2017, **12**, 2583–2590.
31. A. Felten, D. McManus, C. Rice, L. Nittler, J.-J. Pireaux and C. Casiraghi, *Appl. Phys. Lett.*, 2014, **105**, 183104.
32. W. Feng, P. Long, Y. Feng and Y. Li, *Adv. Sci.*, 2016, **3**, 1500413.
33. M. H. A. Kudus, M. R. Zakaria, H. Md. Akil, F. Ullah and F. Javed, *J. King Saud Univ. Sci.*, 2020, **32**, 910–913.
34. D. D. Chronopoulos, M. Medveď, G. Potsi, O. Tomanec, M. Scheibe and M. Otyepka, *Chem. Commun.*, 2020, **56**, 1936–1939.
35. C. K. Chua and M. Pumera, *Chem. Asian J.*, 2012, **7**, 1009–1012.
36. L. Jin and T. Liu, *J. Macromol. Sci. A.*, 2016, **53**, 433–437.
37. S. K. Ujjain, R. Bhatia and P. Ahuja, *J. Saudi Chem. Soc.*, 2019, **23**, 655–665.
38. T. A. Strom, E. P. Dillon, C. E. Hamilton and A. R. Barron, *Chem. Commun.*, 2010, **46**, 4097–4099.
39. L. Daukiya, C. Mattioli, D. Aubel, S. Hajjar-Garreau, F. Vonau, E. Denys, G. Reiter, J. Fransson, E. Perrin, M.-L. Bocquet, C. Bena, A. Gourdon and L. Simon, *ACS Nano*, 2017, **11**, 627–634.
40. M. Quintana, K. Spyrou, M. Grzelczak, W. R. Browne, P. Rudolf and M. Prato, *ACS Nano*, 2010, **4**, 3527–3533.

41. J. Li, M. Li, L.-L. Zhou, S.-Y. Lang, H.-Y. Lu, D. Wang, C.-F. Chen and L.-J. Wan, *J. Am. Chem. Soc.*, 2016, **138**, 7448–7451.
42. D. R. Dreyer, S. Park, C. W. Bielawski and R. S. Ruoff, *Chem. Soc. Rev.*, 2010, **39**, 228–240.
43. P. Feicht, J. Biskupek, T. E. Gorelik, J. Renner, C. E. Halbig, M. Maranska, F. Puchtler, U. Kaiser and S. Eigler, *Chem. Eur. J.*, 2019, **25**, 8955–8959.
44. H. Yu, B. Zhang, C. Bulin, R. Li and R. Xing, *Sci. Rep.*, 2016, **6**, 36143.
45. D. C. Marcano, D. V. Kosynkin, J. M. Berlin, A. Sinitskii, Z. Sun, A. Slesarev, L. B. Alemany, W. Lu and J. M. Tour, *ACS Nano*, 2010, **4**, 4806–4814.
46. W. Collins, W. Lewandowski, E. Schmois, J. Walish and T. Swager, *Angew. Chem. Int. Ed.*, 2011, **50**, 8848–8852.
47. S. S. Abbas, G. J. Rees, N. L. Kelly, C. E. J. Dancer, J. V. Hanna and T. McNally, *Nanoscale*, 2018, **10**, 16231–16242.
48. I. A. Vacchi, J. Raya, A. Bianco and C. Ménard-Moyon, *2D Mater.*, 2018, **5**, 035037.
49. I. A. Vacchi, S. Guo, J. Raya, A. Bianco and C. Ménard-Moyon, *Chem. Eur. J.*, 2020, **26**, 6591-6598.
50. J. Yao, S. Liu, Y. Huang, S. Ren, Y. Lv, M. Kong and G. Li, *Prog. Nat. Sci. Mater.*, 2020, **30**, 328–336.
51. S. Guo, J. Raya, D. Ji, Y. Nishina, C. Ménard-Moyon and A. Bianco, *Nanoscale Adv.*, 2020, **2**, 4085–4092.
52. H. Thomas, A. Marsden, M. Walker, N. Wilson and J. Rourke, *Angew. Chem. Int. Ed.*, 2014, **53**, 7613-7618.
53. I. A. Vacchi, C. Spinato, J. Raya, A. Bianco and C. Ménard-Moyon, *Nanoscale*, 2016, **8**, 13714–13721.
54. V. Georgakilas, J. N. Tiwari, K. C. Kemp, J. A. Perman, A. B. Bourlinos, K. S. Kim and R. Zboril, *Chem. Rev.*, 2016, **116**, 5464–5519.
55. J. Feng, Y. Ye, M. Xiao, G. Wu and Y. Ke, *Chem. Pap.*, 2020, **74**, 3767–3783.

Chapter 2

Covalent functionalization of graphene with redox-active organic molecules for energy storage

2. Introduction

Graphene-based materials have attracted considerable interest in electrochemical applications due to their abundance, processability, stability, and relatively environmentally friendly characteristics.[1] Graphene has been widely used as electrode materials. Some of the useful properties of GO and graphene-based electrodes include electrochemical stabilities and wide potential windows for repetitive redox reactions.[2] The sp^2 and/or sp^3 hybridized carbons and some of the oxygenated functional groups provide reactive sites for surface functionalization, which is beneficial to electrochemical applications, especially for electrode materials.

The covalent functionalization could significantly change the electrical structure and properties of the graphene.[3,4] In particular, acid (*e.g.*, nitric acid or sulfuric acid)-promoted oxidation is one of the most commonly used methods for covalent functionalization.[5,6] The carbon atoms in graphene can form robust covalent bonds with organic molecules, giving rise to a variety of composites with distinguished properties. The surface functionalized graphene and GO have been used for a number of applications such as catalysis,[7,8] energy conversion,[9,10] sensing,[11,12] separation media,[13–17] and biomedicine.[18–20] However, most of the applications rely on the concept of electrochemistry.[21,22]

The fundamental components in electrochemical processes are the electrodes. graphene shows high chemical stability,[23] good mechanical properties,[24,25] and high electrical conductivity.[26,27] However, despite the potentials of graphene-based material, a common problem is the low surface wettability,[28] which lead to a low utilization rate of specific surface area, and result in low energy storage. Change of the surface chemistry by functionalization is a common route to optimize the interaction of the graphene surface with the external environment. The modification of the surface chemistry of graphene strongly improves their interaction with aqueous and organic environments, providing improve performance as electrode materials in energy storage systems.

Covalent modification with organic molecules is expected to allow fine control of the function and physical properties at atomic or molecular levels. The covalent functionalization

of graphene with redox-active materials (organic molecules and conductive polymer) have been performed by nitrene and diazonium chemistry for sp^2 carbons, ring-opening reaction of epoxide group, etherification reaction, esterification reaction, amidation reaction and cyclization reaction (Figure 1). The detail explanation of each functionalization method is already discussed in section 1.

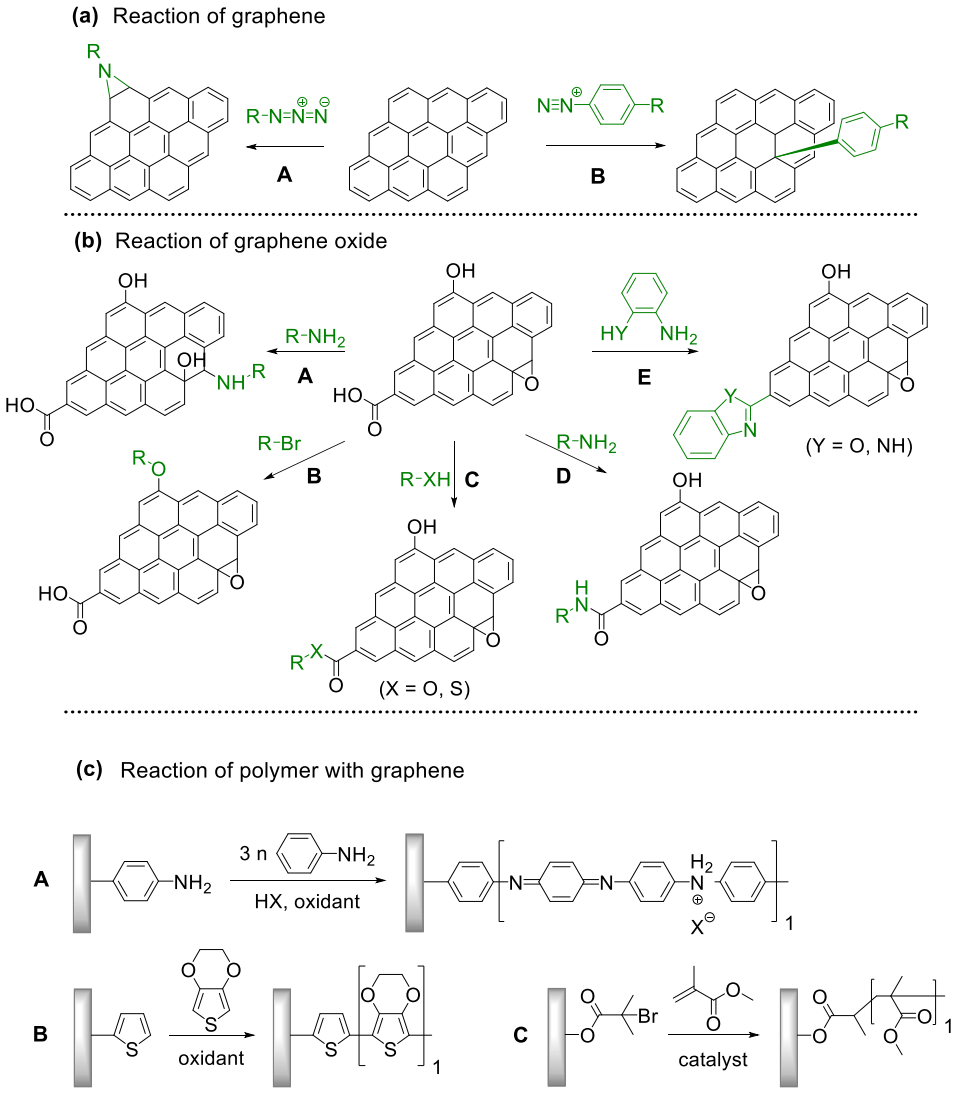

Figure 1: Various functionalization routes of graphene with redox-active molecules (a) toward sp^2 carbons framework of graphene and (b) toward oxygenated functional groups on GO. (c) Preparation strategies of graphene-polymer composites

2.1. Redox-active organic molecules and their operating mechanism

According to the growth of renewable energy utilization, demands for advanced energy storage devices with high efficiency are increasing. To solve the problems of global energy consumption, the development of high-performance and low-cost clean energy devices is required. LIBs and SCs are two of the most promising energy storage devices due to their notable characteristics, such as high energy density,[29] high power density,[30] and long cycle life.[31] For instance, widespread success has been achieved for LIBs since their commercialization in the 1990s.[32] Current commercial LIBs are constructed with metal-based materials, such as $LiMn_2O_4$,[33] $LiCoO_2$,[34] and $LiFePO_4$,[35] on the cathode side and carbon-based materials such as graphite on the anode side. In the case of SCs, pseudocapacitive materials, such as metal oxides, sulfides, selenides and phosphides, are widely explored to enhance energy density.[36] However, the concerns of high cost, limited availability, and electronic hazards of transition metals, as well as poor cycling stability, would hinder their practical use.[37] Thus, metal-free redox-active organic materials for the fabrication of electrodes have been widely studied and can be potential candidates for the next-generation energy storage.

The first organic electrode was introduced by Williams using dichloroisocyanuric acid as an active material for a primary battery in 1969.[38] After this study, a variety of redox-active organic molecules have been studied, including small organic molecules such as quinones, dianhydrides and conjugated polymers such as polypyrrole and polyacetylene. The reported redox-active organic molecules can be categorized into carbonyl compounds,[39] organic radicals,[40] organosulfur compounds,[41] phenazine derivatives,[42] and conductive polymers (Figure 2).[43]

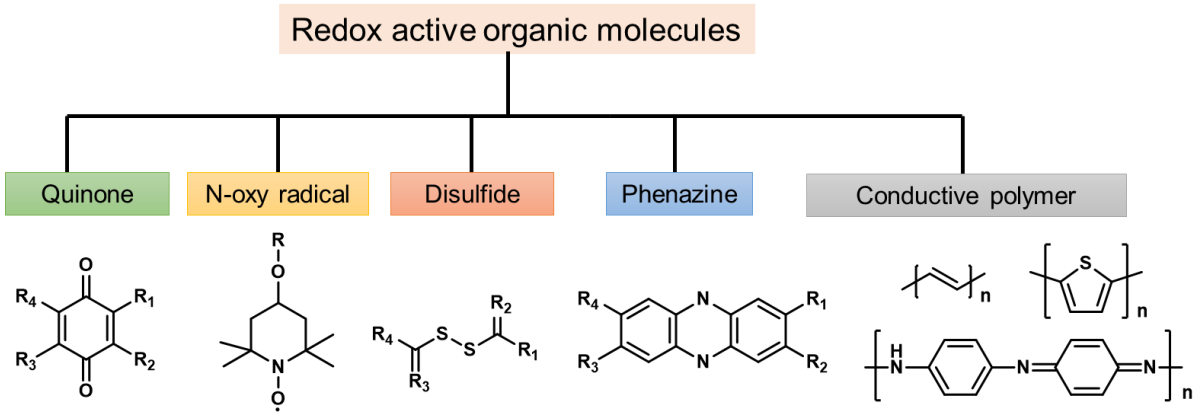

Figure 2: Classification of organic redox-active molecules

Redox-active organic molecules have attracted more and more interest recently, due to their intrinsic and reliable redox behavior, which can be readily utilized for charge-storage memory applications. A redox-active molecule contains a redox component acting as the charge-storage center surrounded by insulators/barriers. The electrons tunnel through the barrier during the oxidation and reduction processes. Typically, the application of an oxidation voltage will cause electron loss in the redox molecules; reversely, the electrons will be driven back to the molecules by applying a reduction voltage. Generally, the redox molecules have multiple stable states. The switching between these states is dynamically reversible through the loss or capture of a charge, that is, oxidation and reduction of the redox centers (Figure 3).

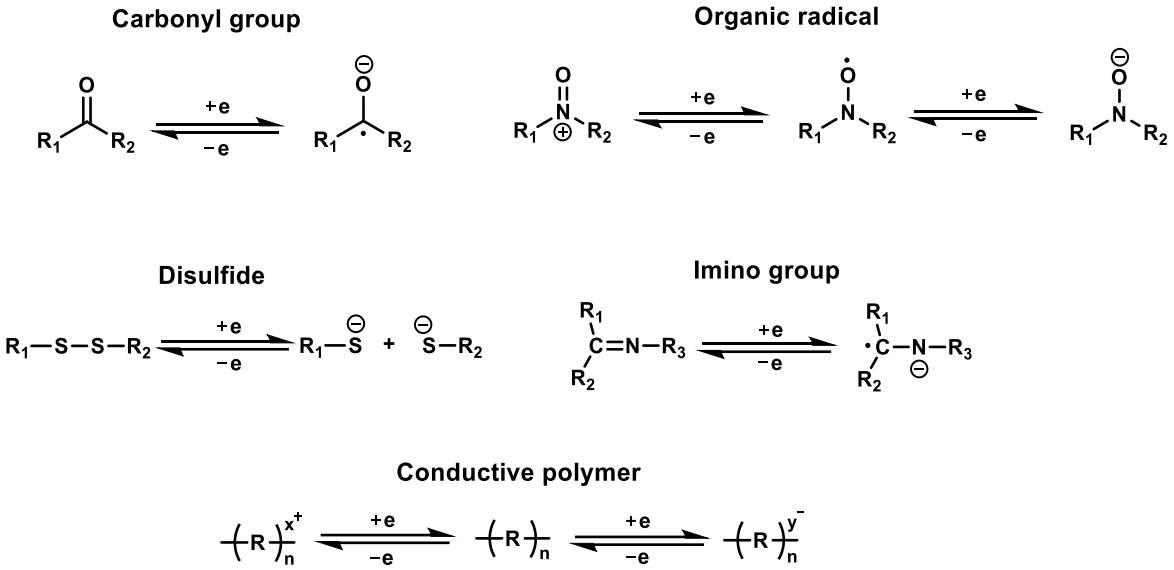

Figure 3: Redox mechanisms of various types of organic redox-active molecules

Up to now, several reviews were published on the organic electrode for energy devices; Schon,[44] Shanmukaraj,[45] Shea,[46] Han,[47] and Song,[48] independently reported the progress of the organic-based electrode for SCs and LIBs, all of which have mentioned difficulties in the development of organic electrodes. First, the organic molecules on electrodes tend to dissolve into the electrolytes, which results in a poor cycle life.[49] Second, their poor conductivity, resulting in limited electrochemical performance; as a result, their potential cannot be withdrawn completely due to the insulative effect.[50] Covalent functionalization strategy is expected to solve these problems.

2.2. Scope of the research

The organic modification of nanocarbons can be classified into covalent,[51] non-covalent,[52] and ionic bond[53] formations. Organic molecules have been functionalized on nanocarbon through non-covalent interactions and ionic bonding; as a result, high capacity, energy density, and power density were obtained.[54] Li,[55] Yuan,[56] Notarianni,[57] and Iqbal[58] independently reviewed the progress of the carbon-based composites as electrode materials for SCs and LIBs (Figure 4), focusing mainly on physical (non-covalent) interactions. However, since physical interactions are weak, molecular dissociation occurs readily.[59,60]

Also, the rapid fading of electrode performance due to the volume change during charge–discharge cycles is a problem that needs to be addressed. The covalent functionalization of graphene results in the formation of durable materials.[61] The electrochemical performance of redox-active organic molecules can be properly regulated by introducing redox-active molecules via diverse organic reactions. Covalent binding of redox-active organic molecules with graphene improves the transfer rate of electron and prevents the dissolution of the redox-active material, resulting in good conductivity and long cycle life.[62,63] In this literature review, I will summarize and discuss the reported literature based on the covalent modification of redox-active organic molecules on graphene and their electrochemical stability as electrode material in SCs and LIBs.

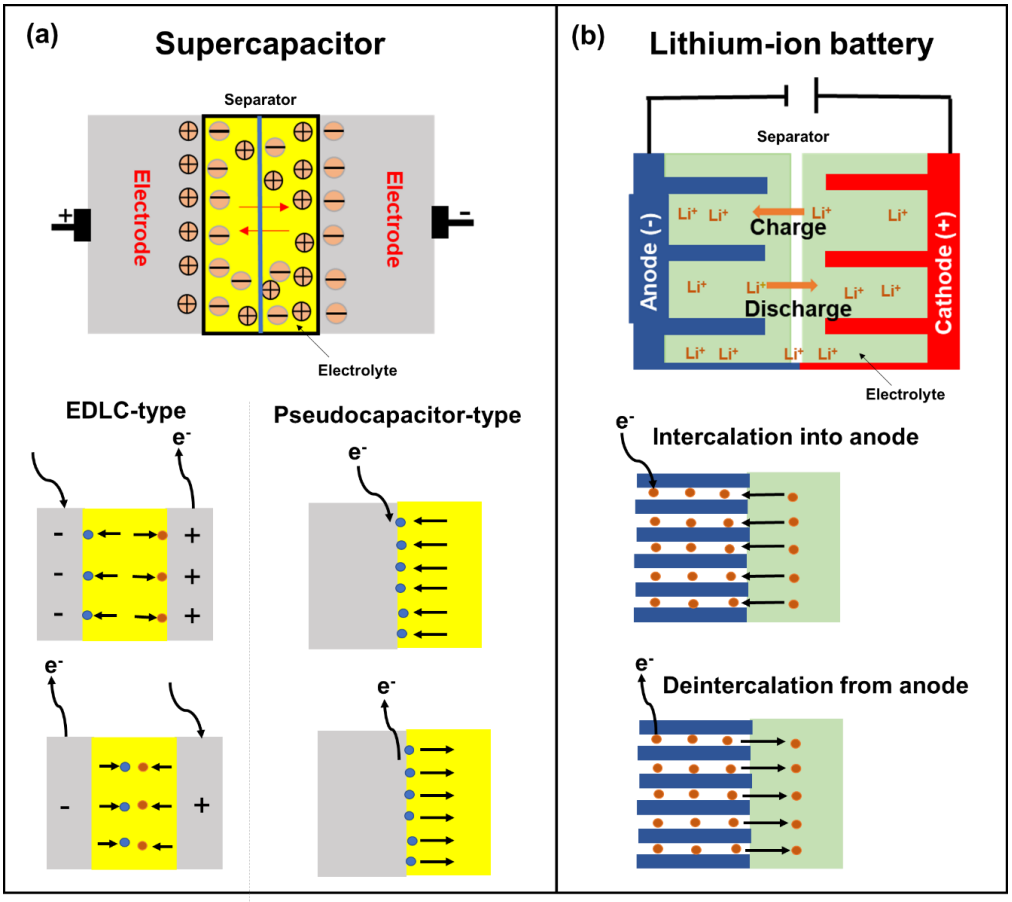

Figure 4: Schematic representation of the working principle of (a) SCs and (b) LIBs

2.3. Covalent functionalization of graphene with redox-active organic molecules for SCs

2.3.1. Small redox-active molecules-functionalized graphene for SCs

SCs are attractive for high power applications because of their ability to rapidly store/release electrical energies.[64–66] High-performance SCs should have large specific capacitances, high-power capabilities, and ultra-long cycle lives. Among the proposed applications of graphene-based materials, SCs, also known as electrochemical capacitors, have attracted much attention for the past decade. Compared with secondary batteries, graphene-based SCs are electrochemical energy storage devices that promise outstanding power density, charge/discharge rate, cycling stability, and operational safety.[67] SCs are often utilized individually or in tandem with batteries for energy storage and supply. Based on their energy storage mechanisms, SCs are mainly classified into electrical double-layer capacitors (EDLCs) and pseudocapacitor.[68,69] EDLCs store energy by electrostatic charge accumulation at electrode/electrolyte interfaces, while the pseudocapacitance is mainly attributed to the redox reactions at electrode surfaces (Figure 4a).

The covalent attachment of redox-active molecules to graphene has been proven to be a viable means of increasing electron transfer rates and preventing the dissolution of redox-active material, leading to a good cycle life.[70] When redox-active molecules are covalently attached on graphene, they can represent reversible reactions; therefore, electrodes can have both pseudocapacitance and EDLC mechanism simultaneously. Thus, the energy density of the electrode enhances and results in a stable behavior without any structural disturbance. Selected examples are summarized in Table 1. RGO was functionalized with phenylenediamine (RGO-PD),[71] 2-aminoanthraquinone (RGO-AAQ),[72] and 2-aminopyrene-3,4,9,10-tetraone (RGO-PYT)[73] through nucleophilic ring-opening reaction of epoxide group and applied for SCs. The resulting composite materials showed a capacitance retention of 92%, 100%, and 100%, respectively. The covalently bonded redox-active moieties contribute to the pseudocapacitance. Graphene provides a large specific surface area for forming electric double layers, works as a host material for the redox-active molecules, and promotes charge transfer and electrolyte diffusion. Edges of graphene can be functionalized by cyclization

reaction at carboxylic groups.[74,75] The prepared composite material displays a capacitance retention of 98% after 9000 cycles. The cyclization reaction does not destroy the in-plane sp^2 framework of graphene, allowing better electrical conductivity. However, this functionalization method requires phosphoric acid catalyst and multistep reactions. Thiourea functionalized GO (RGO-TU) was prepared through amide bond.[76] The specific capacitance of the material increases slightly in the initial cycles and then become stable with no obvious loss in specific capacitance after long cycling. We assume that the sulfur-containing thiourea is activated in the first few cycles and undergoes redox reaction. In another report, adenine (AD) was functionalized on GO (GO-AD) through amide bond.[77] The GO-AD electrode exhibited excellent cycling retention of 100% after 1000 cycles. But, the reaction was performed at room temperature; therefore, the functionalization might occur only at the epoxide groups instead of carboxyl groups. Another approach for graphene functionalization is diazonium chemistry. Anthraquinone (AQ) molecules were grafted on graphene through diazonium chemistry, forming covalently linked graphene framework (G-AQ). Covalently linked AQ molecules worked as pillars to construct graphene framework and prevented the restacking of graphene sheets during fabrication processes. The capacitance retention of G-AQ was 96% after 5000 cycles.[78] Similarly, 2-amino-3-chloro-1,4-naphthoquinone (ACNQ) molecules were introduced onto graphene via diazonium chemistry (G-CNQ).[79] The electrode exhibited a long cycling life, nearly no loss after 10,000 cycles. Diazonium chemistry is simple, fast, and efficient. The key species of the reaction is an aryl radical, which readily adds to carbon frameworks at the basal planes and edges, achieving a sufficient introduction of functional groups. To summarize this section, the order of the desirable functionalization is diazonium chemistry > cyclization > amidation reaction > reaction through epoxide group (Figure 5), although the investigation may not be comprehensively performed.

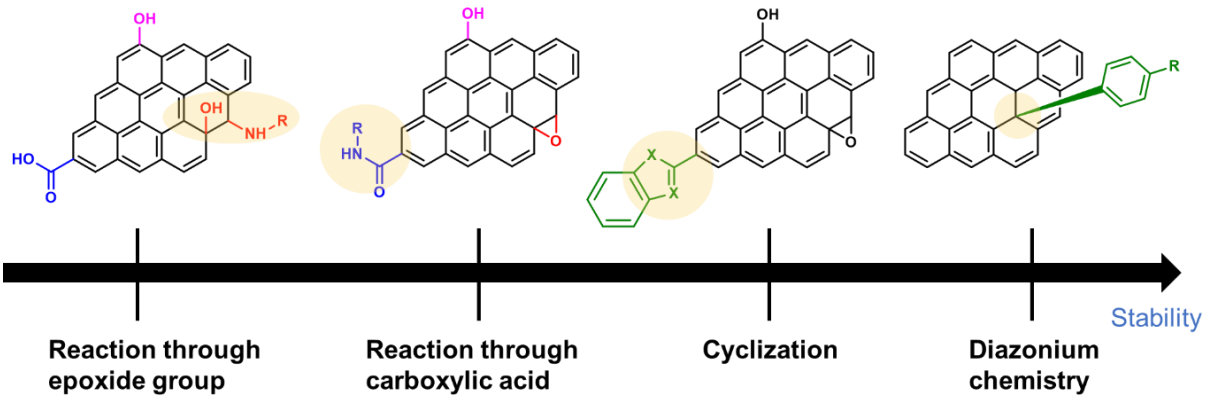

Figure 5: Comparison of different covalent functionalization methods toward electrochemical stability

Table 1: Small redox-active molecules-functionalized graphene for SCs

Material	Functionalization reaction	Cycle number	Capacity retention	Ref.
RGO-PD	Ring opening of epoxide	1000	92%	[71]
RGO-AAQ	Ring opening of epoxide	1000	100%	[72]
RGO-PYT	Ring opening of epoxide	25000	100%	[73]
G-BBO	Cyclization (phosphoric acid-catalyzed cyclization reaction)	9000	98%	[74]
G-BO	Cyclization (phosphoric acid-catalyzed cyclization reaction)	2000	100%	[75]
RGO-TU	Amidation and ring opening of epoxide	10000	100%	[76]
GO-AD	Amidation (mixing and heating)	1000	100%	[77]
G-AQ	Diazonium chemistry	5000	96%	[78]
G-CNQ	Diazonium chemistry	10000	100%	[79]

2.3.2. Conductive polymer functionalized graphene for SCs

Polymer-based SCs offer some unique properties such as controllable solubility, precise optimization of potential, variety of counter ions, flexible or even bendable electrodes and, subsequently, devices can be fabricated.[80] Various graphene–polymer composites with non-covalent and covalent interaction have been synthesized, and high capacitive performances have been achieved. The non-covalent interaction between graphene and polymers limits charge transfer at their interface and causes volumetric change during the charge-discharge cycles, reducing the cycling stability when applied for electrode materials.[81–84] To overcome this issue, polymers were introduced on graphene through covalent bond. At the same time, the polymer structure plays important roles, both in stability and capacitance. Various types of polymers have been introduced on graphene through covalent bond and applied for SCs (Table 2). PANI was functionalized on RGO (RGO-PANI) through introduction of carboxyl group on RGO, amidation, followed by oxidative polymerization. Diazonium chemistry is widely employed for the covalent functionalization of RGO, because it can prevent the graphene sheets from aggregating during the functionalization. In addition, RGO can provide an excellent conducting path to the grafted PANI and improve the charge transport of PANI. The cycling stability of nanocomposite after 1000 cycles was 72% of the initial capacitance.[85] Similarly, poly(3,4-ethylenedioxythiophene) was covalently grafted onto RGO, which was prefunctionalized with thiophene by diazonium chemistry (RGO-PEDOT). Thiophene was used as linker, followed by chemical polymerization. Thiophene unit on GO promotes the selective polymerization with EDOT at the 2- and 5-positions of thiophene, forming covalently grafted GO-PEDOT. The prepared material showed a capacitance retention of 80% after 1000 cycles.[86] Also, PANI was introduced on RGO using PD as an linker. The capacitance retention in a range of 82%-90% was obtained.[87–89] These results suggest that the type of linker affect the electrochemical stability. Using cyclization reaction, 1,3-bis(2-benzimidazolyl)-5-aminobenzene was functionalized on RGO (RGO-BOA). The capacitance retention of electrode materials was 88% after 5000 cycles.[90] Through amide linkage, melamine was functionalized on RGO (RGO-M), and then nanocomposite with

polyorthoaminophenol was prepared (RGO-M-PAP). The prepared material was applied as an electrode, with a capacity retention of 90% after 1000 cycles.[91] This result suggests that nitrogen-containing RGO has the potential to improve the electrochemical behavior of SCs. In another work, PPD was functionalized on RGO (RGO–PPD) through amide bond, using thionyl chloride activation method, followed by polymerization. The composite exhibits excellent cycling stability, maintaining 90% of its initial capacitance after 1000 cycles.[92] The excellent SCs properties rely on the polymer nanoparticles wrapped within or on the graphene surface, providing a large surface area and high pore volume of RGO. To further improve the electrochemical performance, organic dopant was introduced into the structure of PANI which is covalently functionalized on the surface of graphene (G-PANI) through diazonium chemistry. The resulting material showed high electrochemical stability in cycling, with 95% of capacitance retention after 1000 cycles.[93] The synthesized composites showed a unique hierarchical morphology, which increased the accessible surface area for the redox reaction and allowed faster ion diffusion for excellent electrochemical performance. Recently, we reported graphene–polymer composite through ring opening reaction of epoxides (RGO-SBP). The composite was synthesized using a three-step reaction involving a cross-linker, initiator, and monomer. The prepared material demonstrated a cycling stability of 98% after 1000 cycles.[94] Furthermore, RGO was functionalized with a redox-active thiourea-formaldehyde polymer (TF), yielding a multifunctional hybrid system (RGO-TF). The functionalization of the RGO was performed by thiol-carboxylic-acid esterification. The presence of multiple functional groups comprising sulfur, nitrogen, and oxygen provide additional contribution of faradaic redox reaction in SCs, leading to effective pseudocapacitances. The prepared material exhibited good cycling stability with a capacitance retention of 100% after 5000 cycles.[95] The literature reveals that the most important point for the electrochemical stability is the structure of polymer along with covalent connection. The introduction of proper linker, and construction of multifunctional polymer increase the stability as well as the specific capacitance of polymer-graphene composites.

Table 2: Conductive polymer functionalized graphene for SCs

Materials	Functionalization reaction	Cycle number	Capacity retention	Ref.
RGO-PANI	Diazonium chemistry	1000	72%	[85]
RGO-PEDOT	Diazonium chemistry	1000	80%	[86]
RGO-PANI	Diazonium chemistry	2000	83%	[87]
RGO-PANI	Ring opening of epoxide	10000	82%	[88]
RGO-PANI	Ring opening of epoxide	1000	81%	[89]
RGO-BOA	Cyclization	5000	88%	[90]
RGO-M-PAP	Amidation	1000	90%	[91]
RGO-PPD	Amidation ($SOCl_2$ activation)	1000	90%	[92]
G-PANI	Diazonium chemistry	1000	95%	[93]
RGO-SBP	Ring opening of epoxide	1000	98%	[94]
RGO-TF	Esterification	5000	100%	[95]

2.4. Covalent functionalization of graphene with redox-active organic molecules for LIBs

2.4.1. Small redox-active molecules-functionalized graphene for LIBs

Small organic molecules covalent grafted onto the surface of graphene can result in a high capacity and maintain excellent cycling stability in LIBs. To date, several approaches for covalent functionalization of graphene have been reported (Table 3). AQ was grafted on RGO (RGO-AQ) through nitrene chemistry. The material showed a capacity retention of 70% after ten cycles in LIBs.[96] The cycling stability of the material decreases significantly, indicating the formation of RGO-AQ via nitrene is not ideal. To further improve the electrochemical stability, graphene was functionalized with an organic radical, 4-hydroxy-2,2,6,6-tetramethylpiperidin-1-oxyl (4-hydroxy-TEMPO), through esterification reaction. This composite has an electrically conductive network of graphene sheets with abundant electrochemically active nitroxide radical functionalities. However, when the prepared material was applied as an electrode, the capacity decreases in the first few cycles, suggesting the instability of the ester bond.[97] Esterification was also investigated for the functionalization of tetrahydroxybenzoquinone (THBQ) on GO (GO-THBQ). GO-THBQ was applied as electrode for LIBs and demonstrated a cycling stability of 68% after 2000 cycles.[98] Similarly, carboxyl-enriched RGO was functionalized with nitroxide radical (RGO-NO) via one-step esterification. The capacity retention of RGO-NO was 89% after 2000 cycles, derived from the folded RGO-NO structure that shortens the distance of electron transport between radicals.[99] These results suggest that ester bonding is not stable. In another report, *N,N′*-diamino-1,4,5,8-naphthalenetetracarboxylic bisimide (DNTCB)-functionalized GO (GO-DNTCB) was prepared by amidation. The resulting material showed a capacity retention of 85% after 50 cycles in LIBs electrode.[100] Similarly, GO was functionalized with naphthalenediimide diamine (NDIDA) through amide bond (GO-NDIDA), using conjugating linker. GO-NDIDA exhibits a capacity retention of 100% after 50 cycles with the aid of conjugated linker (aniline).[101] These results suggested that the introduction of a conjugated linker between graphene and redox-active molecules can improve the electrochemical stability. The functionalization of graphene through the amide bond is the

better approach to achieve stability under electrochemical reactions. This is because amide is the most stable form in carboxyl acid derivatives.

To summarize this section, the order of the desirable functionalization is amidation > esterification > nitrene chemistry (Figure 6), although there is still room for consideration.

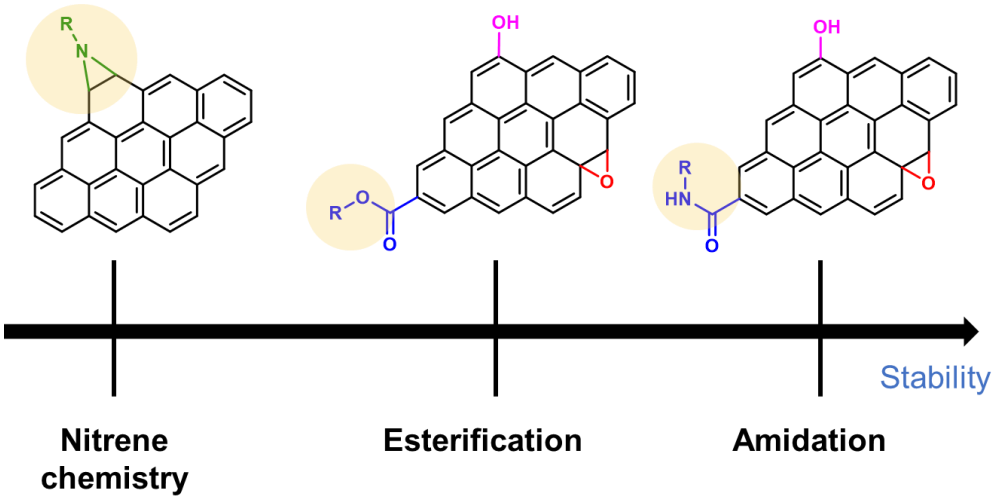

Figure 6: Comparison of different covalent functionalization methods of graphene toward electrochemical stability

Table 3: Small redox-active molecules-functionalized graphene for LIBs

Material	Functionalization reaction	Cycle number	Capacity retention	Ref
RGO-AQ	Cyclization (nitrene chemistry)	10	70%	[96]
GO-TEMPO	Esterification ($SOCl_2$ activation)	400	65%	[97]
GO-THBQ	Esterification (simple mixing)	2000	68%	[98]
RGO-NO	Esterification ($SOCl_2$ activation)	200	89%	[99]
GO-DNTCB	Amidation (coupling reagent)	50	85%	[100]
GO-NDIDA	Amidation (coupling reagent) and conductive linker	50	100%	[101]

2.4.2. Conductive polymer functionalized graphene for LIBs

Surface covalent functionalization of graphene sheets by polymers has been verified as an effective approach to keep the sheets from restacking in the composite materials, which is a different solution to allow utilization of the surface groups of graphene sheets (Table 4).[102,103] Covalently grafted graphene with polysulfur (G-PS) was synthesized through inverse vulcanization, and applied for ultra-high loading Li−polyS batteries.[104] The prepared material showed a capacity retention of 67% after 100 cycles. Graphene sheets improve the conductivity and stability of polysulfides matrix. The nitroxide radical polymer, poly(2,2,6,6-tetramethylpiperidinyloxy-4-ylmethacrylate) (PTMA), gains attention as a promising cathode material for high-rate, organic radical batteries, which is also called as organic radical polymer battery.[105] Graphene covalently functionalized with radical polymer (G-PTMA), via surface-initiated atom transfer radical polymerization, and applied for LIBs. After 250 cycles, the capacity retention of the prepared material was almost 70%. The covalently bonded PTMA could interact with graphene sheets at a molecular level, improving electron and ion transportation. G-PTMA could also inhibit the restacking of graphene sheets during the electrode fabrication process.[106] However, this method requires several preparation steps, which is time-consuming and requires metallic catalyst.

To summarize this section, atom transfer radical polymerization reaction showed relatively good electrochemical stability than synthesis and grafting of polymer through inverse vulcanization.

Table 4: Conductive polymer functionalized graphene for LIBs

Materials	Functionalization reaction	Cycle number	Capacity retention	Ref.
G-PS	Ring opening of epoxide and Inverse vulcanization	100	67%	[104]
G-PTMA	Diazonium chemistry and atom transfer radical polymerization	250	70%	[106]

2.5. Conclusion and challenges

Here, I summarized the covalent functionalization of graphene with redox-active small molecules and polymers and compared their performances for SCs and LIBs. Covalent binding of redox-active organic molecules to graphene has been demonstrated to be a promising strategy. The covalently bonded composites prevent the dissolution of small redox-active molecules, stabilize the polymer structure, and shows better electrochemical stability than non-covalently bonded ones. However, the current covalent functionalization methods required harsh reaction conditions, complicated procedures and accompanied with biproduct formation (Table 5). Therefore, the improvement of the current functionalization method is needed to achieve cost effective, eco-friendly and high-performance electrode materials. Also, the literature survey reveals that comprehensive research has not been done on the covalent functionalization of graphene for energy storage applications, despite the development of various types of organic transformations in recent years. Therefore, further investigation is needed for developing advanced electrode materials.

Table 5: Characteristics and issues of each covalent functionalization method

Methods for functionalization of graphene	**Characteristics**	**Issues**
Diazonium chemistry	Simple, stable, basal-plane functionalization	Disrupt the sp^2 framework, side reactions can occur
Amidation	Preserve the sp^2 framework, well-established chemistry, stable	Functionalization only at the edge, harsh reaction condition, hydrolysis can occur
Ring opening of epoxide	Simple, mild condition, basal-plane functionalization	Disrupt the sp^2 framework, less stable
Cyclization	Stable, preserve the sp^2 framework	Harsh reaction conditions (phosphoric acid), multistep reaction
Esterification	Preserve the sp^2 framework, strong	Harsh reaction condition ($SOCl_2$ activation), less stable (hydrolysis), functionalization only at the edge
Nitrene chemistry	Simple, basal-plane functionalization	Harsh reaction conditions (180 °C), less stable
Etherification	Stable, basal-plane functionalization	Harsh reaction condition, disrupt the sp^2 framework

2.6. References

1. A. Borenstein, O. Hanna, R. Attias, S. Luski, T. Brousse and D. Aurbach, *J. Mater. Chem. A*, 2017, **5**, 12653–12672.
2. P. R. Unwin, A. G. Güell and G. Zhang, *Acc. Chem. Res.*, 2016, **49**, 2041–2048.
3. A. Kasprzak, K. Fateyeva, M. Bystrzejewski, W. Kaszuwara, M. Fronczak, M. K. Stawinska and M. Poplawska, *Dalton Trans.*, 2018, **47**, 11190–11202.
4. T. J. M. Fraga, M. N. Carvalho, M. G. Ghislandi, M. A. D. M. Sobrinho, T. J. M. Fraga, M. N. Carvalho, M. G. Ghislandi and M. A. D. M. Sobrinho, *Brazilian J. Chem. Eng.*, 2019, **36**, 1–31.
5. M. N. Tchoul, W. T. Ford, G. Lolli, D. E. Resasco and S. Arepalli, *Chem. Mater.*, 2007, **19**, 5765–5772.
6. C. Li, X. Chen, L. Shen and N. Bao, *ACS Omega*, 2020, **5**, 3397–3404.
7. E. Lam and J. H. T. Luong, *ACS Catal.*, 2014, **4**, 3393–3410.
8. M. J. Lázaro, S. Ascaso, S. Pérez-Rodríguez, J. C. Calderón, M. E. Gálvez, M. J. Nieto, R. Moliner, A. Boyano, D. Sebastián, C. Alegre, L. Calvillo and V. Celorrio, *C. R. Chim.*, 2015, **18**, 1229–1241.
9. W. J. Liu, H. Jiang and H. Q. Yu, *Energy Environ. Sci.*, 2019, **12**, 1751–1779.
10. C. Hu, Y. Xiao, Y. Zou and L. Dai, *Electrochem. Energ. Rev.*, 2018, **1**, 84–112.
11. M. D. Angione, R. Pilolli, S. Cotrone, M. Magliulo, A. Mallardi, G. Palazzo, L. Sabbatini, D. Fine, A. Dodabalapur, N. Cioffi and L. Torsi, *Mater. Today*, 2011, **14**, 424–433.
12. M. Pan, Z. Yin, K. Liu, X. Du, H. Liu and S. Wang, *Nanomaterials*, 2019, **9**, 1330. DOI:10.3390/nano9091330.
13. E. Kanao, T. Kubo and K. Otsuka, *Bull. Chem. Soc.*, 2020, **93**, 482–489.
14. X. Yang, Y. Wan, Y. Zheng, F. He, Z. Yu, J. Huang, H. Wang, Y. S. Ok, Y. Jiang and B. Gao, *Chem. Eng. J.*, 2019, **366**, 608–621.
15. A. Azari, R. Nabizadeh, S. Nasseri, A. H. Mahvi and A. R. Mesdaghinia, *Chemosphere*, 2020, **250**, 126238.
16. R. Gusain, N. Kumar and S. S. Ray, *Coord. Chem. Rev.*, 2020, **405**, 213111.

17. M. Selvaraj, A. Hai, F. Banat and M. A. Haija, *J. Water Process Eng.*, 2020, **33**, 100996.
18. C. Cha, S. R. Shin, N. Annabi, M. R. Dokmeci and A. Khademhosseini, *ACS Nano*, 2013, **7**, 2891–2897.
19. A. M. Monaco and M. Giugliano, *Beilstein J. Nanotechnol.*, 2014, **5**, 1849–1863.
20. L. S. Porto, D. N. Silva, A. E. F. de Oliveira, A. C. Pereira and K. B. Borges, *Rev. in Anal. Chem*, 2019, **38**. DOI:10.1515/revac-2019-0017.
21. Y. E. Jeun, B. Baek, M. W. Lee and H. S. Ahn, *Chem. Commun.*, 2018, **54**, 10052–10055.
22. M. Starowicz, B. Stypuła and J. Banaś, *Electrochem. Commun.*, 2006, **8**, 227–230.
23. L. Fagiolari and F. Bella, *Energy Environ. Sci.*, 2019, **12**, 3437–3472.
24. X. Zhang, L. Ge, Y. Zhang and J. Wang, *Materials*, 2019, **12**. DOI:10.3390/ma12223759.
25. A. Takakura, K. Beppu, T. Nishihara, A. Fukui, T. Kozeki, T. Namazu, Y. Miyauchi and K. Itami, *Nat. Commun.*, 2019, **10**, 3040.
26. I. M. Alarifi, *J. Mater. Res. Technol.*, 2019, **8**, 4863–4893.
27. S. Zhang, W. Xiao, Y. Zhang, K. Liu, X. Zhang, J. Zhao, Z. Wang, P. Zhang and G. Shao, *J. Mater. Chem. A*, 2018, **6**, 22555–22565.
28. J. Feng and Z. Guo, *Nanoscale Horiz.*, 2019, **4**, 339–364.
29. Y. Qiao, K. Jiang, H. Deng and H. Zhou, *Nat. Catal.*, 2019, **2**, 1035–1044.
30. C. Choi, D. S. Ashby, D. M. Butts, R. H. DeBlock, Q. Wei, J. Lau and B. Dunn, *Nat. Rev. Mater.*, 2020, **5**, 5–19.
31. Y. Zhao, C. Wu, J. Li and L. Guan, *J. Mater. Chem. A*, 2013, **1**, 3856–3859.
32. J. B. Goodenough, *Nat. Electron.*, 2018, **1**, 204–204.
33. J. Drews, R. Wolf, G. Fehrmann and R. Staub, *J. Power Sources*, 1997, **65**, 129–132.
34. J. Qian, L. Liu, J. Yang, S. Li, X. Wang, H. L. Zhuang and Y. Lu, *Nat. Commun.*, 2018, **9**, 4918.
35. C. T. Hsieh, C. T. Pai, Y. F. Chen, P. Y. Yu and R. S. Juang, *Electrochim. Acta*, 2014, **115**, 96–102.

36. J. H. Kim, S. Lee, J. Choi, T. Song and U. Paik, *J. Mater. Chem. A*, 2015, **3**, 20459–20464.
37. M. E. Bhosale, S. Chae, J. Man Kim and J. Y. Choi, *J. Mater. Chem. A.*, 2018, **6**, 19885–19911.
38. D. L. Williams, J. J. Byrne and J. S. Driscoll, *J. Electrochem. Soc.*, 1969, **116**.
39. L. I. U. Mengyun, G. U. Tiantian, Z. Min, W. Kangli, C. Shijie and J. Kai, *Energy Storage Sci. Technol.*, 2018, **7**, 1171.
40. C. Friebe and U. S. Schubert, *Top. Curr. Chem.*, 2017, **375**, 19–19.
41. B. Boateng, Y. Han, C. Zhen, G. Zeng, N. Chen, D. Chen, C. Feng, J. Han, J. Xiong, X. Duan and W. He, *Nano Lett.*, 2020, **20**, 2594–2601.
42. M. Lee, J. Hong, B. Lee, K. Ku, S. Lee, C. B. Park and K. Kang, *Green Chem.*, 2017, **19**, 2980–2985.
43. H. Wang, J. Lin and Z. X. Shen, *Adv. Mater. Dev.*, 2016, **1**, 225–255.
44. T. B. Schon, B. T. McAllister, P. F. Li and D. S. Seferos, *Chem. Soc. Rev.*, 2016, **45**, 6345–6404.
45. D. Shanmukaraj, P. Ranque, H. B. Youcef, T. Rojo, P. Poizot, S. Grugeon, S. Laruelle and D. Guyomard, *J. Electrochem. Soc.*, 2020, **167**, 070530.
46. J. J. Shea and C. Luo, *ACS Appl. Mater. Interfaces*, 2020, **12**, 5361–5380.
47. C. Han, H. Li, R. Shi, T. Zhang, J. Tong, J. Li and B. Li, *J. Mater. Chem. A*, 2019, **7**, 23378–23415.
48. Z. Song and H. Zhou, *Energy Environ. Sci.*, 2013, **6**, 2280–2301.
49. Y. Lu, Q. Zhang, L. Li, Z. Niu and J. Chen, *Chem*, 2018, **4**, 2786–2813.
50. Y. Lu and J. Chen, *Nat. Rev. Chem.*, 2020, **4**, 127–142.
51. V. Georgakilas, M. Otyepka, A. B. Bourlinos, V. Chandra, N. Kim, K. C. Kemp, P. Hobza, R. Zboril and K. S. Kim, *Chem. Rev.*, 2012, **112**, 6156–6214.
52. D. Tuncel, *Nanoscale*, 2011, **3**, 3545–3554.
53. Z. Liu, T. Rios-Carvajal, M. P. Andersson, M. Ceccato, S. L. S. Stipp and T. Hassenkam, *Environ. Sci. Nano*, 2019, **6**, 2281–2291.
54. F. Tournus, S. Latil, M. I. Heggie and J. C. Charlier, *Phys. Rev. B*, 2005, **72**, 075431.

55. Q. Li, M. Horn, Y. Wang, J. MacLeod, N. Motta and J. Liu, *Materials*, 2019, **12**, 703.
56. W. Yuan, Y. Zhang, L. Cheng, H. Wu, L. Zheng and D. Zhao, *J. Mater. Chem. A*, 2016, **4**, 8932–8951.
57. M. Notarianni, J. Liu, K. Vernon and N. Motta, *Beilstein J. Nanotechnol.*, 2016, **7**, 149–196.
58. S. Iqbal, H. Khatoon, A. H. Pandit and S. Ahmad, *Mater. Sci. Energy Technol.*, 2019, **2**, 417–428.
59. C. A. Dyke and J. M. Tour, *J. Phys. Chem. A*, 2004, **108**, 11151–11159.
60. G. Speranza, *J. Carbon Res.*, 2019, **5**, 84.
61. I. A. Vacchi, C. Ménard-Moyon and A. Bianco, *Phys. Sci. Rev.*, 2017, **2**, 035037. DOI:10.1515/psr-2016-0103.
62. A. Bakandritsos, P. Jakubec, M. Pykal and M. Otyepka, *FlatChem.*, 2019, **13**, 25–33.
63. A. Jaffe, A. S. Valdes and H. I. Karunadasa, *Chem. Mater.*, 2015, **27**, 3568–3571.
64. N. A. Elessawy, J. E. Nady, W. Wazeer and A. B. Kashyout, *Sci. Rep.*, 2019, **9**, 1129.
65. R. Vellacheri, A. Al-Haddad, H. Zhao, W. Wang, C. Wang and Y. Lei, *Nano Energy*, 2014, **8**, 231–237.
66. F. Zhang, T. Zhang, X. Yang, L. Zhang, K. Leng, Y. Huang and Y. Chen, *Energy Environ. Sci.*, 2013, **6**, 1623–1632.
67. L. L. Zhang, R. Zhou and X. S. Zhao, *J. Mater. Chem.*, 2010, **20**, 5983–5992.
68. H. Ji, X. Zhao, Z. Qiao, J. Jung, Y. Zhu, Y. Lu, L. L. Zhang, A. H. MacDonald and R. S. Ruoff, *Nat. Commun.*, 2014, **5**, 3317.
69. Y. M. Volfkovich, A. A. Mikhailin, D. A. Bograchev, V. E. Sosenkin and V. S. Bagotsky, Recent Trend Electrochem. *Sci. Technol*., 2012, **159**.
70. S. Seo, M. Min, S. M. Lee and H. Lee, *Nat. Commun.*, 2013, **4**, 1920.
71. M. M. Sk and C. Y. Yue, *RSC Adv.*, 2014, **4**, 19908–19915.
72. Q. Wu, Y. Sun, H. Bai and G. Shi, *Phys. Chem. Chem. Phys.*, 2011, **13**, 11193–11198.
73. J. Shi, Z. Zhao, J. Wu, Y. Yu, Z. Peng, B. Li, Y. Liu, H. Kang and Z. Liu, *ACS Sustain. Chem. Eng.*, 2018, **6**, 4729–4738.

74. W. Ai, W. Zhou, Z. Du, Y. Du, H. Zhang, X. Jia, L. Xie, M. Yi, T. Yu and W. Huang, *J. Mater. Chem.*, 2012, **22**, 23439–23446.
75. W. Ai, X. Cao, Z. Sun, J. Jiang, Z. Du, L. Xie, Y. Wang, X. Wang, H. Zhang, W. Huang and T. Yu, *J. Mater. Chem. A*, 2014, **2**, 12924–12930.
76. W. S. V. Lee, M. Leng, M. Li, X. L. Huang and J. M. Xue, *Nano Energy*, 2015, **12**, 250–257.
77. D. M. El-Gendy, N. A. A. Ghany, E. E. F. El Sherbini and N. K. Allam, *Sci. Rep.*, 2017, **7**, 43104.
78. Y. Qin, J. Li, X. Jin, S. Jiao, Y. Chen, W. Cai and R. Cao, *Ceram. Int.*, 2020, **46**, 15379–15384.
79. L. Hou, Z. Hu, H. Wu, X. Wang, Y. Xie, S. Li, F. Ma and C. Zhu, *Dalton Trans.*, 2019, **48**, 9234–9242.
80. J. Kim, J. H. Kim, K. Ariga, *Joul*, 2017, **1**, 739-768.
81. D. Majumdar, *Innovative Energy Res.*, 2016, **5**, 1–9.
82. Q. Zhao, J. Chen, F. Luo, L. Shen, Y. Wang, K. Wu and M. Lu, *J. Appl. Polym. Sci.*, 2017, **134**, 44808. DOI:10.1002/app.44808.
83. Y. Teng, S. Li, C. Xue, H. Zhang, L. Zhu and Y. Tang, 2017, **134**. https://doi.org/10.1155/2020/8730852
84. X. Liu, Y. Zheng and X. Wang, *Chem. A. Eur. J.*, 2015, **21**, 10408–10415.
85. R. Li, Y. Yang, D. Wu, K. Li, Y. Qin, Y. Tao and Y. Kong, *Chem. Commun.*, 2019, **55**, 1738–1741.
86. M. Wang, R. Jamal, Y. Wang, L. Yang, F. Liu and T. Abdiryim, *Nanoscale Res Lett*, 2015, **10**, 370.
87. Z. F. Li, H. Zhang, Q. Liu, Y. Liu, L. Stanciu and J. Xie, *Carbon*, 2014, **71**, 257–267.
88. Y. Zou, R. Liu, W. Zhong and W. Yang, *J. Mater. Chem. A*, 2018, **6**, 8568–8578.
89. C. Wang, Y. Yang, R. Li, D. Wu, Y. Qin and Y. Kong, *Chem. Commun.*, 2020, **56**, 4003–4006.
90. A. Roy, S. Dhibar, S. Kundu and S. Malik, *RSC Adv.*, 2019, **9**, 24646–24653.

91. F. B. Ajdari, E. Kowsari, A. Ehsani, L. Chepyga, M. Schirowski, S. Jäger, O. Kasian, F. Hauke and T. Ameri, *Appl. Surf. Sci.*, 2018, **459**, 874–883.
92. Z. Liu, H. Zhou, Z. Huang, W. Wang, F. Zeng and Y. Kuang, *J. Mater. Chem. A*, 2013, **1**, 3454–3462.
93. A. Mohammadi, S. J. Peighambardoust, A. A. Entezami and N. Arsalani, *J. Mater. Sci. Mater. Electron*, 2017, **28**, 5776–5787.
94. R. Khan and Y. Nishina, *J. Mater. Chem. A*, 2020, **8**, 13718-13724.
95. S. Witomska, Z. Liu, W. Czepa, A. Aliprandi, D. Pakulski, P. Pawluć, A. Ciesielski and P. Samorì, *J. Am. Chem. Soc.*, 2019, **141**, 482–487.
96. S. B. Sertkol, B. Esat, A. A. Momchilov, M. B. Yılmaz and M. Sertkol, *Carbon*, 2017, **116**, 154–166.
97. Z. Du, W. Ai, L. Xie and W. Huang, *J. Mater. Chem. A*, 2014, **2**, 9164–9168.
98. Y. Wang, X. Li, L. Chen, Z. Xiong, J. Feng, L. Zhao, Z. Wang and Y. Zhao, *Carbon*, 2019, **155**, 445–452.
99. C. Lu, G. Pan, Q. Huang, H. Wu, W. Sun, Z. Wang and K. Sun, *J. Mater. Chem. A*, 2019, **7**, 4438–4445.
100. Y. Song, Y. Hu, Y. Sha, H. Rong, H. Wen, H. J. Liu and Q. Liu, *Ionics*, 2019, **25**, 2987–2995.
101. Y. Song, Y. Gao, H. Rong, H. Wen, Y. Sha, H. Zhang, H. J. Liu and Q. Liu, *Sustain. Energy Fuels*, 2018, **2**, 803–810.
102. A. Maio, R. Fucarino, R. Khatibi, S. Rosselli, M. Bruno and R. Scaffaro, *Compos. Sci. Technol.*, 2015, **119**, 131–137.
103. J. L. Suter, R. C. Sinclair and P. V. Coveney, *Adv. Mater.*, 2020, **32**, 2003213.
104. C. H. Chang, A. Manthiram, ACS. *Energy. Lett.*, 2018. **3**, 72-7.
105. J. K. Kim, G. Cheruvally, J. H. Ahn, Y. G. Seo, D. Choi, S.-H. Lee and C. Song, *J. Ind. Eng. Chem.*, 2008, **14**, 371–376.
106. Y. Li, Z. Jian, M. Lang, C. Zhang and X. Huang, *ACS Appl. Mater. Interfaces*, 2016, **8**, 17352–17359.

Chapter: 3

A Simple and Robust Functionalization of Graphene for Advanced Energy Devices

Abstract: Efficient and selective methods for graphene functionalization are needed because they allow tuning of the graphene surface and electronic properties. To date, graphene has been functionalized using ionic bonds, π–π interactions, and covalent bonds. Graphene derivatives based on these methods have been used in various applications, but a new functionalization strategy that improves the properties of graphene is still needed. Herein, a new concept for graphene functionalization using halogenated graphene has been developed, in which brominated graphene is successfully functionalized by heteroatom-containing molecules to form onium bonds, such as pyridinium or ammonium. The counter ion, bromide, is replaced with other anions, such as sulfate, by treating with sulfuric acid, while retaining the molecules, which demonstrates the durable properties of onium bonding. To emphasize the advantages of this strategy for graphene functionalization, the performance for energy-related applications, such as biofuel cells, SCs, and LIBs, is evaluated after introducing redox-active moieties onto graphene through onium bonding. This new graphene functionalization concept will provide a new approach to the design of tailor-made materials with targeted functions.

3.1. Introduction

Two-dimensional nanocarbons, as represented by graphene, have been the subject of active research owing to their outstanding physical properties, such as toughness,[1,2] high specific surface area,[3,4] and high electrical[5–7] and thermal conductivities.[8,9] As the basic physical properties of graphene and its analogues have mostly been elucidated by intense research over more than 15 years, the development of functionalization methods to further enhance their physical/chemical properties is in great demand. To date, elemental doping,[10,11] complexing with metal nanoparticles,[12,13] complexing with polymers,[14] and chemical modification with organic molecules[15] have been studied to improve the function of carbon materials. Among these methods, this study focuses on chemical modification with organic molecules, which is expected to allow fine control of the function and physical properties at atomic or molecular levels. The organic modification of nanocarbons can be further classified into covalent, noncovalent, and ionic bond formations, each of which has advantages and

disadvantages (Table 1). Covalent bonds are durable and can adequately reflect the function of the molecules introduced.[16]

However, strict and severe reaction conditions are required for their formation, and the carbon atom forming the covalent bond in the basal plane is converted to sp^3 hybridization, which can diminish the physical properties expected of an sp^2 carbon framework.[17-23] Noncovalent interactions, such as π– π interactions or hydrophobic interactions between a carbon material and molecule, are advantageous because they do not destroy the sp^2 carbon framework. However, as these interactions are weak, molecule dissociation occurs readily.[24] Ionic bonds can be formed using a negatively charged functional group on carbon (hydroxyl or carboxyl group) and a positively charged molecule. This method is simple and forms a robust bond under mild conditions, but the ionic bond is fragile toward different environments, such as acid or base.[25]

Table 1: Comparison and functionalization method of graphene

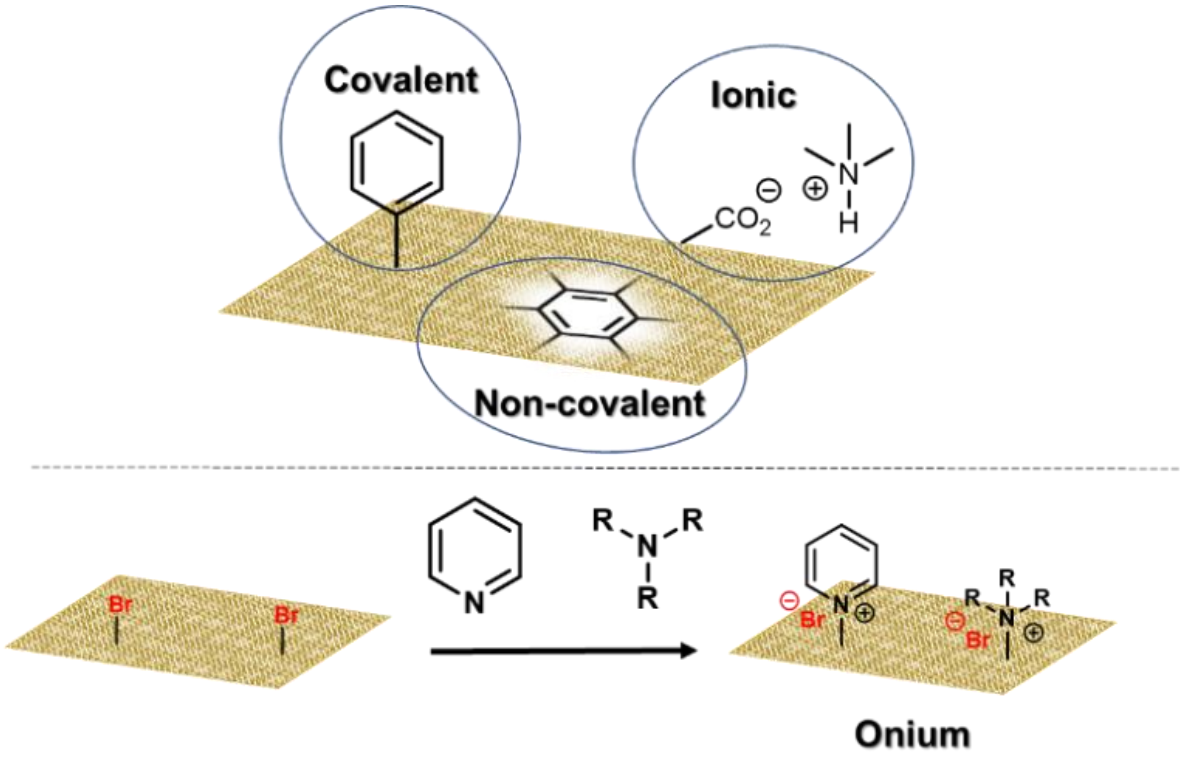

Method	Advantages	Disadvantage	Ref.
Covalent bond	Strong	Severe reaction conditions	[26]
Noncovalent bond	Mild, simple	Fragile, limited to hydrophobic molecules	[27]
Ionic bond	Mild, simple	Fragile, limited to hydrophilic molecules	[28]
Onium bond	Strong, simple		This work

In particular, the stability of ionic interactions is of concern when applied to bioapplications and batteries in which other ionic species are present.[29] In this study, we have developed a new chemical modification method for graphene to compensate for these drawbacks. This method involves the formation of the strong interaction, similar to a covalent bond, without generating any byproduct using a simple procedure similar to ionic bond formation. Specifically, we aimed to construct quaternary ammonium or phosphonium species on graphene using halogenated graphene and amines or phosphines. Such quaternary species can be synthesized simply by heating and mixing halides with the corresponding tertiary nitrogen or phosphorus species.[30] Unlike amines and phosphines, ammonium and phosphonium species are stable toward electrophiles, nucleophiles, oxidants, acids, and bases. Owing to their stability and ionic character, we have referred to such species formed on graphene as "onium" species herein. We succeeded in introducing various organic molecules onto graphene through onium formation. Furthermore, to clarify the usefulness of this method, the performance of the resulting onium–graphene hybrids as functional electrodes in energy devices (LIBs, biofuel cell, and SCs) is disclosed.

3.2. Results and discussion

Brominated graphene (**Br-G**) was prepared using the hydrothermal method,[31] and then subsequently functionalized with different nitrogen-containing compounds, such as pyridine (Py), diisopropylamine (iPr_2NH), and trimethylamine (Et_3N). To emphasize the advantages of this method, a redox-active quinone molecule bearing a pyridine moiety, 5,8-

isoquinolinedione (IQD), was also used to functionalize graphene. To confirm the formation of a robust carbon–nitrogen bond between graphene and the nitrogen-containing molecules, the products were washed with dilute H_2SO_4 (Figure 1).

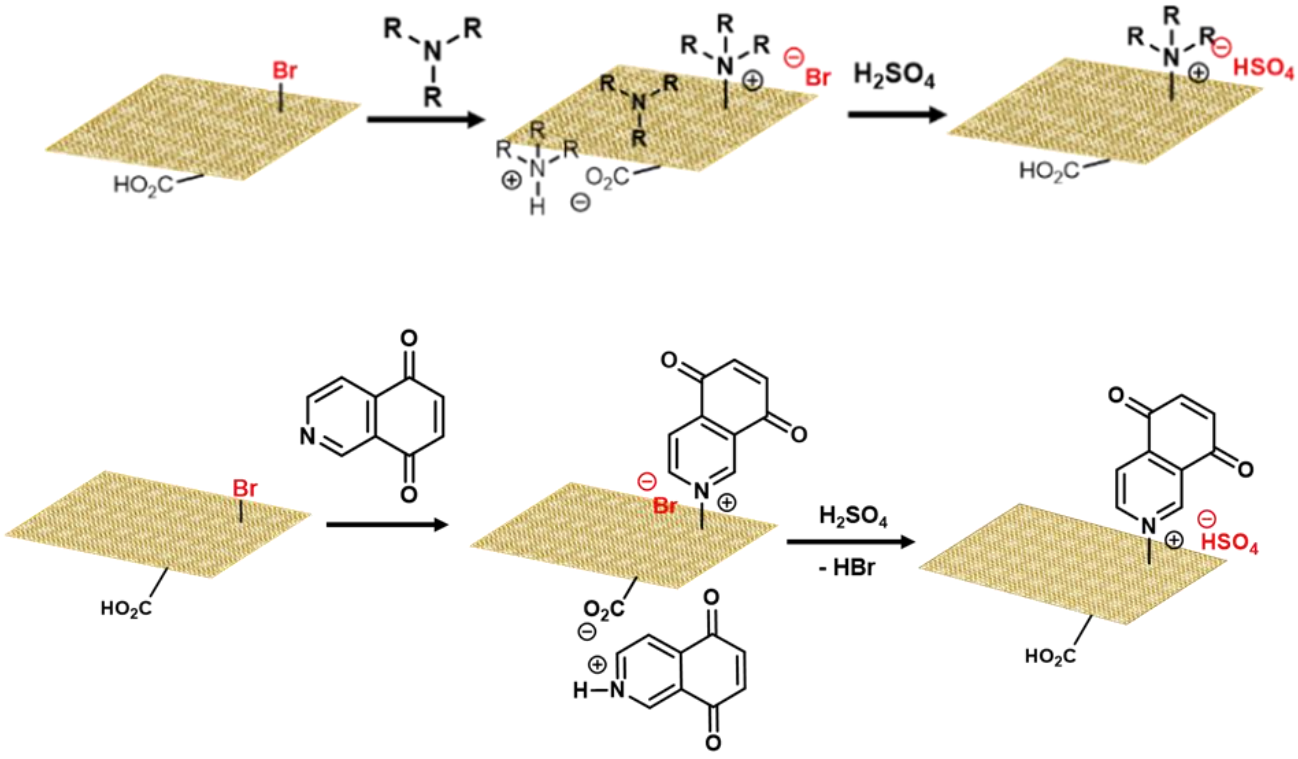

Figure 1: Preparation of onium–graphene hybrid

The prepared materials were characterized by XPS, FT-IR, energy-dispersive X-ray spectroscopy (EDS), and Raman spectroscopy. For comparison, we also prepared chlorinated graphene (**Cl-G**) and iodinated graphene (**I-G**), to investigate the formation of onium bonds. XPS analysis showed that **Br-G** predominantly formed onium bonds compared with other halogenated graphenes.

Initially, the elemental composition was analyzed by wide-scan XPS analysis. The wide-scan XPS spectra of **Br-G** contained a C 1s peak at 284.5 eV, O 1s peak at 532.5 eV, and Br 3p and Br 3d peaks at 184.1 eV and 69.9 eV, respectively (Figure 2i). In contrast, wide-scan XPS analysis of the pyridine-, diisopropylamine-, trimethylamine-, and 5,8-

isoquinolinedione-functionalized graphenes (**Py-G**, **iPr$_2$NH-G**, **Et$_3$N-G**, and **IQD-G**, respectively) showed N 1s, S 2s, and S 2p$_{1/2}$ peaks, but no Br 3p and Br 3d peaks, suggesting successful ammonium or pyridinium formation on graphene (Figure 2 (ii-v)).[32] The results of elemental analysis by XPS are summarized in Table 2.

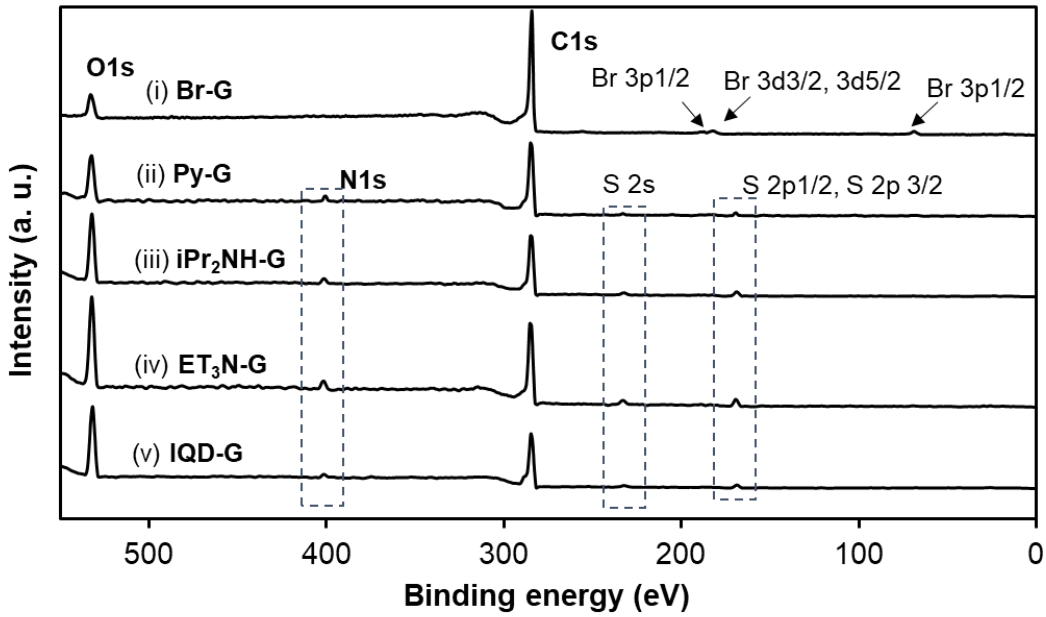

Figure 2: Wide scan XPS spectra of, (i) **Br-G**, (ii) **Py-G**, (iii) **iPr$_2$NH-G**, (iv) **Et$_3$N-G**, and (v) **IQD-G**

Table 2: Elemental analysis by XPS

Sample	**Elemental analysis (at%)**				
	C	O	N	S	Br
Br-G	89.0	8.4	-	-	2.5
Py-G	70.7	24.4	2.0	2.7	-
iPr$_2$NH-G	72.1	22.2	2.7	2.8	-
Et$_3$N-G	72.6	20.2	3.1	3.3	-
IQD-G	70.3	24.6	2.5	2.4	-

Next, to gain further insight into the chemical state of each element, high-resolution XPS analysis was performed. **Br-G** showed a peak at 69.9 eV in the Br 3d region, which suggested the formation of a covalent C–Br bond (Figure 3).[33]

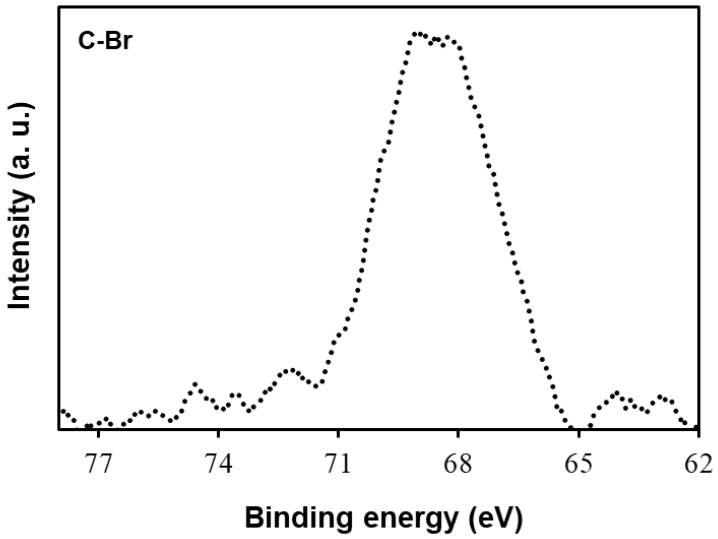

Figure 3: High-resolution XPS spectra at Br 3p1/2 region of **Br-G** to confirm the presence of the C-Br bond

After washing with H_2SO_4, all functionalized graphene products, **Py-G**, **iPr$_2$NH-G**, **Et$_3$N-G**, and **IQD-G**, showed only ionic nitrogen in the N 1s region (400–402 eV, Figures 4ai–4aiv), which supported the formation of onium species on graphene.[34] Before washing with H_2SO_4, a neutral C–N bond was also observed in the N 1s XPS spectra of **IQD-G** at 399 eV (Figure 4av), which was derived from the nitrogen-containing molecule physically adsorbed on the graphene surface. The functional groups on each graphene were analyzed by FT-IR spectroscopy (Figure 4b). A peak at 570 cm^{-1} was attributed to a C–Br bond (Figure 4bi).[35] After onium bond formation, new peaks appeared at 1200–1300, 1340, 1633, and 2900 cm^{-1}, which were associated with C–N, S=O, C=O, and C–H bonds, respectively,[36] while the C–Br bond peak disappeared (Figures 4bii–4bv). These observations indicated the successful substitution of Br by nitrogen-containing molecules and sulfonate ions.

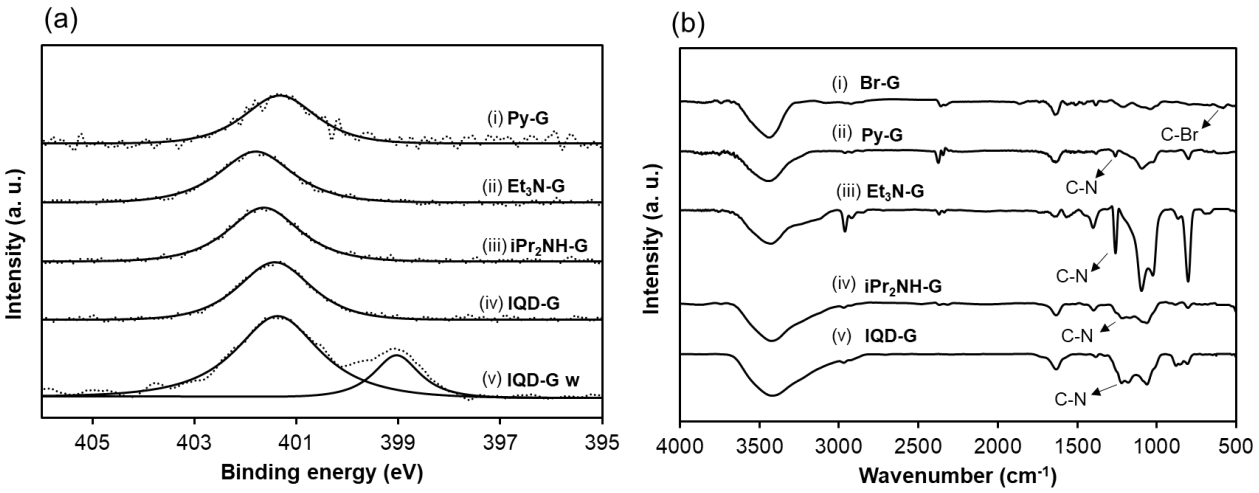

Figure 4: (a) N1s XPS raw data (dotted line) and deconvolution (continuous line) for (i) **Py-G**, (ii) **Et$_3$N-G**, (iii) **iPr$_2$NH-G**, (vi) **IQD-G**, and (v) **IQD-G** without acid washing. (b) FT-IR spectra of (i) **Br-G**, (ii) **Py-G**, (iii) **iPr$_2$NH-G**, (vi) **Et$_3$N-G**, and (v) **IQD-G**

To obtain more information on the structure of the functionalized graphene, Raman spectra were obtained. Two major peaks corresponding to the defect (D-band, at 1340 cm^{-1}) and graphene (G-band, at 1570 cm^{-1}) domains were found in all Raman spectra (Figure 5 (i-v)). The intensity ratio of these bands (I_D/I_G) can be used to indicate the density of defects present in the graphene framework. The I_D/I_G ratio for **Br-G** was 1.5, and the other functionalized graphenes, **Py-G**, **iPr$_2$NH-G**, **Et$_3$N-G**, and **IQD-G**, showed similar values. This suggested that graphene had been selective functionalized by the nitrogen-containing molecules.

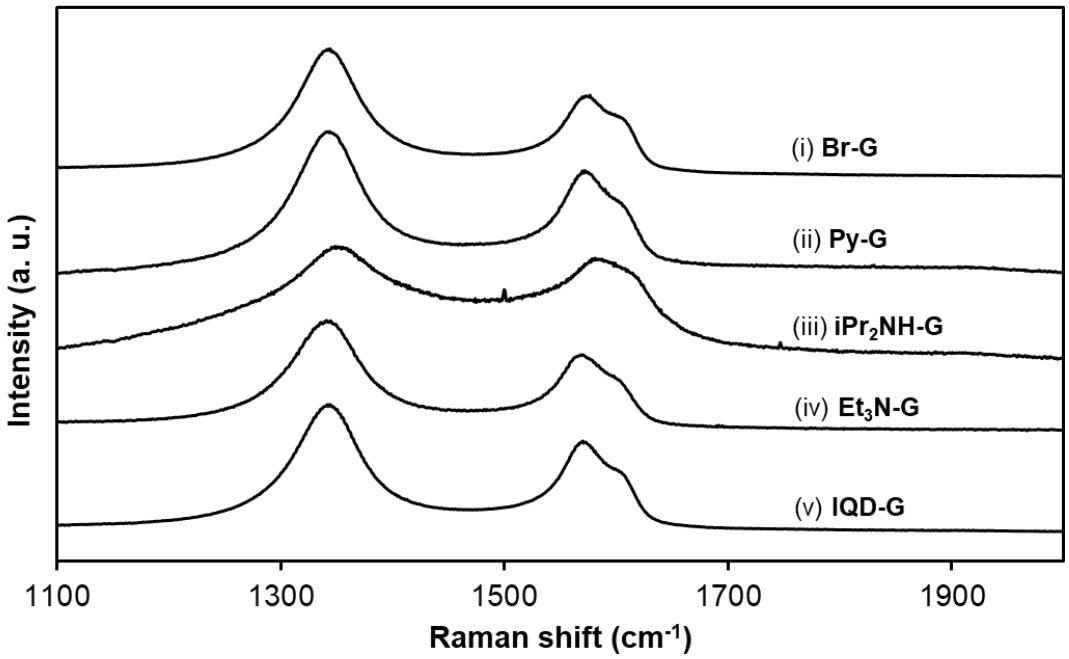

Figure 5: Raman analysis of (i) **Br-G**, (ii) **Py-G**, (iii) **iPr$_2$NH-G**, (iv) **Et$_3$N-G**, and (v) **IQD-G**

For comparison, we also prepared chlorinated graphene (**Cl-G**) and iodinated graphene (**I-G**) and investigated the formation of onium bond. The formation of halogenated graphene was confirmed by EDS analysis (Figure 6 (a-c)). **Cl-G** contains 0.5% chlorine, **Br-G** contains 1.8% bromine and **I-G** contains 1.5% iodine (Table 3). The presence of halogen atom in EDS spectra confirmed the synthesis of halogenated graphene. The formation of onium bond was further confirmed by XPS analysis. The wide scan XPS spectra showed the presence of nitrogen atom, confirming the formation of onium bonding (Figure 7). The amount of nitrogen in **Cl-G**, **Br-G**, and **I-G** was 0.8%, 2.5% and 0.7% respectively (Table 4). The high-resolution N 1s XPS spectra showed that **Br-G** predominantly formed the onium bond as compared to other halogenated graphene (Figure 8).

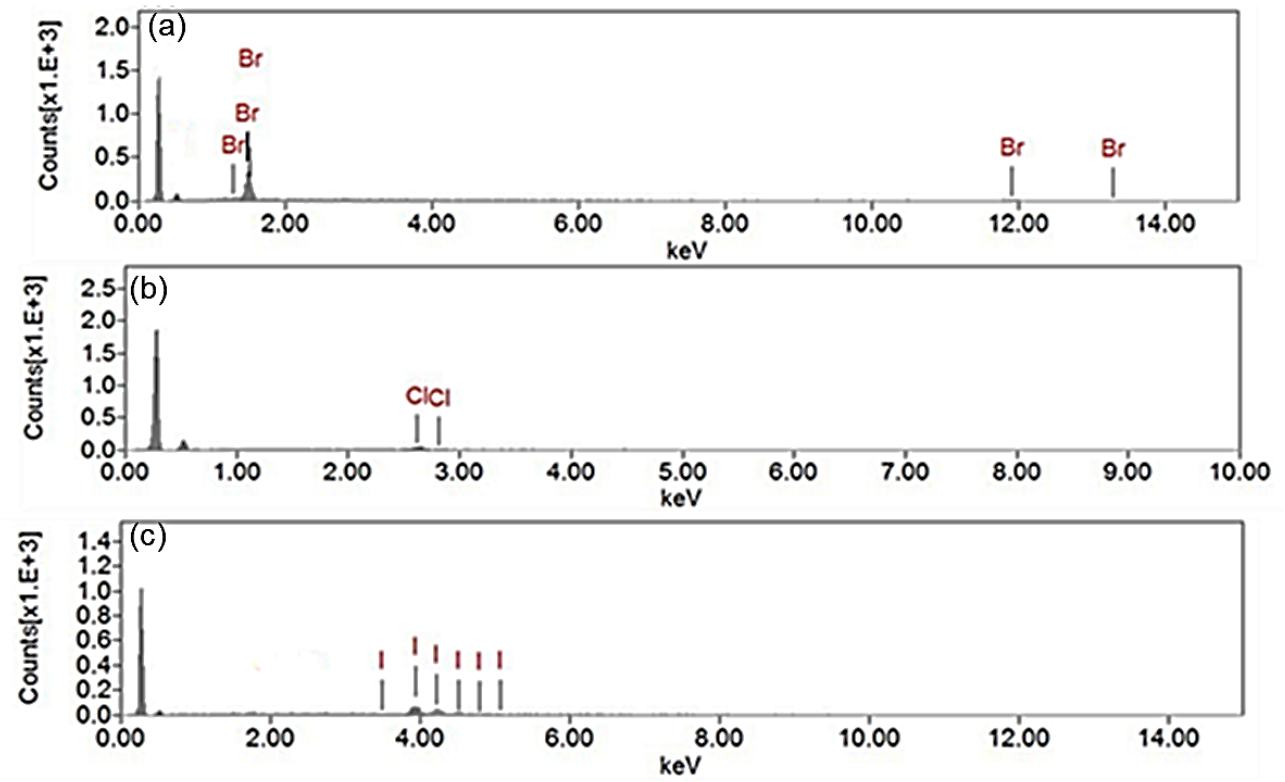

Figure 6: EDS analysis of (a) brominated graphene (**Br-G**), (b) chlorinated graphene (**Cl-G**), and (c) Iodinated graphene (**I-G**)

Table 3: Quantitative comparison of detected elements from EDS analysis of halogenated graphene

Sample	**Elemental analysis (at %)**				
	C	O	Cl	Br	I
Cl-G	84.8	14.7	0.5	-	-
Br-G	89.1	9.3	-	1.8	-
I-G	89.9	8.6	-	-	1.5

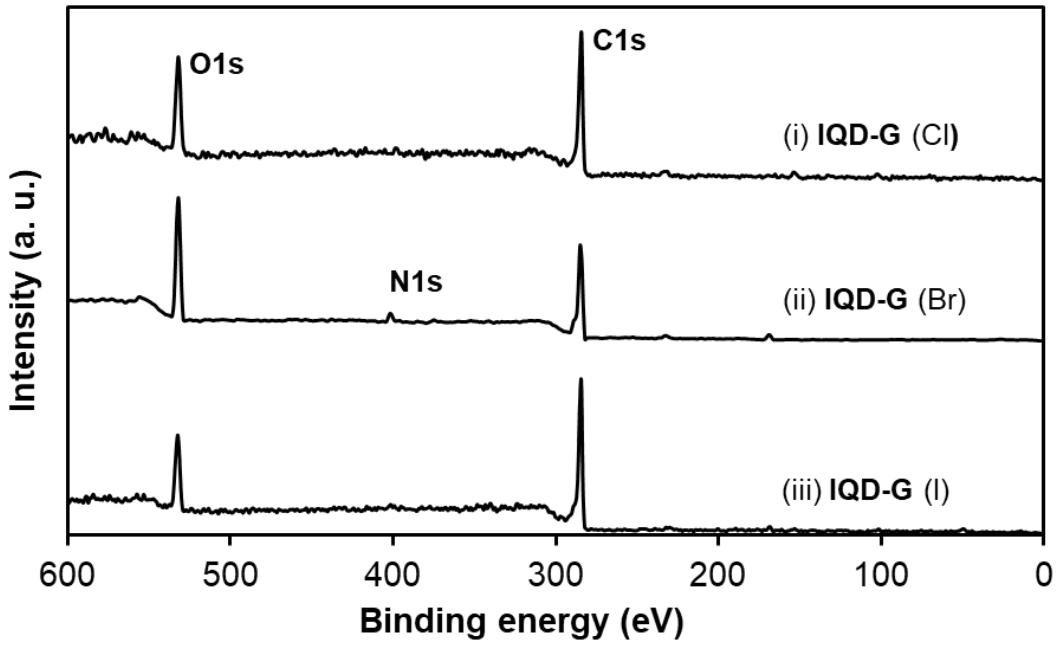

Figure 7: Wide scan XPS spectra of **IQD-G** prepared from, (i) **IQD-G (Cl)**, (ii) **IQD-G (Br)**, and (iii) **IQD-G (I)**

Table 4: Elemental analysis by XPS analysis

Sample	**Elemental analysis (at %)**						
	C	O	N	S	Cl	Br	I
IQD-G (Cl)	77.6	20.5	0.8	0.7	0.3	-	-
IQD-G (Br)	70.3	24.6	2.5	2.4	-	-	-
IQD-G (I)	81.2	17.4	0.7	0.6	-	-	0.5

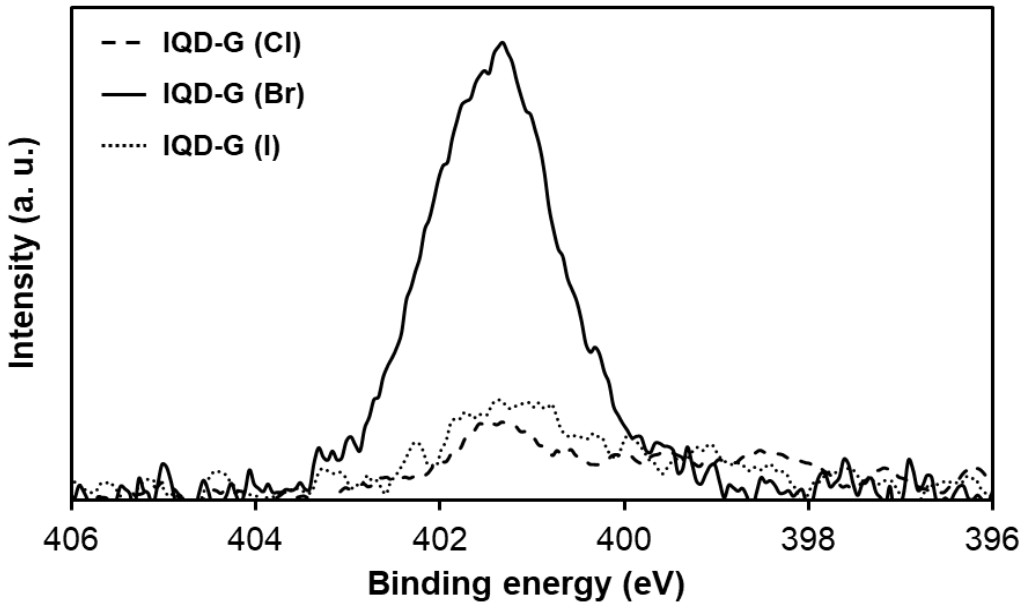

Figure 8: High-resolution XPS spectra at N 1s region of **IQD-G** prepared from, (i) **IQD-G (Cl),** (ii) **IQD-G (Br)**, and (iii) **IQD-G (I)**

Functionalized graphenes are expected to work as electrode.[37] To show the proof of the concept of our strategy, graphene functionalized with a redox-active molecule, **IQD-G**, was evaluated as an electrode in biofuel cell, SCs, and LIBs applications mainly in the viewpoint of stability (e.g., leaching of IQD) in the following sections.

3.2.1. Biofuel cell application

Initially, the performance of the **IQD-G** electrode was evaluated in a biofuel cell. Power curves were obtained by scanning from the open-circuit voltage (OCV) of the cell to 0 V at a constant scan rate of 1 mV s^{-1} in Phosphate buffer saline (PBS) solution containing 1 mol L^{-1} D-glucose. As a result, a power density of 47.7 μW cm^{-2} was obtained (Figure 9). After 2 h, the power density of the **IQD-G** electrode had decreased to 50%. This decrease was due to the decomposition of IQD. In contrast, the power density of a biofuel cell composed of an electrode prepared by simply mixing IQD and graphene was reduced to 20%

(Figure 10). Therefore, **IQD-G** showed better stability and improved performance compared with a just mixed sample of IQD, and graphene (IQD-graphene mixture), confirming the usefulness of onium bond formation. Furthermore, the non-catalytic cyclic voltammograme (CV) of **IQD-G** was measured at different scan rates (Figure 11a). The current was proportionally increased as the scan rate increased. The **IQD-G** showed narrower Δ Ep than the electrode prepared by just mixing of graphene and IQD (Figure 11b), suggesting a successful electron transfer of **IQD-G**. Further, the effect of flavin adenine dinucleotide-glucose dehydrogenase (FAD-GDH) and glucose on the biofuel cell performance of **IQD-D** was investigated (Figure 12a and 12b).

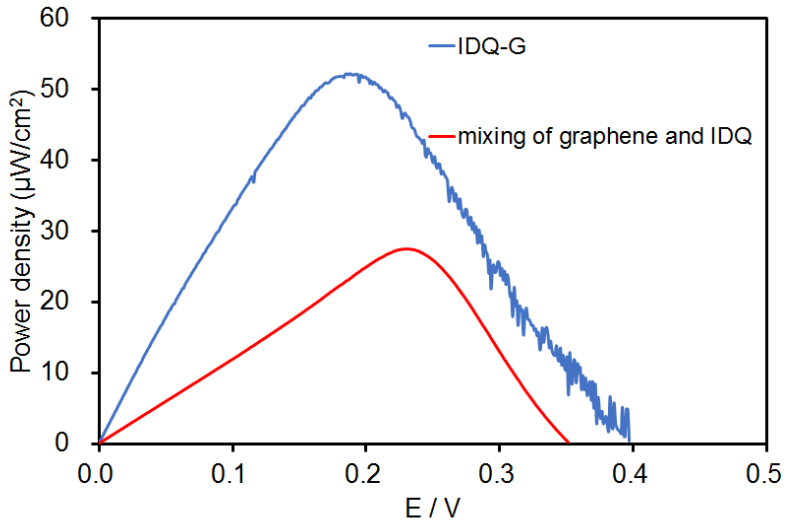

Figure 9: Power density vs voltage

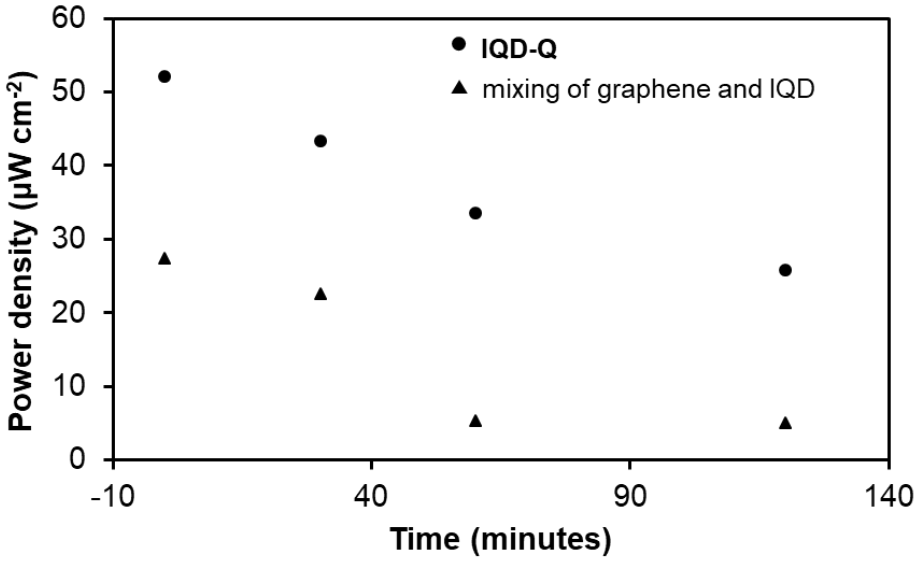

Figure 10: The power density of biofuel cells derived from (i) **IQD-G**, and (ii) a simple mixture of IQD with graphene after different time intervals in PBS–glucose solution (1 M) at a scan rate of 1 mV s^{-1}

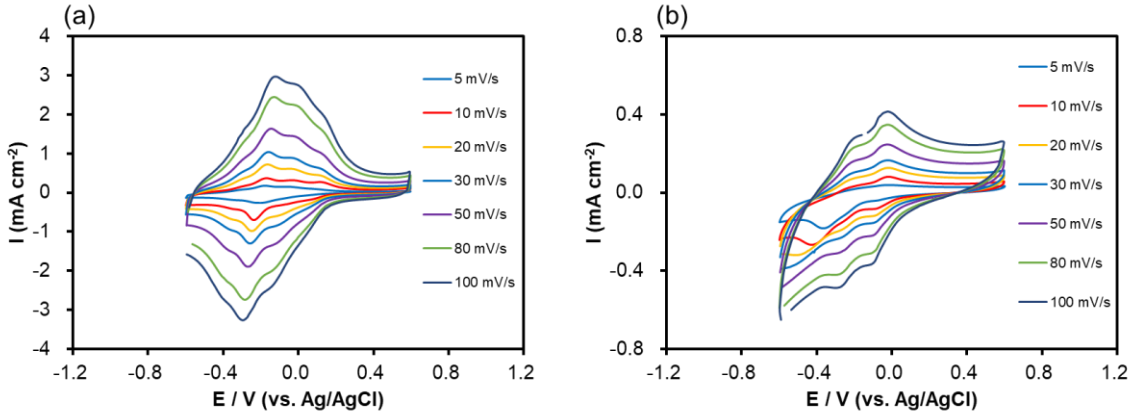

Figure 11: Cyclic voltammogram of (a) **IQD-G**, and (b) mixing of graphene and IQD without glucose at different scan rate using PBS (0.5 M) as electrolyte

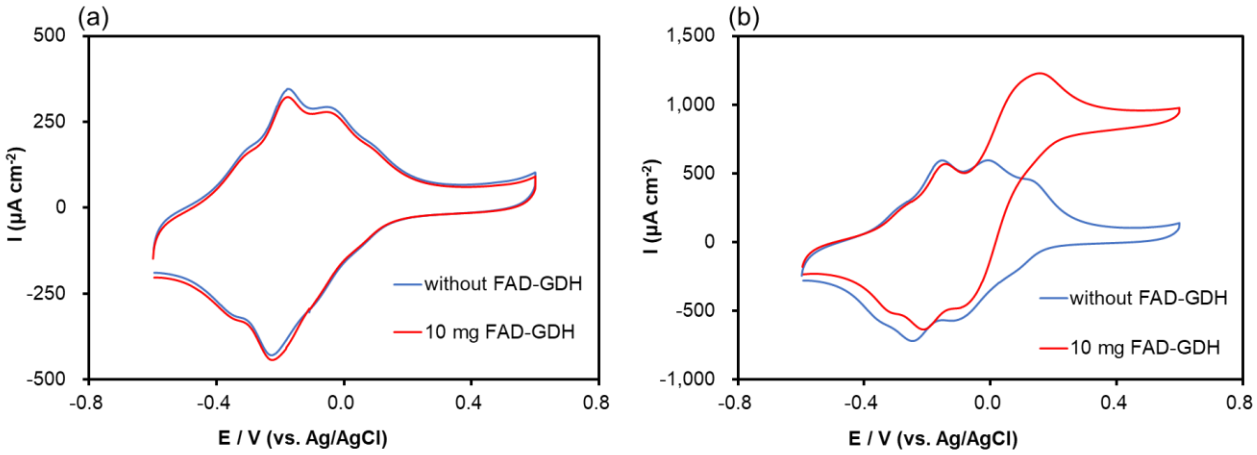

Figure 12: Cyclic voltammogram of **IQD-G** electrode. (a) without glucose, and (b) with 0.1 M glucose

3.2.2. Supercapacitor application

Next, symmetric electrochemical cells were assembled using **IQD-G** as electrodes with an electrolyte of 0.5 M Na_2SO_4 to evaluate the SCs performance. The rate capability was measured by increasing the current density from 1 to 20 A g^{-1}. The rate capabilities of the **IQD-G** composite and just mixing of IQD–graphene was similar (Figure 13a). The capacity value was calculated after five cycles during each measurement. The cycling stability of the fabricated symmetric cells was evaluated, with the capacitance of **IQD-G** electrodes maintained without any noticeable fading after 10,000 cycles (Figure 13b). Furthermore, the retention was 100% after 10,000 cycles. For comparison, the cycling stability of the just mixing IQD–graphene was measured, showing that the capacity decreased to 120 F g^{-1} after 3,000 cycles. This decrease in capacity was due to the leaching of IQD from the graphene surface after a certain time in the aqueous electrolyte. In contrast, the onium bond between IQD and graphene was strong and stable in the aqueous electrolyte. These results were among the best values reported for small conjugated carbonyl compounds functionalized on carbon materials (Table 5).

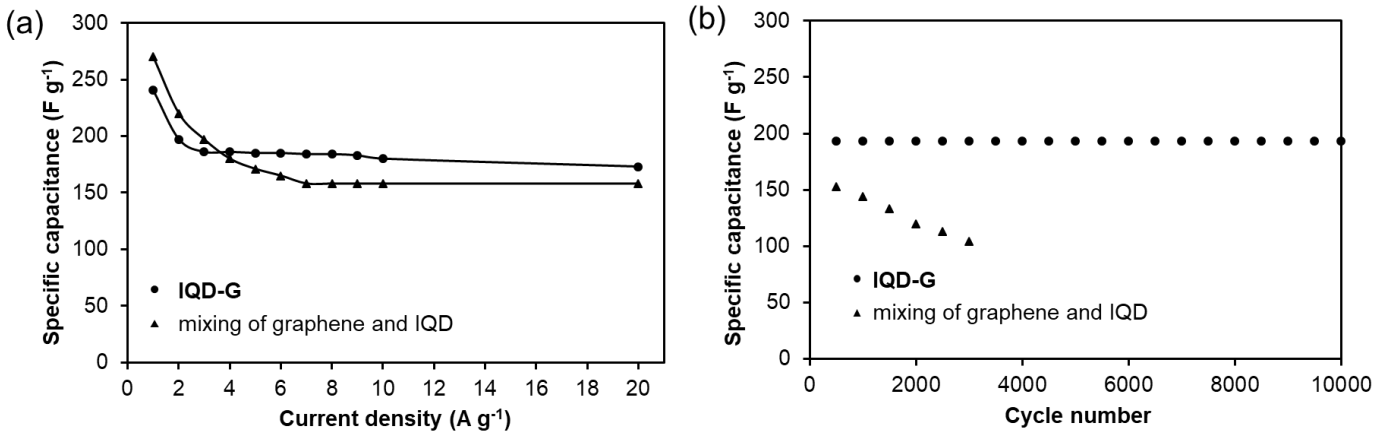

Figure 13: (a) Galvanostatic charge-discharge curve of **IQD-G** at different current densities; (b) cycling stability test at a current density of 20 A g^{-1}

Next, the electrochemical performance was evaluated by CV. The redox peak for **IQD-G**, and just mixing sample was observed at different potential. Further, the electrochemical performance of **IQD-G** was higher than that of just mixing sample (Figure 14a). When the CV curves of **GO 3** were acquired using different scan rates, all the curves maintained their shapes (Figure 14b).

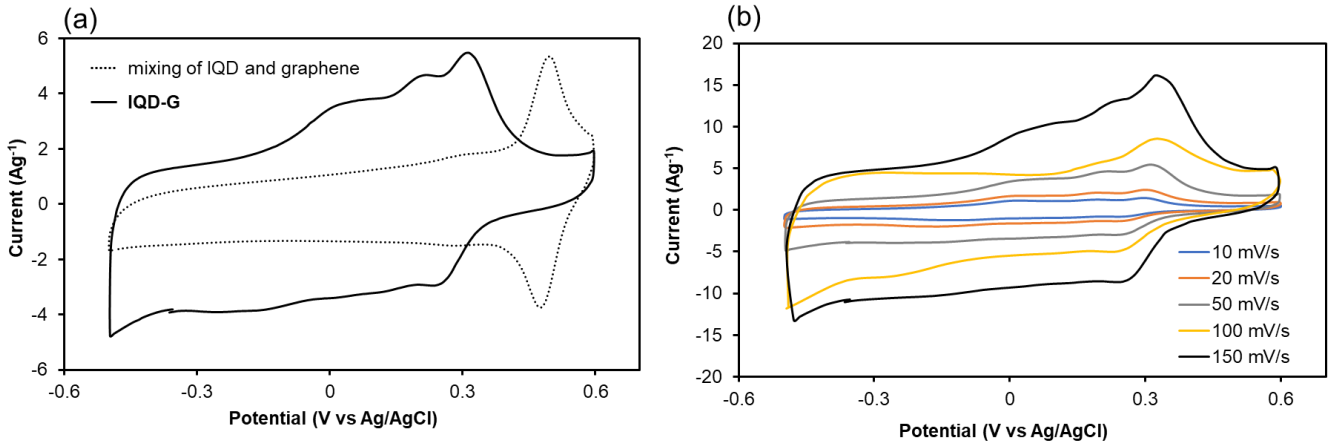

Figure 14: The electrochemical evaluation in three-electrode setup for SCs in Na_2SO_4 (0.5M) aqueous electrolyte: (a) CV curve of **IQD-G**, and just mixing of IQD, and graphene at a scan rate of 50 mVs^{-1}, (b) CV curve of **IQD-G** at different scan rates (10 mVs^{-1} to 150 mVS^{-1})

Table 5: Comparison of **IQD-G** with the published data for quinone-containing carbon-based electrodes

Electrode material	Electrolyte	Retention (%) (cycle number)	Current density/scan rate	Ref.
TBHQ@gr	1 M H_2SO_4	92 (800)	1 A g^{-1}	[38]
AQ@CFs	1 M H_2SO_4	89 (5000)	20 A g^{-1}	[39]
AQ@gr	1 M HCl	77 (10 000)	10 A g^{-1}	[40]
AT@AC	1 M H_2SO_4	90 (1000)	200 mA g^{-1}	[41]
HQ@gr	1 M H_2SO_4	86 (10 000)	10 A g^{-1}	[42]
PQ@OLC	1 M H_2SO_4	90 (10 000)	200 mV s^{-1}	[43]
NQ@OLC	1 M H_2SO_4	92 (10 000)	50 mV s^{-1}	[44]
PQ@AC	1M KOH	80 (1000)	2 A g^{-1}	[45]
HQ@AC	1 M H_2SO_4/HQ	65 (4000)	4.42 mA cm^{-2}	[46]
Catechol/AC	1 M H_2SO_4	75 (10 000)	7.5 A g^{-1}	[47]
BPA/gr.	1 M H_2SO_4	90 (4000)	1 A g^{-1}	[48]
AQ/gr	1 M H_2SO_4	97 (2000)	10 A g^{-1}	[49]
RGO/AQDS	1 M H_2SO_4	82 (10,000)	1 A g^{-1}	[50]
THAQ/RGO	1 M H_2SO_4	97 (10,000)	1 A g^{-1}	[51]
IQD/gr	0.5 M Na_2SO_4	100 (10,000)	20 Ag^{-1}	This work

3.2.3. Lithium-ion battery application

Finally, the performance of the **IQD-G** electrode and mixed graphene–IQD electrode were comparatively evaluated in a half-cell LIBs. The charge-discharge behavior of the **IQD-G** coin cell between 1.5 and 4.3 V at 10 mA g^{-1} showed a discharge plateau at 3.2 V and expressed a reversible capacity of 118 mAh g^{-1}(Figure 15a), while just mixing of IQD and graphene sample showed no discharge plateau and a reversible capacity as low as 40 mAh g^{-1} (Figure 15b). This absence of a plateau and lower capacity demonstrated that just mixing of IQD and graphene sample was inactive for LIBs. The rate capability evaluation showed

that **IQD-G** still exhibited a capacity of 30 mAh g^{-1} at 1 A g^{-1}, while just mixing of IQD and graphene showed a capacity of only 13 mAh g^{-1} at the same rate (Figure 16a). The cyclability study at 1 A g^{-1} showed that **IQD-G** remained stable, highlighting the stability of the onium bonding for LIBs (Figure 16b). These results demonstrated that onium bonding has great potential for use in high-performance LIB electrodes. The above electrical applications demonstrated the superior electrode performance of **IQD-G** compared with just mixing of IQD and graphene.

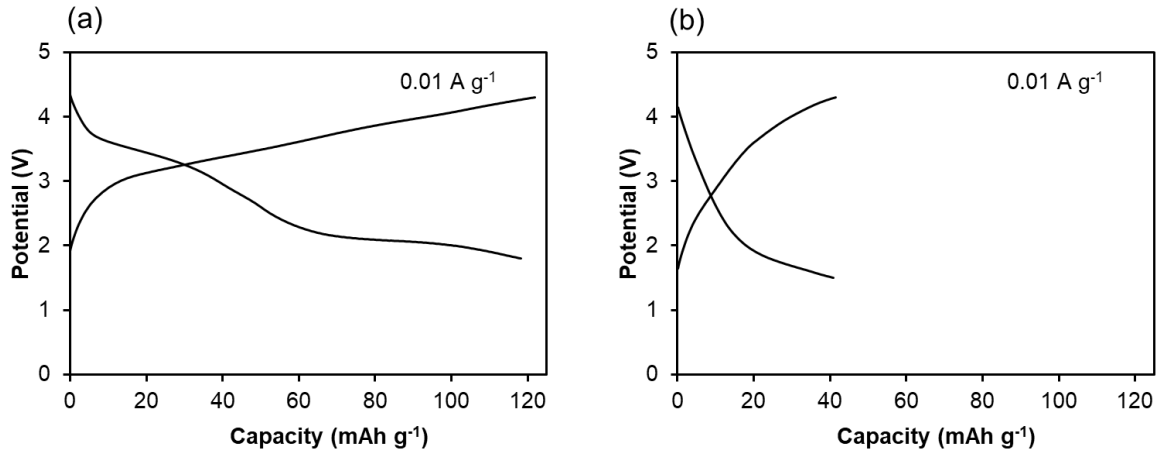

Figure 15: LIB charge-discharge behavior of (a) **IDQ-G**, and (b) mixing of graphene and IDQ at 10 mA g^{-1}

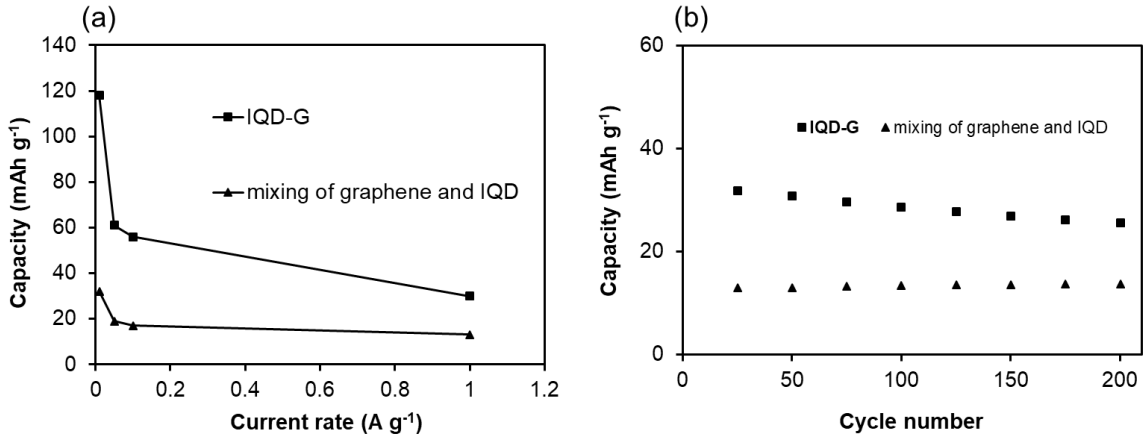

Figure 16: (a) Galvanostatic charge-discharge curve of **IQD-G** at different current densities; (b) cycling stability test at a current density of 1 A g^{-1}

The difference between these two materials was investigated by soaking each electrode material in organic and aqueous electrolyte solutions for 2 h, and then analyzing the eluted IQD by UV–Vis spectroscopy (Figure 17a and 17b). The results showed that onium bonding prevented the release of IQD into the electrolyte, allowing superior performance.

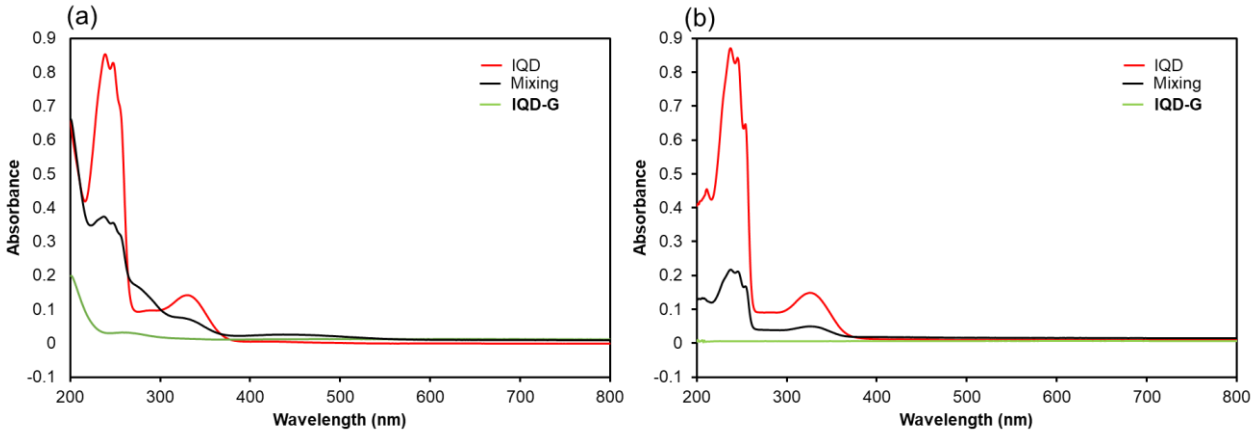

Figure 17: UV/Vis measurement of leached IQD from an electrode prepared by mixing IQD and graphene, and **IQD-G**; (a) Leaching test in aqueous electrolyte (Na_2SO_4). (b) Leaching test in an organic electrolyte (diethyl carbonate)

3.3. Conclusions

We have produced functional graphenes with strong onium bonding. This functionalization can be achieved by simply mixing brominated graphene with nitrogen-containing molecules. Graphene functionalized with a redox-active molecule was evaluated as an electrode in biofuel cell, SCs, and LIBs applications, exhibiting excellent electrochemical performance. Among applications such as LIBs, SCs, and biofuel cell, SCs was found to be promising. The high SCs performance is due to the synergistic effect of IQD and graphene which act as pseudo-capacitance and EDLC at the same time. Stability of the LIB using **IQD-G** was acceptable, but capacity was low due to the small amount of IQD molecule on graphene. **IQD-G** worked also as an electrode for a biofuel cell, however, stability was not adequate due to the decomposition of IQD moiety during enzymatic reaction. The performance of biofuel cell can be improved by optimizing the structure of redox-active molecules by attaching substituents or linkers to improve the stability and electron transfer efficiency. Although further improvement is needed, functionalized graphene through onium bonding will provide the long-lasting performance required for future practical applications.

3.4. Experimental section

3.4.1. Materials

Hydrobromic acid (HBr), Et_3N, and iPr_2NH were obtained from Nacalai Tesque. Ethanol, 8-hydroxy isoquinoline, and H_2SO_4 were purchase from WAKO Co., Ltd. pyridine was obtained from Kanto Chemical Co. Ltd. All chemicals were used as received.

3.4.2. Synthesis of GO

Graphite powder (100 g) was dispersed into concentrated H_2SO_4 (2.5 L). After cooling the mixture in an ice bath, $KMnO_4$ (300 g) was added, and the reaction mixture was kept below 55 °C. The mixture was stirred at 35 °C for 2 h to complete the oxidation process. Next, deionized water (5 L) was added slowly and the temperature was kept below 50 °C with continuous stirring, then followed by the addition of H_2O_2 (30% aq., 250 ml) into the mixture. Finally, the brown crude graphite oxide was purified by performing 10 times centrifugation, and GO is prepared. The concentration of GO was measured by drying the GO dispersion under vacuum at 50 °C.

3.4.3. Synthesis of Br-G

GO (200 mg) and HBr (20 ml, 47%) were placed in the Teflon-lined autoclave. The autoclave was heated at 240 °C for 5 h. The unreacted bromine was evaporated at room temperature, and the product was washed from the reaction vessel using deionized water. Next, the reaction mixture was directly filtrated by suction filtration on the nylon membrane and repeatedly washed with deionized water and methanol. In comparison, **Cl-G** and **I-G** were synthesized in the same way.[30]

3.4.4. Synthesis of IQD

A solution of 5-hydroxyisoquinoline (312 mg, 2.14 mmol) in acetonitrile (30 ml) was cooled to 0 °C under argon atmosphere. Then [bis(trifluoroacetoxy)iodo] benzene (PIFA) (2 g, 4.7 mmol) was dissolved in 2:1 acetonitrile–water solution (60 ml). The PIFA solution was added dropwise to the pre-cooled solution of 5-hydroxyisoquinoline over a 30-min and continued for 1 h. The reaction solvent was concentrated under reduced pressure to afford a dark brown aqueous solution. The aqueous solution was extracted with ethyl acetate (20 ml) three times. The organic extract was washed with brine (50 ml), dried over magnesium sulfate,

filtered, and concentrated under reduced pressure to give a dark yellow residue. The residue was purified by silica gel column chromatography eluting with 1:4 ethyl acetate–hexanes to give 160 mg (51%) IQD as bright yellow crystals.[52] ^{1}H NMR (300 MHz, $CDCl_3$) δ 9.36 (S, 1H), 9.10 (d, J= 2.1Hz, 1H), 7.87 (d, J= 2.1Hz, 1H), 7.00 (m, 2H).

3.4.5. Br-G substitution with iPr_2NH and Et_3N

Br-G dispersion was prepared by adding **Br-G** (100 mg) into ethanol (20 ml), which was sonicated for 30 min. Then the dispersion was injected to the flask, and to this was added Et_3N (0.681 ml, 0.5 mmol). The mixture solution was stirred for three days at 70 °C. After completion of the reaction, solid product was filtered, washed with H_2SO_4 and distilled water several times, respectively.

3.4.6. Br-G substitution with pyridine

In a typical experiment, **Br-G** (100 mg) was sonicated for 30 minutes in ethanol (50 ml) to obtain fine dispersion. To this dispersion, pyridine (51 µl, 0.632 mmol) was added. The mixture solution was then refluxed for 40 h with constant stirring. After completion of the reaction, the mixture solution was filtered and washed with sulfuric acid and distilled water respectively.

3.4.7. Br-G substituted with IQD:

Br-G (100 mg) and IQD were added to the flask containing ethanol (50 ml), which was sonicated for 30 minutes. The dispersion was then refluxed for 40 h under constant stirring. After completion of the reaction, the mixture solution was filtered and washed a few times with sulfuric acid and water, respectively, to obtain the final product.

3.4.8. Characterization

FT-IR were recorded on a SHIMADZU IR Tracer-100 in the range of 500-4500 cm^{-1}. The samples for FT-IR were dried and mixed with KBr, and then pressed up to 1.3 mm-diameter pellets. The XPS was carried out on a JPS-9030 with a pass energy of 20 eV. Raman spectroscopic measurements were conducted at room temperature by a Raman spectrometer. The UV-Vis measurements were conducted on a JASCO V-670 spectrophotometer. SEM-EDS was performed using JSM-IT 100 LA.

3.4.9. Electrochemical characterization:

For biofuel cell, the anode was fabricated by mixing electrode material (16 mg) and carbon black (1.8 mg) in 1 mL NMP, which is sonicated to make fine dispersion. Then 3 μL suspension using a pipet gun was dropped onto the glassy carbon electrode (diameter: 3 mm) and completely dried at 50 °C *in vacuo* for 1 h. The cathode used a curled platinum wire. Using a dialysis membrane, the anode and the cathode were separated, then phosphate buffer (PBS, pH = 7, 25 mL) was added to the cathode side, the PBS solution of 1 mol L^{-1} D-glucose (25 mL) was added to the anode side. In addition, O_2 bubbling was performed on the cathode side and the 10 mg enzyme (FAD-GDH) was added to the anode side. The power curves were obtained by scanning the voltage between the OCV of the cell to 0 V at a constant scan rate of 1 mV s^{-1}. To confirm the correctness of the data, we performed power density measurement of **IQD-G** for three times, as a result, 47.7±4.3 μW (n=3) were obtained.

For SCs the working electrode was prepared by mixing electrode material (40 mg), carbon black (5 mg), and PVDF (5 mg) in NMP (2 mL), which was sonicated for 1 h. The prepared past was then coated on nickel foil and dried under vacuum at 50 °C for 24 h. The electrochemical performance was tested in a two-electrode system separated by a glass fiber membrane. The cycling test and rate capability test are evaluated by charge/discharge measurement with a potential range from 0-1 V. Specific capacitance of the SCs (C, F g^{-1}) is calculated from discharge curve according to the following formula:

$$C = \frac{2\ I \bullet \Delta t}{m \bullet \Delta V}$$

where I is the constant current in discharging, m is the mass of active material on working electrode, Δt is the discharge time, and ΔV is the voltage change during discharge. The rate capability and cycling stability test was measured in 0.5 M Na_2SO_4 electrolyte solution with a Solartron SI1287 electrochemical workstation.

In the three-electrode system, the platinum foil and Ag/AgCl electrode were used as the counter electrode and reference electrode, respectively. The working electrode was fabricated by mixing electrode material (20 mg) and carbon black (2.2 mg) in 1 mL NMP solution,

which is sonicated to make fine dispersion. Then 3 μL above suspension using a pipet gun was dropped onto the glassy carbon electrode (5 mm) and completely dried at 50 °C for 1 h under vacuum. The electrochemical performance was measured in a potential range of -0.6-0.5 V, with a scan rate of 50 mVs^{-1}. To confirm the correctness of the data, we performed capacitance measurement of **IQD-G** for three times at 20 A g^{-1}, as a result, 200± 6 F g^{-1} (n=3) were obtained.

For LIBs battery the working electrodes were made of active material: carbon black: PVDF= 7: 2: 1 by using NMP as a solvent and a copper foil as the current collector. For both **IQD-G** and just mixing of IQD and graphene, the amount of IQD was adjusted to 17 wt%. In order to obtain the homogeneous active and conductive material powder, both materials were mixed together in a distilled water-ethanol solution (v/v, 1/1). After mixing, the solution was filtered using Merck Millipore JAWP04700 filter. The powder was freeze and then freeze-dry under vacuum at 30 °C for 24 h. The dry powder was set into ball-milling for 30 min at 300 RPM to reduce the particle size. Then the powder was at first mixed with NMP to obtain a homogeneous slurry and then with the binder. The slurry (active material, a conductive material, binder) was spread on a copper foil using a Doctor blade of 100 μm. The sheet was dry under vacuum at atmospheric temperature for 24 h and in air at 120 °C for 20 min. Finally, the 15.95 mm sheets were punched and pressed. To confirm the correctness of the data, we performed a capacity measurement of **IQD-G** for three coin-cells at 1 A g^{-1}. As a result, 30.8±1.3 mAh g^{-1} (n=3) were obtained.

3.4.10. Electrode sheet preparation for LIBs

The working electrodes were made of active material: carbon black: PVDF= 7: 2: 1 by using NMP as a solvent and aluminum foil as the current collector. The powder was at first mixed with NMP to obtain a homogeneous slurry and then with the binder. The slurry (mixture of active material, conductive material, and binder) was spread on aluminum foil using a Doctor blade of (100 μm thickness). The sheet was dry dried under vacuum at atmospheric room temperature for 24 h and in air and at 120 °C for 20 min. Finally, the sheets with a diameter of 15.95 mm were punched and pressed.

3.4.11. Preparation of LIBs

The LIB was assembled in an argon-filled glow box using our electrode at the cathode, lithium foil at the anode, a Whatman 1823-257 as separator, 70 µl electrolyte. The electrolyte was 1 M L^{-1} LiPF6 dissolved in a mixture of ethylene carbonate, diethyl carbonate (v/v, 3/7).

3.4.12. Evaluation of LIBs

The charge and discharge cycling tests were performed using a multi-channel battery tester (580 8 channel Battery Cycler Scribner Associates Incorporated) with a voltage window of 1.5 - 4.3 V. Each cell was subject to charge-discharge cycle at different current rates: 0.01C, 0.05C, 0.1C, 1C. All currents have been calculated with 1C = 1 A g^{-1}.

3.5. References

1. S. Chandrasekaran, N. Sato, F. Tölle, R. Mülhaupt, B. Fiedler, K. Schulte,. *Compos. Sci. Technol.* 2014, **97**, 90–99.

2. Y. Qian, I. M. Ismail, A. Stein, A, *Carbon,* 2014, **68,** 221–231.

3. C. Zheng, X. Zhou, H. Cao, G. Wang, Z. Liu, *J. Power Sources* 2014, **258,** 290–296.

4. A. Klechikov, G. Mercier, T. Sharifi, I. A. Baburin, G. Seifert, A. V. Talyzin, *Chem. Commun.* 2015, **51**, 15280–15283.

5. R. Xiong, K. Hu, A. M. Grant, R. Ma, W. Xu, C. Lu, X. Zhang, V. V. Tsukruk, *Adv. Mater.* 2016, **28,** 1501–1509.

6. H. Murata, Y. Nakajima, N. Saitoh, N. Yoshizawa, T. Suemasu, K. Toko, *Sci. Rep.* 2019, **9,** 1–5.

7. M. Cao, D. B. Xiong, L. Yang, S. Li, Y. Xie, Q. Guo, Z. Li, H. Adams, J. Gu, T. Fan, X. Zhang, D. Zhang, *Adv. Funct. Mater.* 2019, **29,** 1806792.

8. X. Xu, L. F. C. Pereira, Y. Wang, J. Wu, K. Zhang, X. Zhao, S. Bae, C. T. Bui, R. Xie, J. T. L. Thong, B. H. Hong, K. P. Loh, D. Donadio, B. Li, B. Ozyilmaz, *Nat. Commun.* 2014, **5,** 3689.

9. A. Balandin, *Nat. mater.* 2011, **10,** 569–581.

10. S. Kawai, S. Saito, S. Osumi, S. Yamaguchi, A. S. Foster, P. Spijker, E. Meyer, *Nat. Commun.* 2015, **6,** 8098.

11. D. Usachov, O. Vilkov, A. Grüneis, D. Haberer, A. Fedorov, V. K. Adamchuk, A. B. Preobrajenski, P. Dudin, A. Barinov, M. Oehzelt, C. Laubschat, D. K. Vyalikh, *Nano Lett.* 2011, **11,** 5401–5407.

12. J. Li, S. Zhang, C. Chen, G. Zhao, X. Yang, J. Li, X. Wang, *ACS Appl. Mater. Interfaces.* 2012, **4**, 4991–5000.

13. F. Parnianchi, M. Nazari, J. Maleki, M. Mohebi, *Int. Nano Lett.* 2018, **8,** 229–239.

14. B. He, Q. Tang, M. Wang, C. Ma, S. Yuan, *J. Power Sources* 2014, **256,** 8–13.

15. J. Liu, J. Tang, J. J. Gooding, *J. Mater. Chem.* 2012, **22,** 12435–12452.

16. P. Katti, K. V. Kundan, S. Kumar, S. Bose, *Polymer* 2017, **122,** 184–193.

17. V. Georgakilas, M. Otyepka, A. B. Bourlinos, V. Chandra, N. Kim, K. C. Kemp, P. Hobza, R. Zboril, K. S. Kim, *Chem. Rev.* 2012, **112,** 6156–6214.

18. A. Keerthi, B. Radha, D. Rizzo, H. Lu, V. D. Cabanes, I. C. Y. Hou, D. Beljonne, J. Cornil, C. Casiraghi, M. Baumgarten, K. Mullen, J. Am. Chem. Soc. **2017, 139,** 16454–16457.

19. X. Y. Wang, X. Yao, K. Müllen, Era. Sci. China Chem. 2019, **62,** 1099–1144.

20. S. Eigler, A. Hirsch, Phys. *Sci. Rev.* 2017, **2**, 30-66.

21. G. Bottari, M. A. Herranz, L. Wibmer, M. Volland, L. Rodríguez-Pérez, D. M. Guldi, A. Hirsch, N. Martín, F. D'Souza, T. Torres, Chem. Soc. Rev. 2017, **46,** 4464–4500.

22. H. Au, N. Rubio, M. S. P. Shaffer, *Chem. Sci.* 2017, **9,** 209–217.

23. S. Eigler, *Chem. Eur. J.* 2016, **22,** 7012–7027.

24. Z. Liu, H. Zhou, Z. Huang, W. Wang, F. Zeng, Y. Kuang, *J. Mater. Chem. A* 2013, **1**, 3454–3462.

25. Y. Liang, D. Wu, X. Feng, K. Müllen, *Adv. Mater.* 2009, **21**, 1679–1683.

26. M. Fang, K. Wang, H. Lu, Y. Yang, S. Nutt, *J. Mater. Chem.* 2009, **19,** 7098–7105.

27. C. C. Teng, C. C. M. Ma, C. H. Lu, S. Y. Yang, S. H. Lee, M. C. Hsiao, M. Y. Yen, K. C. Chiou, T. M. Lee, *Carbon* 2011, **49,** 5107–5116.

28. J. Balapanuru, J. X. Yang, S. Xiao, Q. Bao, M. Jahan, L. Polavarapu, J. Wei, Q. H. Xu, K. P. A. Loh, *Angew. Chem. Int. Ed.* 2010, **49,** 6549–6553.

29. V. Georgakilas, J. N. Tiwari, K. C. Kemp, J. A. Perman, A. B. Bourlinos, K. S. Kim, R. Zboril, *Chem. Rev.* 2016, **116,** 5464–5519.

30. S. Bag, A. Samanta, P. Bhunia, C. R. Raj, *Int. J. Hydrog. Energy* 2016, **41,** 22134–22143.

31. O. Jankovský, P. Šimek, K. Klimová, D. Sedmidubský, S. Matějková, M. Pumera, Z. Sofer, *Nanoscale* 2014, **6,** 6065–6074.

32. S. Lai, Y. Jin, X. Sun, J. Pan, W. Du, L. Shi, *Res. Chem. Intermed.* 2018, **44,** 3523–3536.

33. H. Li, Y. Shi, L. J. Li, *Carbon* 2018, **127,** 602–610.

34. X. Hu, X. Lin, H. Zhao, Z. Chen, J. Yang, F. Li, C. Liu, F. Tian, *Materials*, 2016, **9,** 376.

35. G. Shukla, V. K. Shahi, *Sustain. Energy Fuels* 2017, **1,** 932–940.

36. J. Ederer, P. Janoš, P. Ecorchard, J. Tolasz, V. Štengl, H. Beneš, M. Perchacz, P. Georgievski, *RSC Adv.* 2017, **7**, 12464–12473.

37. M. Liang, L. Zhi, *J. Mater. Chem.* 2009, **19,** 5871-5878.

38. H. Wang, H. Wu, Y. Chang, Y. Chen, Z. Hu, *Chin. Sci. Bull.* 2011, **56,** 2092–2097.

39. H. Wang, H. Yi, C. Zhu, X. Wang, H. J. Fan, *Nano Energy* 2015, **13,** 658–669.

40. P. G. Campbell, M. D. Merrill, B. C. Wood, E. Montalvo, M. A. Worsley, T. F. Baumann, J. Biener, *J. Mater. Chem. A* 2014, **2,** 17764–17770.

41. S. Isikli, R. Díaz, Carbon. *J. Power Sources* 2012, **206,** 53–58.

42. Y. Xu, Z. Lin, X. Huang, Y. Wang, Y. Huang, X. Duan, *Adv. Mater.* 2013, **25,** 5779–5784.

43. M. Zeiger, D. Weingarth, V. Presser, *Chem. Electro. Chem.* 2015, **2,** 1117–1127.

44. D. M. Anjos, J. K. McDonough, E. Perre, G. M. Brown, S. H. Overbury, Y. Gogotsi, V. Presser, *Nano Energy* 2013, **2,** 702–712.

45. A. L. Comte, D. Chhin, A. Gagnon, R. Retoux, T. Brousse, D. Bélanger, *J. Mater. Chem. A* 2015, **3**, 6146–6156.

46. S. Roldán, C. Blanco, M. Granda, R. Menéndez, R. Santamaría, *Angew. Chem. Int. Ed.* 2011, **50,** 1699–1701.

47. G. Pognon, C. Cougnon, D. Mayilukila, D. Bélanger, *ACS Appl. Mater. Interfaces* 2012, **4,** 3788–3796.

48. H. Hu, Z. Hu, X. Ren, Y. Yang, R. Qiang, N. An, H. Wu, *Chinese J. Chem.* 2015, **33,** 199–206.

49. N. An, F. Zhang, Z. Hu, Z. Li, L. Li, Y. Yang, B. Guo, Z. Lei, *RSC Adv.* 2015, **5,** 23942–23951.

50. L. Gao, S. Gan, H. Li, D. Han, F. Li, Y. Bao, L. Niu, *Nanotechnol,* 2017, **28,** 275602.

51. L. Xu, R. Shi, H. Li, C. Han, M. Wu, C. P. Wong, F. Kang, B. Li, *Carbon* 2018, **127,** 459–468.

52. M. Paige, G. Kosturko, G. Bulut, M. Miessau, S. Rahim, J. A. Toretsky, M. L. Brown, A. Uren, *Bioorg. Med. Chem.* 2014, **22,** 478–487.

Chapter: 4

Grafting conductive polymers on graphene oxide through cross-linker: a stepwise approach

Abstract: A three-step reaction furnished a composite of graphene and a conductive polymer. In the first step, GO was modified with a diamine, which acted as a linker for polymer attachment. In the second step, an initiating site was attached to the free amine of the linker. Finally, a polymer was grown from the initiation site, and GO was reduced during polymer growth. The method does not require any catalyst, acid, or reducing agent, furnishing the graphene–polymer composite in a straightforward procedure. Various instrumental techniques, including step-by-step AFM analysis, were used to characterize the structure of the products in each step and confirm the covalent functionalization among GO, cross-linker, and polymer. The average surface height was sequentially increased after each step, indicating the success of the sequential reactions. The graphene-polymer composite showed excellent electrochemical performance and stability compared with a composite prepared by physical mixing of graphene and polymer.

4.1. Introduction

Among the many proposed applications of graphene-based materials, SCs, also known as electrochemical capacitors, have been an active area of research for the past decade.[1–3] Compared with secondary batteries, graphene based SCs are electrochemical energy storage devices that promise outstanding power density,[4] charge/discharge rate,[5] cycling stability,[6] and operational safety.[7] SCs are often utilized individually or in tandem with batteries for energy storage and supply (Figure 1ai). They can be classified into two types: the electric double-layer capacitor (EDLC) (Figure 1aii) and the pseudocapacitor (Figure 1aiii). The energy storage mechanism of the EDLC involves a simple charge separation at the interface between the conductive electrode and the electrolyte. Because there is no chemical transformation at the EDLC electrodes, the system is quite stable, although the specific capacitance is relatively low.[8,9] In comparison, charge storage in a pseudocapacitor is predominantly achieved via the redox or faradic transformation of capacitive electrode materials, such as metal oxides[10] and conductive polymers.[11] The specific capacitance of the pseudocapacitor is generally high, but gradually decays because of structural collapse and degradation. A composite of a conductive substance and a

pseudocapacitive material is desirable to enhance the overall capacitance, charge/discharge rate, and cycling lifetime. Graphene is a promising conductive component because it has a large surface area,[12-14] and excellent electronic[15,16] and mechanical properties.[17,18] To develop a high-performance pseudocapacitor, we focused on developing a conductive polymer as an electrode counterpart to graphene. Various graphene–polymer composites with non-covalent and covalent interactions have been synthesized, and high capacitive performances have been achieved. The non-covalent interaction between graphene and polymers limits charge transfer at their interface, and hence constrains the cycling stability (Figure 1bi).[19] To address this issue, we propose the formation of the covalent bond between graphene and redox-active polymers.

Liu covalently functionalized graphene using amidation to graft phenylenediamine to chlorinated GO, followed by polymerization and reduction.[20] Gao,[21] Baek,[22] Liu,[23] and Shen, [24] independently reported the covalent grafting of polyaniline to graphene; all these methods initially functionalized graphene with phenylenediamine, then added aniline to initiate polymerization under acidic and oxidative conditions (Figure 1bii). As a result, a covalently cross-linked graphene–polymer composite was formed. Herein, I synthesized a new type of composite containing a linker between the polymer and graphene (Figure 1biii). The graphene–polymer composite was synthesized using a three-step reaction involving a cross-linker, initiator, and monomer. The prepared polymer–graphene composite was used as an electrode material for a SCs.

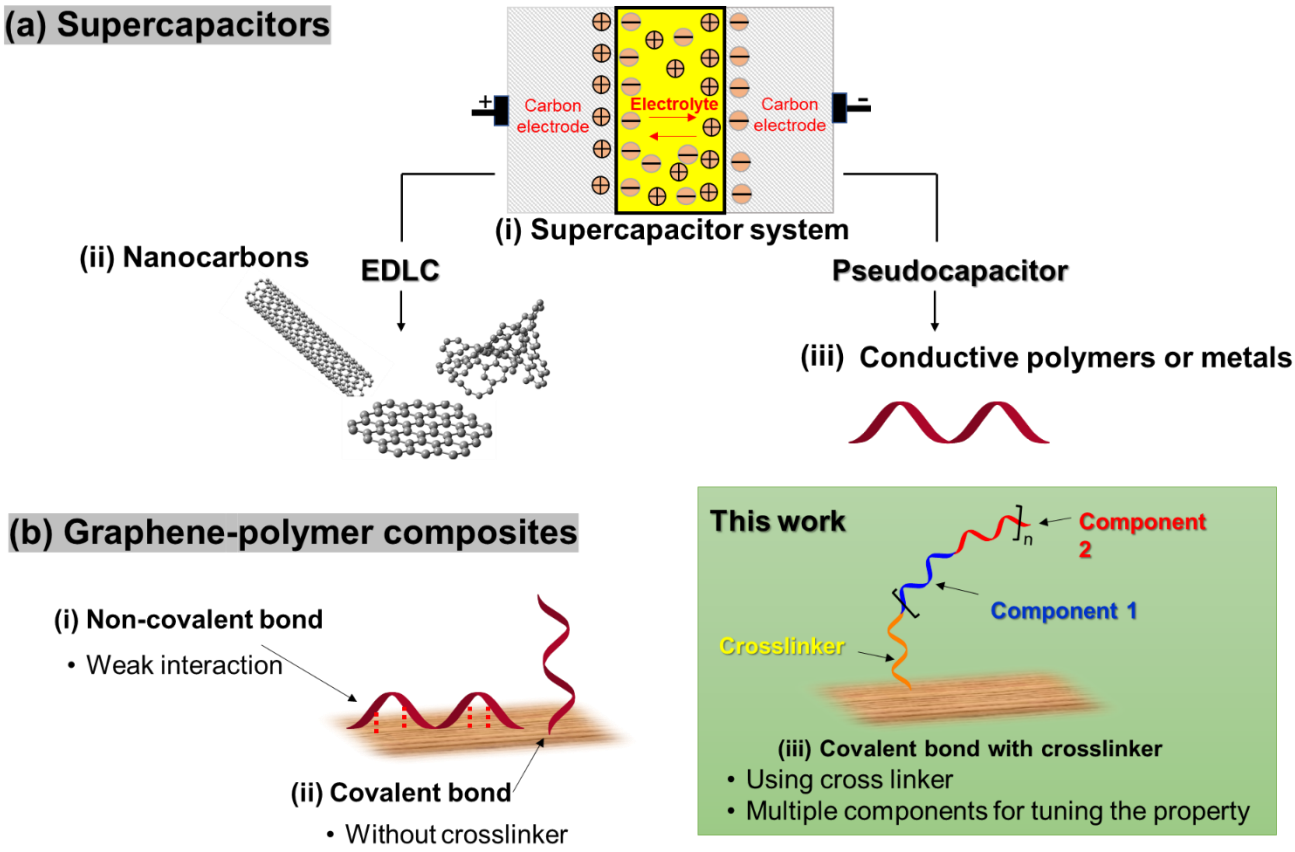

Figure 1: (a) (i) SCs systems, (ii) EDLC-type carbon materials, and (iii) pseudocapacitor-type conductive polymer or metals. (b) Synthesis of graphene-polymer through (i) non-covalent bond, (ii) covalent bond, and (iii) present work: covalent bond with cross-linker

4.2. Results and Discussion

Our strategy to synthesize a graphene–polymer composite with a linker (**GO 3**) involved three steps: (1) functionalization of graphene with 1,3-diaminopropane to obtain **GO 1**; (2) addition of a monomer (*N,N'*-bissulphinyl-*m*-benzenediamine) to **GO 1** to obtain **GO 2**; (3) addition of another monomer (1,4-phenylenediamine) to **GO 2** to initiate polymerization (Figure 2). The polymer synthesis[25] and amine functionalization of GO[26] were independently reported, and we prepared **GO 1**, **GO 2**, and **GO 3** following these previous reports.

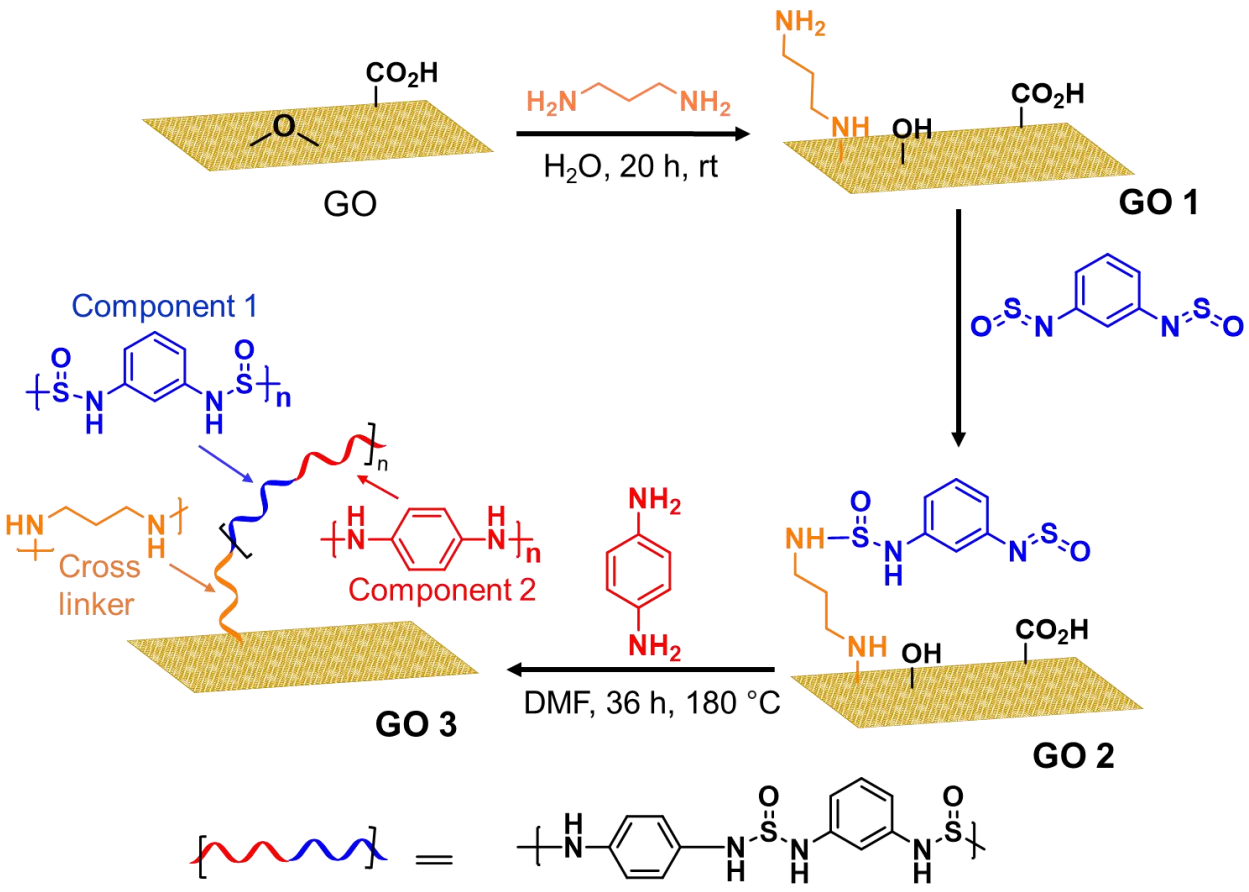

Figure 2: Synthetic route for producing **GO 3**

The structure of the product was confirmed using XPS, TGA, FT-IR, AFM, and SEM. Initially, the elemental compositions of **GO 1**, **GO 2**, and **GO 3** were analyzed using XPS (Figure 3). Survey XPS spectra of **GO 1** showed the presence of nitrogen, which confirmed the functionalization of GO with 1,3-diaminopropane (Figure 3ai).[27]

The XPS analysis of **GO 2** showed the presence of nitrogen (N) and sulphur (S), which confirmed the functionalization of the initiation site (Figure 3aii). Analysis of the XPS spectra showed the amount of N and S in **GO 2** was 4.1% and 1.2%, respectively; after polymerization, the amount of N and S was increased to 6.5% and 1.6%, respectively (Figure 3aiii). The greater amount of N and S in **GO 3** compared with **GO 2** confirms the progress

of the polymerization. The amount of oxygen in **GO 1**, **GO 2**, and **GO 3** was 25.6%, 17.5%, and 11.0%, respectively (Table 1). The smaller amount of oxygen in **GO 3** suggested reduction of GO occurred during heating.

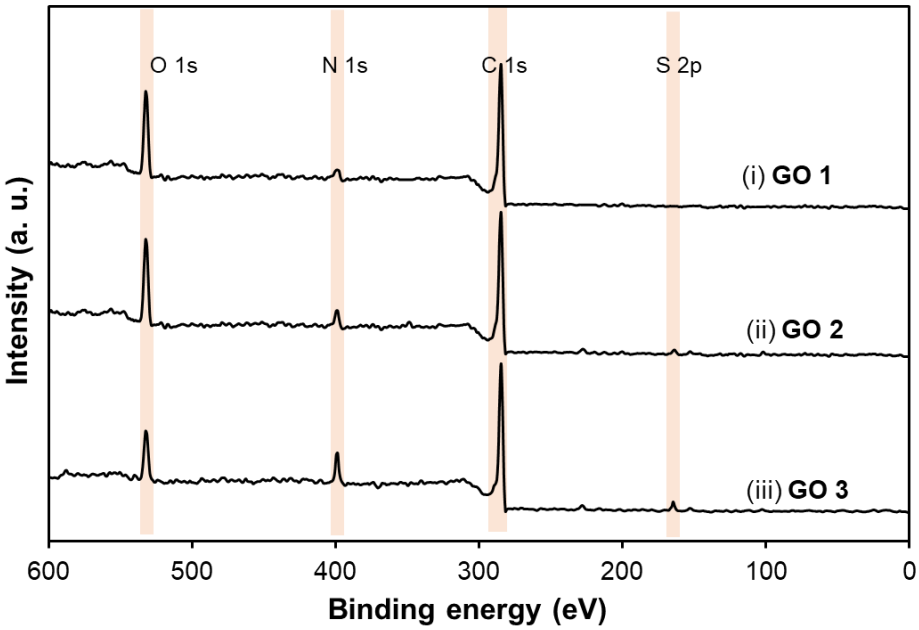

Figure 3: (a) Wide-scan X-ray photoelectron spectra of (i) **GO 1**, (ii) **GO 2**, and (iii) **GO 3**

Table 1: Quantitative comparison of detected elements from XPS spectra

Sample	**Element (at.%)**			
	C	O	N	S
GO 3	81.1	11.0	6.5	1.6
GO 2	76.6	17.5	4.1	1.2
GO 1	71.9	25.6	2.4	--

To gain further insight into the chemical composition, each element was analyzed using high-resolution XPS (Figure 4). The spectrum of **GO 1** showed a peak at 398.5 eV in the N 1s region, which suggested the formation of a covalent C–N bond,[28] and confirmed the functionalization of GO with 1,3-diaminopropane (Figure 4a). Similarly, a new peak was observed in the S 2p region of **GO 3** at 163.5 eV, which could be attributed to a C–S=O bond from the polymer (Figure 4c).[29] These spectral changes indicate the successful grafting of the polymer onto graphene.

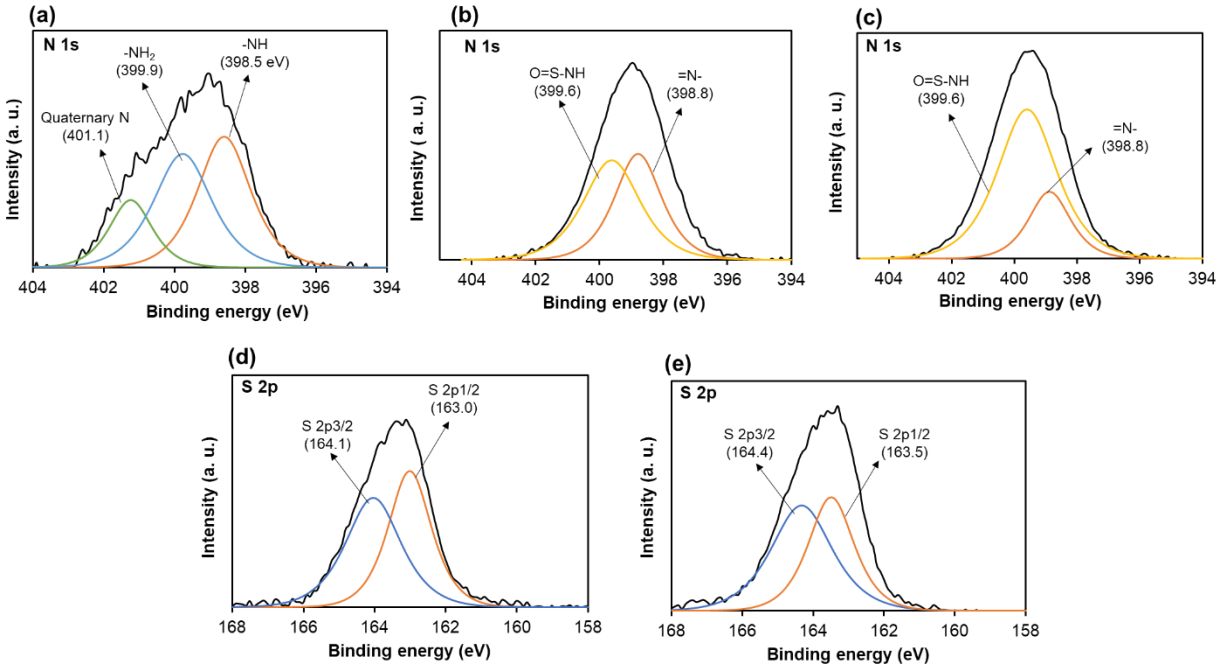

Figure 4: High-resolution XPS spectra of (a) N 1s of (a) **GO 1**, (b) **GO 2**, (c) **GO 3**, and S 2p of (d) **GO 2**, and (e) **GO 3**

Next, the thermal stability of each material was measured using TGA (Figure 5a). The TGA curve of GO showed that most weight loss occurred below 150 °C in the N_2 atmosphere, which was due to the removal of adsorbed water and oxygen-containing groups (Figure 5ai).[30] In the case of **GO 1**, a slow weight loss was observed, starting from 150–250 °C, due to the thermal decomposition of remaining oxygenated functional groups and 1,3-

diaminopropane,[31] from the GO (Figure 5aii). The lower weight loss observed in **GO 1** compared with GO could be attributed to the partial reduction of GO by diamine, as reported previously.[32] The TGA curve of the pristine polymer suggested that the polymer decomposed only gradually above 250 °C, with almost 50 wt% remaining even at 850 °C (Figure 5aiii). Comparing the TGA curve of **GO 3** with these data, the weight loss between 150 °C and 200 °C could be ascribed to the removal of oxygen functional groups and 1,3-diaminopropane from GO, and the weight loss between 300 °C and 400 °C could be attributed to the decomposition of the polymer (Figure 5aiv). Both of these observations suggest that the polymer was successfully cross-linked to the graphene in **GO 3.**

The FT-IR spectrum of GO (Figure 5bi) revealed the presence of O–H (3435 cm^{-1}), C=O (1735 cm^{-1}), C=C (1615 cm^{-1}), and C–O (1052 cm^{-1}) functional groups.[33] The FT-IR spectrum of **GO 1** exhibited a peak at 2900 cm^{-1}, which was attributed to the alkyl chain of 1,3-diaminopropane (Figure 5bii).[34] The spectrum **GO 2** contained a small peak corresponding to S=O at 1430 cm^{-1}, and the intensity of this peak was greater in the FT-IR spectra of the pristine polymer,[25] and **GO 3**.

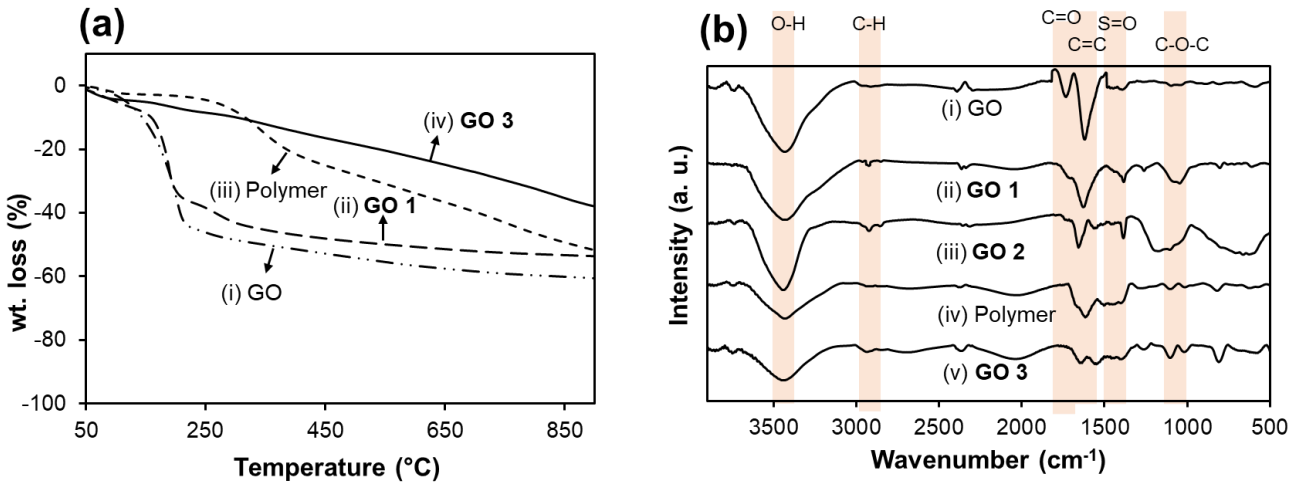

Figure 5: (a) Thermogravimetric analysis of (i) GO, (ii) **GO 1**, (iii) polymer, and (iii) **GO 3**; (b) FT-IR analysis of (i) GO, (ii) **GO 1**, (iii**) GO 2**, (iv) polymer, and (v) **GO 3**

The stepwise functionalization of graphene was confirmed by AFM (Figure 6). The average height of GO was approximately 0.9 nm (Figure 6a). The height of a **GO 1**, and **GO 2** was 1.3 nm, and 1.5 nm, respectively. The values are only slightly larger than that of the pristine GO (Figure 6b and 6c); therefore, we consider 1,3-diaminopropane and/or *N,N'*-bissulphinyl-*m*-benzenediamine are bent or almost horizontal to GO plane. The height of **GO 3** was about 16 nm, much higher than others, due to the growth of polymer on graphene (Figure 6d). This dramatic increase in the surface height of **GO 3** proves the bonding of the polymer on the surface of graphene.

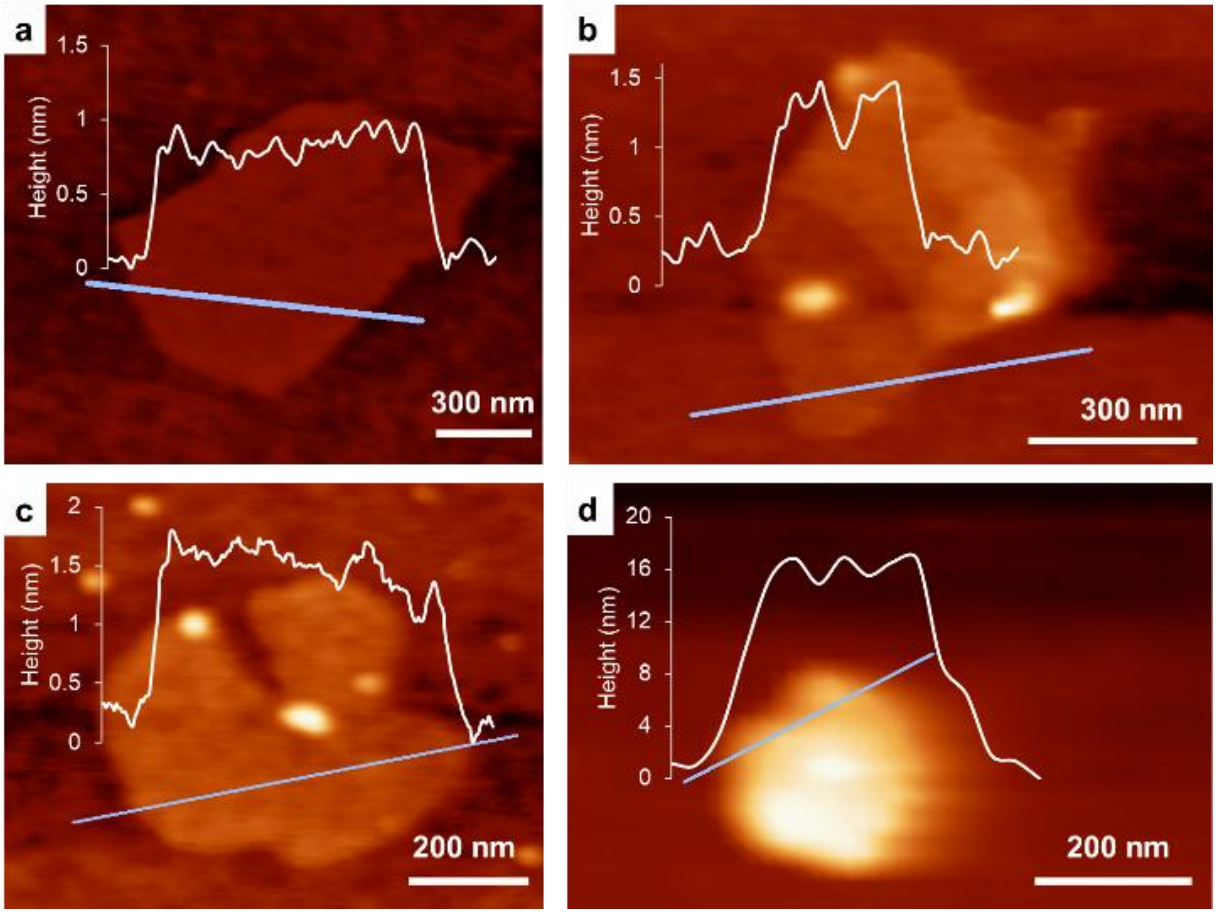

Figure 6: Atomic force microscope image analysis of (a) GO, (b) **GO 1**, (c) **GO 2**, and (d) **GO 3**

The morphologies of GO, **GO 1**, **GO 2**, and **GO 3** were further analyzed using SEM, which indicated that GO consisted of thin single-layer sheets (Figure 7a), and that these structures were retained by **GO 1** (Figure 7b), and **GO 2** (Figure 7c) after their functionalization. These observations were consistent with the AFM analyses. The SEM image of **GO 3** showed a spherical shape (Figure 7d), possibly because of the uniform growth and encapsulation of the graphene by the polymer. GO is negatively charged, and the nitrogen groups on polymer would be positively charged; therefore, ionic interaction would occur. The SEM images showed good agreement with AFM images.

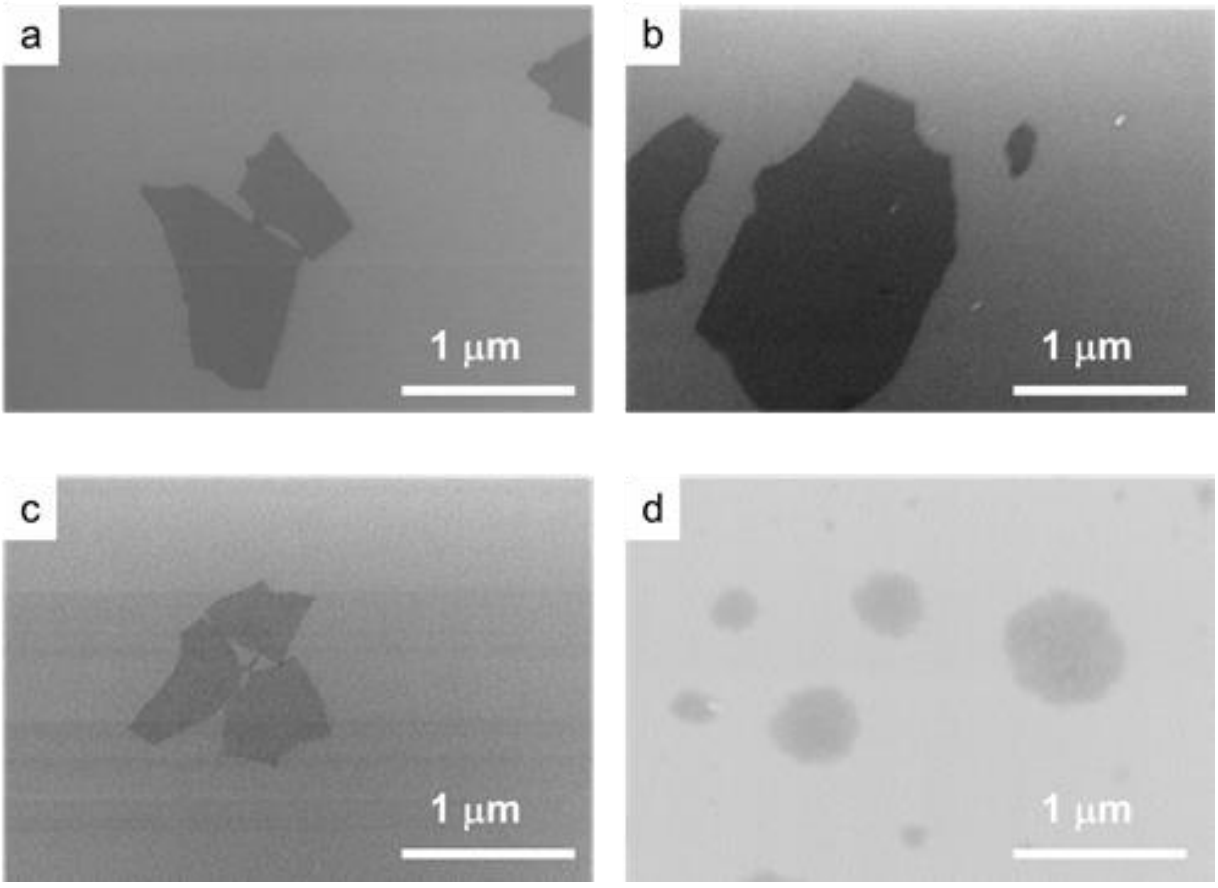

Figure 7: Scanning electron microscope images of (a) GO, (b) **GO 1**, (c) **GO 2**, and (d) **GO 3**

Possible side reactions, such as neutralization of amine and *N,N'*-bissulphinyl-*m*-benzenediamine with acidic functional groups on GO were observed (Figure 8 and 9). The reaction was performed on molecular level and the reaction was confirmed by NMR spectroscopy (Figure 10). After this, the direct reaction of monomer on GO, without 1,3-diaminopropane as a cross-linker, was prepared by the same procedure, except the starting material was GO instead of **GO 1**. The elemental composition of ***d*-GO 2** (without using 1,3-diaminopropane) and **GO 2** (addition of 1,3-diaminopropane) was also measured by XPS analysis (Figure 11). In the case of ***d*-GO 2**, the direct addition of monomer to GO caused the decomposition of the monomer, which might be due to the effect of the carboxylic group of GO. The percentage of each elements are listed in Table 2. In the case of **GO 2**, most of the carboxylic group was neutralized by 1,3-diaminopropane in the first step, which prevented the decomposition of monomer. Therefore, this result confirmed that the addition of 1,3-diaminopropane in the first step is important.

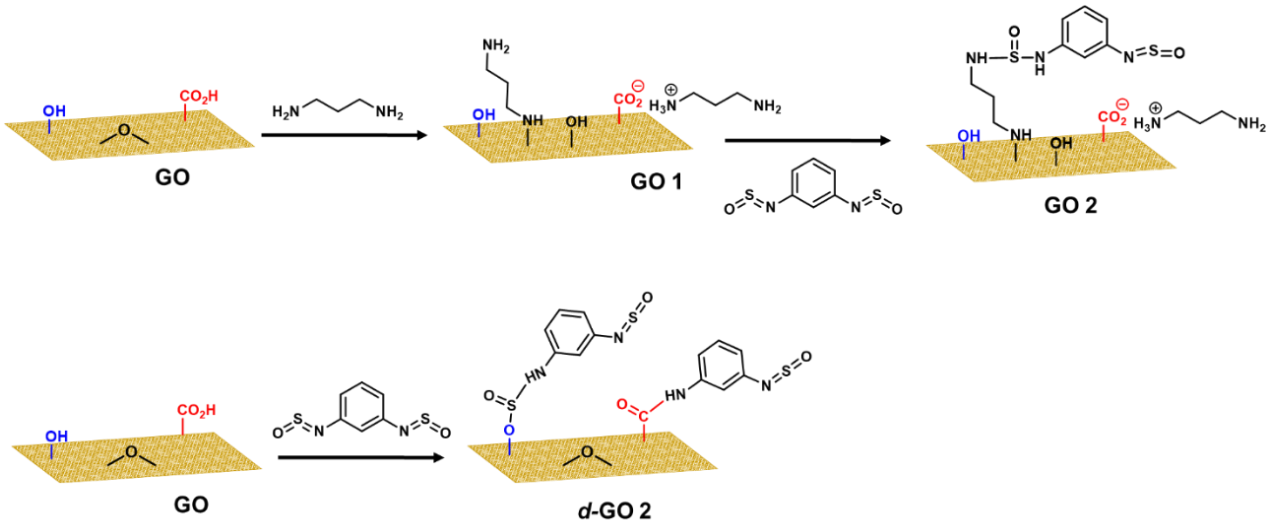

Figure 8: Synthesis of **GO 2**, and ***d*-GO 2**

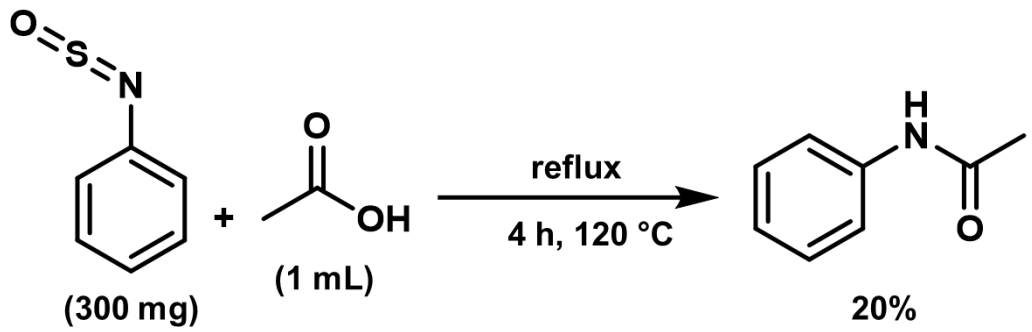

Figure 9: Possible side reaction between the monomer and carboxylic acid of GO

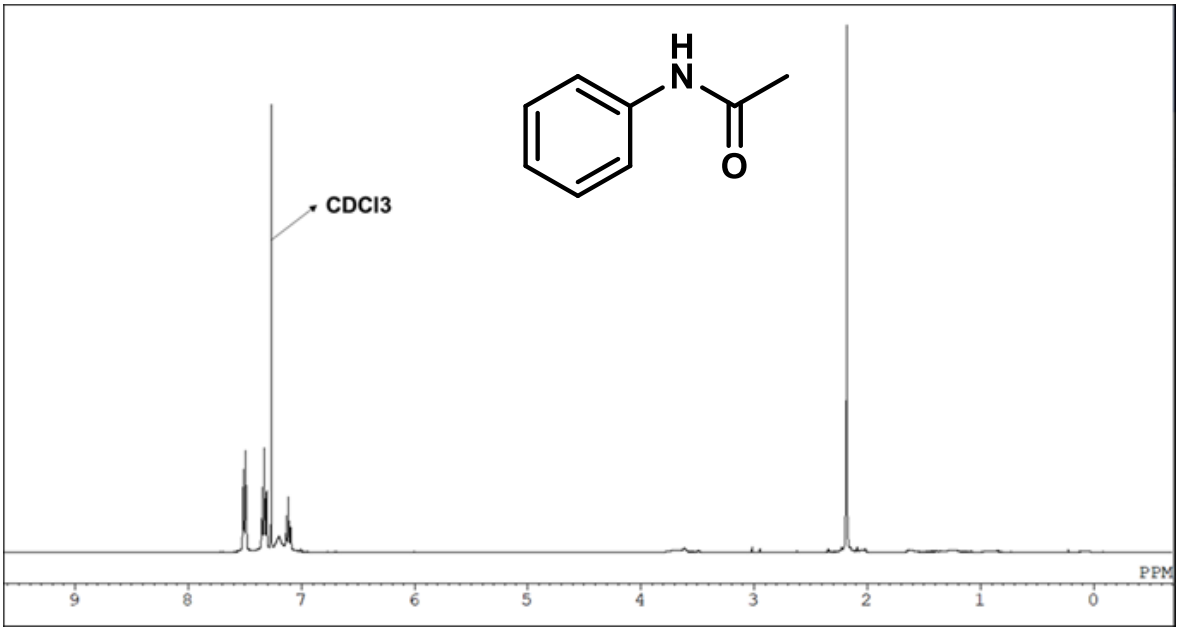

Figure 10: ^{1}H NMR spectra of the product of Figure 9

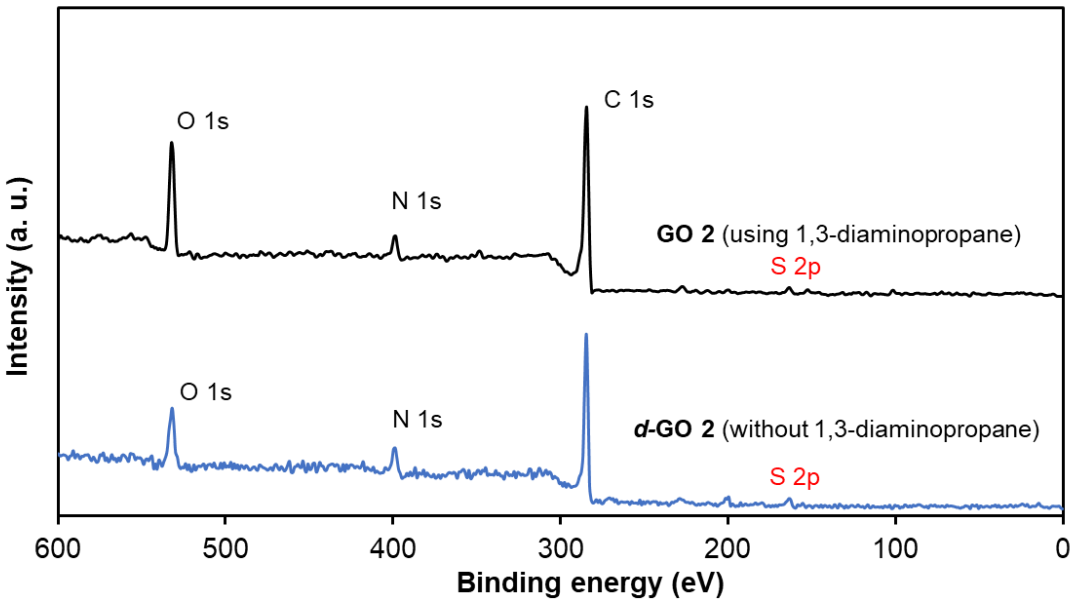

Figure 11: Wide scan XPS spectra of **GO 2 (**functionalization using 1,3-diaminopropane) and ***d*-GO 2** (functionalization without using 1,3-diaminopropane)

Table 2: Quantitative comparison of detected elements from XPS spectra

Sample	**Element (at.%)**			
	C	O	N	S
GO 2	76.6	17.7	4.1	1.2
***d*-GO 2**	76.4	15.5	6.9	1.1

4.2.1. Electrochemical performance as a SCs

CV is an effective method to determine pseudocapacitive performance. There should be a suitable mass ratio of polymer to GO of the composite that displays good electrochemical performance. Therefore, the effect of the mass ratio of polymer to GO on electrochemical performance was also studied. The polymer content in composite was determined by energy dispersive X-rays. The details percentage of each element is listed in Table 3. The CV shows that the **GO 3** with a mass ratio of 2:1 possesses a maximum specific capacitance

characteristic (Figure 12). By further increasing the ratio of polymer to GO the capacitance was decreased, possibly the polymer covers the pore of graphene which decreased the ion accessibility to the pore of graphene.

Table 3: Quantitative comparison of detected elements from EDS analysis of **GO 3** (different ratios of polymer/graphene).

Polymer:GO (wt ratio)	**Element (at%)**				**Polymer content (wt.%)***
	C	O	N	S	
1 : 1	77.7	13.5	6.2	1.2	13.3
2 : 1	80.6	12.0	5.2	1.8	19.9
3 : 1	83.4	10.8	4.3	2.4	26.6

* Polymer contents were calculated based on the molecular weight of the unit and sulfur content. Unit structure for calculation is as follows:

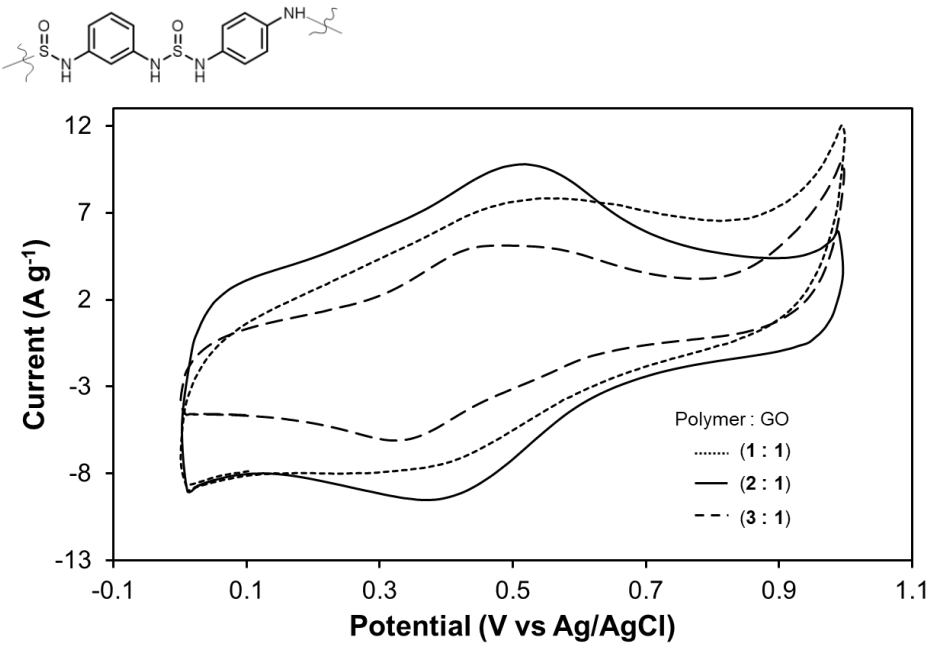

Figure 12: CV study of **GO 3** with different mass ratios of polymer to graphene at a scan rate of 50 mVs^{-1}

Next, the electrochemical performance of **GO 3**, just mixing sample (physical interact), polymer and RGO was measured by CV. The CV curve of **GO 3** (Figure 13ai) showed a peak that may be attributed to the pseudocapacitance of the polymer. **GO 3** displayed excellent electrochemical performance, possibly resulting from the larger surface area associated with the uniform polymer distribution on the graphene. Secondly, the high performance of **GO 3** might be due to the synergistic effect of pseudocapacitance and EDLC, which contribute to the overall capacitance. The CV curve of non-crosslinked graphene–polymer mixture showed lower electrochemical performance than **GO 3** (Figure 13aii). Graphene cannot maintain a single-layer structure in the solid-state due to strong π–π interactions; therefore, a uniform composite with the polymer cannot be formed. This result suggests the layer-by-layer functionalization of GO, as shown by the AFM analysis, is essential for efficient electrochemical performance. The CV curve of the polymer showed redox peaks, but the electrochemical performance was low, possibly resulting from poor contact with the electrode due to polymer aggregation (Figure 13aiii). The CV curve of graphene (Figure 13aiv) showed a rectangular-like shape without redox peaks, indicating ideal EDLC behavior. The electrochemical performance of graphene is much lower than **GO 3**. The CV curve of **GO 3** composites is much larger than that of the pure polymer, pure graphene, and non-crosslinked graphene-polymer mixture, indicating higher specific capacitance. We believe that this drastic increase of total capacitance depends not only on the amplification effect of the pseudocapacitance by the polymer, but also on the amplification effect of EDLC due to the prevention of the stacking of graphene aided by the polymer. When the CV curves of **GO 3** were acquired using different scan rates, all the curves maintained their shape (Figure 13b), which indicated the stable SCs behavior of **GO 3**. Figure 13c represents the rate capability of **GO 3,** non-crosslinked graphene–polymer mixture, graphene, and polymer. With increasing current density, the capacitance of **GO 3** initially decreased before becoming stable. The capacitance of **GO 3** reached 172 F g^{-1} at 10 A g^{-1}, which is approximately 63% of its capacitance at 1 A g^{-1} (272 F g^{-1}) (Figure 13ci). The specific capacitance of the non-crosslinked sample was 127 F g^{-1} at 10 A g^{-1}, which is 62% of its capacitance at 1 A g^{-1} (205 F g^{-1}) (Figure 13cii). Pure polymer and graphene composite

electrodes can only deliver a specific capacitance of 30 F g^{-1} and 40 F g^{-1}, respectively, at a current density of 1 A g^{-1}, which decreased with increasing current density (Figure 13c (iii and iv)). However, **GO 3** demonstrated high capacitance due to the combined effect of polymer (pseudocapacitance) and isolated graphene (EDLC), which allows fast transport of electrolyte ion. The capacitances of all samples were calculated after five cycles. Measurements of the cycling stability of **GO 3** during repeated charge/discharge cycles (Figure 13di) showed that its specific capacitance remained approximately 98% of its initial capacitance after 1000 cycles with a constant current density of 10 A g^{-1}. Thus, **GO 3** showed good cycling stability in comparison with previous reports (Table 4). This illustrates that **GO 3** possesses good stability, a long lifetime, and a high degree of reversibility during repetitive charge/discharge cycling. In comparison, the non-crosslinked graphene–polymer mixture displayed a lower capacitance that continuously decreased during several hundred cycles (Figure 13dii), its capacitance retention being 63% after 1000 cycles. The high capacitance and good cycling stability of **GO 3** can be attributed to the strong covalent connection between polymer and graphene and its uniform distribution on the graphene surface, allowing fast transport of electrolyte ions

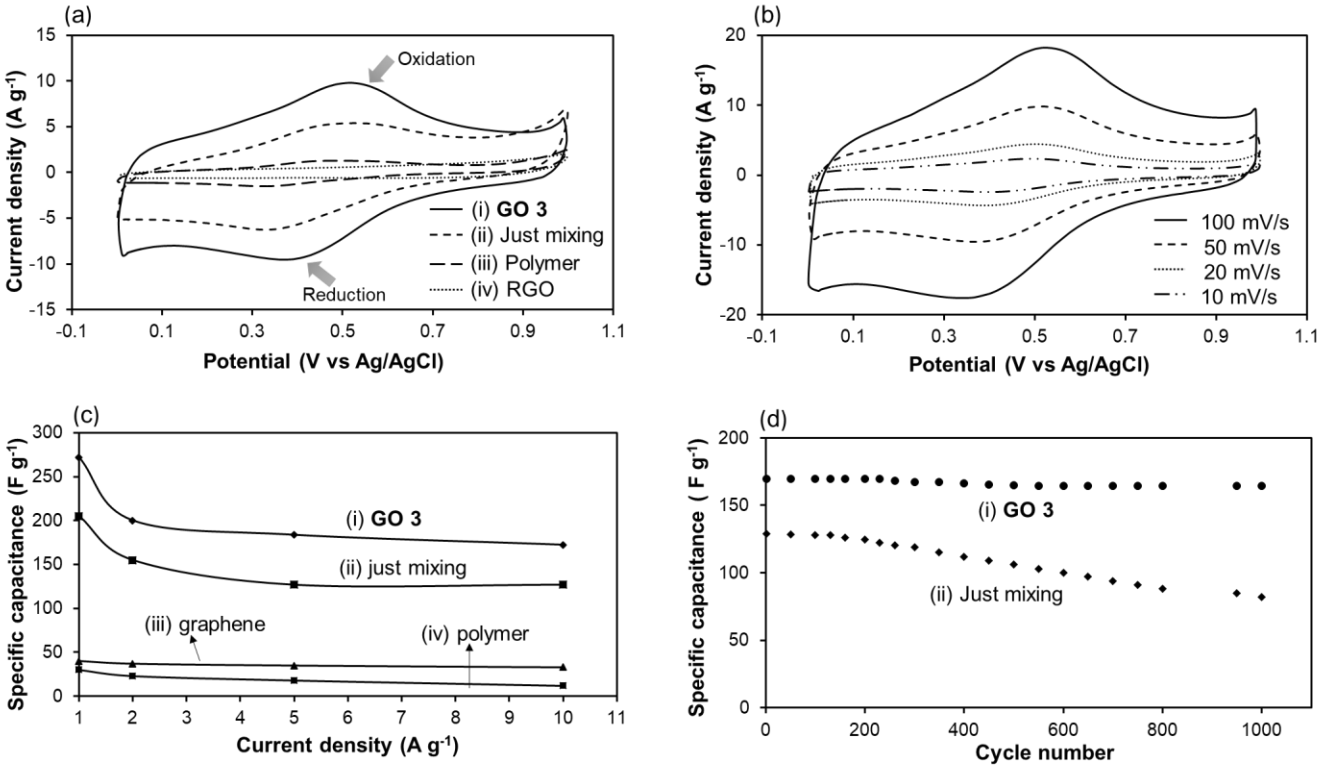

Figure 13: Electrochemical evaluation of a three-electrode system using a scan rate of 50 mV s^{-1}. (a) Cyclic voltammograms of (i) **GO 3**, (ii) just mixing, (iii) polymer, and (iv) graphene. (b) Cyclic voltammograms of **GO 3** at different scan rates. (c) Specific capacitance of (i) **GO 3**, (ii) just mixing (non-crossed linked polymer-graphene), (iii) graphene, and (iv) polymer as a function of current density. (d) Cycling stability of (i) **GO 3**, and (ii) just mixing sample using a current density of 10 A g^{-1}

Table 4: Comparison of SCs performance in three-electrode systems

Material	Cycle number	Capacity retention	Measurement conditions	References
PANI-G	1500	90%	10 A g^{-1}	[35]
PANI-G	1000	91%	2 A g^{-1}	[36]
PANI-G	1500	80%	0.5 A g^{-1}	[37]
PANI-G	200	96%	3 A g^{-1}	[38]
PANI-G	1000	85%	0.5 A g^{-1}	[39]
Ppy-G	1000	92%	1 A g^{-1}	[40]
Ppy-G	200	93%	5 A g^{-1}	[41]
Ppy-G	1500	71%	50 mV s^{-1}	[42]
PEDOT-G	1000	88%	0.3 A g^{-1}	[43]
PEDOT-G	2000	87%	0.5 A g^{-1}	[44]
Ppy-G	500	90%	100 mVs^{-1}	[45]
Ppy-G	1000	91%	1 A g^{-1}	[46]
GO 3	1000	98%	10 A g^{-1}	This work

To comprehensively understand the capacitive response of **GO 3**, an electrochemical impedance test was conducted (Figure 14a). The nearly vertical arm of the AC impedance in the low-frequency region indicates an excellent capacitive behavior, representative of fast ion diffusion and adsorption in or on the electrode material. The low resistance and fast ion diffusion can be attributed to the uniform distribution of polymer on graphene connected by covalent bond through cross-linker, which renders **GO 3** promising as a SCs electrode. Figure 14b indicates the galvanostatic charge/discharge tests at a current density of 0.5, 1, 2, 5, and 10 A g^{-1}. The nonlinear charge/discharge curves indicate the pseudocapacitive behavior of the polymer in **GO 3**

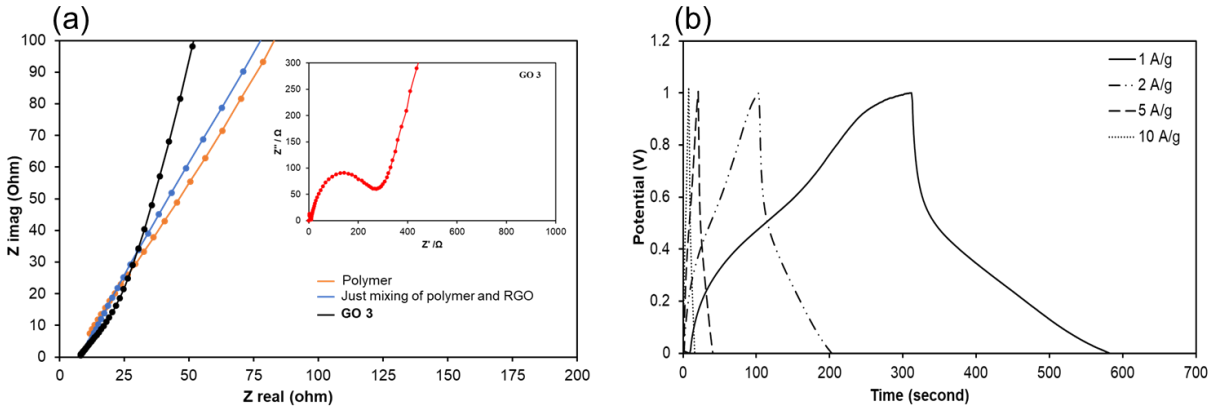

Figure 14: Nyquist plots of **GO 3**, just mixing of polymer and graphene and only polymer. Inset is the high-frequency plot for **GO 3**; (b) Galvanostatic charge/discharge curve of **GO 3** at a current density of 1, 2, 5, and 10 A g^{-1}

Finally, we investigated the capacitive and diffusion-controlled contribution to the whole capacitance of **GO 3**. As a result, the ratios of capacitive/diffusion-controlled contributions were 4.5-1.6, suggesting the success of our strategy to fully utilize the EDLC and pseudocapacitance of **GO 3** (Table 5).

The ratios of capacitive and diffusion were calculated according to the reported method[47] using an equation below.

$i(V) = k_1 v + k_2 v^{1/2}$

$k_1 v$ and $k_2 v^{1/2}$ correspond to the current contributions from the surface capacitive effects and the diffusion-controlled process, respectively.

Table 5: Calculation of Capacitive and diffusion-controlled contribution for **GO 3** at 100 mV/sec

Specific potential	Capacitive charge storage	Diffusion charge storage
0.3 V	71.6%	29.4%
0.4 V	62.3%	37.7%
0.5 V	64.3%	35.7%
0.6 V	82.4%	17.6%

4.3. Conclusion

GO was functionalized with a polymer using simple mixing and heating, without the addition of a catalyst, acid, or oxidant. The graphene–polymer composite **GO 3** was prepared using a sequential three-step reaction. Structural analyses showed that the polymer and the graphene were cross-linked by a strong covalent bond. Polymer particles are uniformly wrapped within or on the surface of graphene. The electrical properties of the composite were evaluated to determine its suitability as an electrode material for a SCs. **GO 3** demonstrated a high capacitance (272 F g^{-1} for **GO 3** vs. 205 F g^{-1} for the non-crosslinked graphene–polymer mixture at 1 A g^{-1}) and good cycling stability (98% @ 1000 cycles for **GO 3** vs. 63% for the non-crosslinked graphene–polymer mixture at 10 A g^{-1}). The superior electrochemical performance of **GO 3** is proposed due to the synergistic interaction of the polymer and graphene, allowing for fast electron transfer. This method of functionalization can be used for the future preparation of another graphene–polymer-based composites.

4.4. Experimental section

4.4.1. Materials

Natural graphite fakes (99.8%) were obtained from Alfa Aesar. *p*-Phenylenediamine, *m*-phenylenediamine, and 1,3-diaminopropane were obtained from Tokyo Chemical Industry Co., Ltd. Potassium permanganate ($KMnO_4$), sulfuric acid (H_2SO_4, 96%), thionyl chloride ($SOCl_2$), dimethylformamide (DMF), and ethanol were obtained from FUJIFILM Wako Pure Chemical Corporation and used as received

4.4.2. Synthesis of GO

Natural graphite (100 g) was dispersed into concentrated H_2SO_4 (2.5 L). After cooling the mixture in an ice bath, $KMnO_4$ (300 g) was added while the reaction mixture was kept below 55 °C. The mixture was stirred at 35 °C for 2 h to complete the oxidation. Next, deionized water (2.5 L) was added slowly, and the temperature was kept below 50 °C with continuous stirring, followed by the addition of H_2O_2 (30% aq., 250 mL) into the mixture. Finally, the brown crude graphite oxide was purified by performing 10 times centrifugation, and GO was prepared. The concentration of GO was measured by drying the GO dispersion under vacuum at 50 °C overnight.

4.4.3. Preparation of *N,N*-bissulphinyl-*m*-benzenediamine (m-monomer)

m-Phenylenediamine (0.5 g) was taken in a 250 mL round-bottomed flask fitted with a dropping funnel containing thermometer. The flask was kept in an ice-bath, and $SOCl_2$ (1 mL) was added dropwise to *m*-phenylenediamine such that the reaction temperature was kept below 0 °C. The flask was taken out from the ice bath and allowed to attain room temperature. Then, the reaction mixture was refluxed for 8 h at 80 °C. The reaction mixture was filtered, washed with benzene, and dried under vacuum.[25]

4.4.4. Synthesis of GO 1

In a typical procedure, 1,3-diaminopropane (0.5 mL) was added dropwise to the suspension of GO (250 mg L^{-1}, 400 mL) under vigorous stirring in a flask. The resulting mixture was allowed to stir for 24 h at room temperature, then filtered and thoroughly washed with ethanol and water several times. The obtained solid was freeze-dried for two days.

4.4.5. Synthesis of GO 2

In a typical procedure, the dispersion of **GO 1** (140 mg) was prepared in DMF (50 mL). Then *m*-monomer (140 mg) was added to the **GO 1** dispersion, and the mixture was sonicated for 1 h. The mixture solution was refluxed at 160 °C for 24 h in an oil bath. After completion of the reaction, the mixture solution was filtered, and the solid product was washed with DMF and water several times. The product was then dried under vacuum for two days.

4.4.6. Synthesis of GO 3

In a typical procedure, *m*-monomer (140 mg) was added into a dispersion of **GO 1** (140 mg) in DMF (50 mL) and sonicated for 1 h. Then the reaction mixture was refluxed at 160 °C for 24 h in an oil bath to obtain **GO 2**. To this mixture, *p*-phenylenediamine (140 mg) was added and refluxed at 180 °C for another 36 h. After completion of the reaction, the reaction mixture was filtered, and the solid product was washed with DMF and water several times. The final product was then dried under vacuum for two days to obtained **GO 3**.

4.4.7. Structural characterization

The thermogravimetry analysis (TGA, RIGAKU TG 8121) was measured at a heating rate of 10 °C min^{-1} from room temperature to 900 °C under a nitrogen atmosphere. FT-IR (SHIMADZU IR Tracer-100) were recorded in the range of 500-4000 cm^{-1}. The samples for FT-IR analysis were dried and mixed with KBr, and then pressed into 1.3 mm-diameter pellets. The morphologies of the composite were characterized using SEM (HITACHI S-5200) and AFM (SHIMADZU SPM-9700HT). Images were obtained through the deposition of the dispersions on oxidized Si wafer in air at 800 °C or freshly cleaved mica substrates by a drop-casting method. The cleaved mica was treated with UV ozone before coated with the samples. The crystalline structure of samples was characterized by X-ray diffraction (XRD, PANalytical Aeris) in the 2θ range of 5–40°. The operating tube current and voltage were 30 mA and 40 kV, respectively. The elemental analysis was conducted using XPS (JEOL JPS-9030) with a pass energy of 20 eV. EDS was performed using JSM-IT 100 LA.

4.4.8. Electrochemical characterization

All electrochemical measurements were carried out with an electrochemical working station (Solartron SI1287) at room temperature in an open three-electrode cell system. The modified glassy carbon electrode (ϕ = 3 mm) was used as the working electrode. A platinum wire and Ag/AgCl were used as a counter electrode and a reference electrode, respectively. Electrode material (20 mg) in NMP (1 mL) was sonicated to make uniform dispersion. 2 µL of the dispersion was taken up using a pipet gun, dropped onto the glassy carbon electrode (ϕ = 3 mm), and dried at 50 °C for 1 h under vacuum, then it was used as a working electrode. The electrochemical performance was measured in a potential range of 0-1 V, with a scan rate of 50 mVs^{-1}. All electrochemical experiments were performed in 0.5 M H_2SO_4 aqueous electrolyte. The electrochemical impedance test was conducted at a frequency range of 100 kHz to 0.01 Hz at 0.4 V with an AC perturbation of 5 mV. The specific capacitance of the SCs (C ($F\ g^{-1}$)) was calculated from the discharge curve according to the following formula:

$$C = \frac{I \times \Delta t}{m \times \Delta V}$$

where I is the constant current in discharging, m is the mass of active material on working electrode, Δt is the discharge time, and ΔV is the voltage change during discharge.

4.5. References

1. Y. Wang, Z. Shi, Y. Huang, Y. Ma, C. Wang, M. Chen, Y, *J. Phys. Chem. C.*, 2009, **113**, 13103-13107.

2. C. Liu, Z. Yu, D. Neff, A. Zhamu, B. Z. Jang, *Nano Lett.,* 2010, **10**, 4863-4868.

3. K. Zhang, L. L. Zhang, X. S. Zhao, J. Wu, *Chem. Mater.*, 2010, **22**, 1392-1401.

4. H. Yang, S. Kannappan, A. Pandian, J.-H. Jang, Y. Lee, W. Lu, *Nanotechnol*., 2017, **28**, 445401.

5. F. Zhang, T. Zhang, X. Yang, L. Zhang, K. Leng, Y. Huang, Y. Chen, *Energy Environ. Sci.*, 2013, **6**, 1623-1632.

6. D. Dutta, J. Y. Jiang, A. Jamaluddin, S. M. He, Y. H. Hung, F. Chen, J. K. Chang, C. Y. Su, *ACS Appl. Mater. Int.*, 2019, **11**, 36560-36570.

7. A. Khosrozadeh, G. Singh, Q. Wang, G. Luo, M. Xing, *J. Mater. Chem. A*., 2018, **6**, 21064-21077.

8. S. Ahmed, A. Ahmed, M. Rafat, *J. Saudi Chem. Soc.*, 2018, **22**, 993-1002.

9. W. Ma, S. Chen, S. Yang, M. Zhu, *RSC Adv.*, 2016, **6**, 50112-50118.

10. T. Nguyen, M. de F. Montemor, *Adv. Sci.*, 2019, **6**, 1801797.

11. G. A. Snook, P. Kao, A. S. Best, *J. Power Sources*, 2011, **196**, 1-12.

12. S. Drieschner, M. Weber, J. Wohlketzetter, J. Vieten, E. Makrygiannis, B. M. Blaschke, V. Morandi, L. Colombo, F. Bonaccorso, J. A. Garrido, *2D Mater.*, 2016, **3**, 045013.

13. A. Klechikov, G. Mercier, T. Sharifi, I. A. Baburin, G. Seifert, A. V. Talyzin, *Chem. Commun*. 2015, **51**, 15280-15283.

14. Y. Qian, I. M. Ismail, A. Stein, *Carbon* 2014, **68**, 221-231.

15. H. Murata, Y. Nakajima, N. Saitoh, N. Yoshizawa, T. Suemasu, K. Toko, *Sci. Rep.*, 2019, **9**, 4068.

16. M. A. Worsley, P. J. Pauzauskie, T. Y. Olson, J. Biener, J. H. Satcher, T. F. Baumann, *J. Am. Chem. Soc.*, 2010, **132**, 14067-14069.

17. D. G. Papageorgiou, I. A. Kinloch, R. J. Young, *Prog. Mater. Sci.*, 2017, **90**, 75-127.

18. L. Liu, J. Zhang, J. Zhao, F. Liu, *Nanoscale* 2012, **4**, 5910-5916.

19. S. Jo, Y. H. Park, S. G. Ha, S. M. Kim, C. Song, S. Y. Park, I. In, *Synth. Met.*, 2015, **209**, 60-67.

20. Z. Liu, H. Zhou, Z. Huang, W. Wang, F. Zeng, Y. Kuang, *J. Mater. Chem. A.*, 2013, **1**, 3454-3462.

21. Z. Gao, F. Wang, J. Chang, D. Wu, X. Wang, X. Wang, F. Xu, S. Gao, K. Jiang, *Electrochim. Acta*, 2014, **133**, 325-334.

22. N. A. Kumar, H. J. Choi, Y. R. Shin, D. W. Chang, L. Dai, J.-B. Baek, *ACS Nano* 2012, **6**, 1715-1723.

23. L. Jianhua, A. Junwei, Z. Yecheng, M. Yuxiao, L. Mengliu, Y. Mei, L. Songmei, *ACS Appl. Mater. Interfaces*, 2012, **4**, 2870-2877.

24. L. Lai, H. Yang, L. Wang, B. K. Teh, J. Zhong, H. Chou, L. Chen, W. Chen, Z. Shen, R.S. Ruoff, J. Lin, *ACS Nano* 2012, **6**, 5941-5951.

25. N. A. El-Ghamaz, T. S. Ahmed, D. A. Salama, Eur. *Polym. J.* 2017, **93**, 8-20.

26. I. A. Vacchi, C. Spinato, J. Raya, A. Bianco, C. Menard-Moyon, *Nanoscale*, 2016, **8**, 13714-13721.

27. B. Qian, C. Liu, J. Xu, Q. Sun, H. Yang, W. Liu, L. Zhang, T. Minari, X. Liu, J. Chen, *J. Phys. D: Appl. Phys.* 2019, **52**, 295502.

28. Z. Yang, Y. Dai, S. Wang, H. Cheng, J. Yu, *RSC Adv*. 2015, **5**, 78017-78025.

29. D. Mhamane, S. Unni, A. Suryawanshi, O. Game, C. Rode, B. Hannoyer, S. Kurungot, S. Ogale, activity, *J. Mater. Chem.* 2012, **22**, 11140-11145.

30. C. C. Caliman, A. F. Mesquita, D. F. Cipriano, J. C. C. Freitas, A. a. C. Cotta, W. a. A. Macedo, A. O. Porto, *RSC Adv.* 2018, **8**, 6136-6145.

31. J. Hu, B. He, J. Lu, L. Hong, J. Yuan, J. Song, L. Niu, *Int. J. Electrochem.* 2012, **7**, 10094-10107.

32. Y. Gong, D. Li, Q. Fu, C. Pan, *Prog. Nat. Sci. Mater. Int.* 2015, **25**, 379-385.

33. H. Zare-Zardini, A. Taheri-Kafrani, A. Amiri, A. K. Bordbar, *Sci. Rep.* 2018, **8**, 586.

34. J. L. Yan, G. J. Chen, C. A. O. Jun, Y. Wei, B. H. Xie, M. B. Yang, *New Carbon Mater.* 2012, **27**, 370-376.

35. Z. Liu, H. Zhou, Z. Huang, W. Wang, F. Zeng, Y. Kuang, *J. Mater. Chem. A*., 2013, 1, 3454–3462.

36. L. Wang, Y. Ye, X. Lu, Z. Wen, Z. Li, H. Hou, Y. Song, *Sci. Rep*., 2013, **3**, 3568.

37. U. Male, J. K. R. Modigunta, D. S. Huh, *Polymer*, 2017, **110**, 242–249.

38. L. Jianhua, A. Junwei, Z. Yecheng, M. Yuxiao, L. Mengliu, Y. Mei, L. Songmei, *ACS Appl. Mater. Inter.*, 2012, **4**, 2870–2876.

39. H. Qiu, X. Han, F. Qiu, J. Yang, *Appl. Surf. Sci*., 2016, **376**, 261–268.

40. Y. Liu, Y. Zhang, G. Ma, Z. Wang, K. Liu, H. Liu, *Electrochim. Acta*., 2013, **88**, 519–525.

41. S. Jo, Y. H. Park, S. G. Ha, S. M. Kim, C. Song, S. Y. Park, I. In, *Synthetic Metals*, 2015, **209**, 60–67.

42. X. Zuo, Y. Zhang, L. Si, B. Zhou, B. Zhao, L. Zhu, X. Jiang, *J. Alloys Compd.*, 2016, **688**, 140–148.

43. J. Zhang, X. S. Zhao, *J. Phys. Chem. C*., 2012, **116**, 5420–5426,

44. J. Wen, Y. Jiang, Y. Yang, S. Li, *J. Mater. Sci. Mater. Electron.*, 2014, **25**, 1063–1071.

45. S. Bose, N. H. Kim, T. Kuila, K. Lau, J. H. Lee, *Nanotechnol*., 2011, **22**, 295202,

46. Y. Song, J. L. Xu, X. X. Liu, *J. Power Sources*, 2014, **249**, 48–58.

47. J. Wang, J. Polleux, J. Lim, B. J. Dunn, *J. Phys. Chem. C.* 2007, **111**, 14925-14931.

Chapter 5

Covalent double functionalization enables multi-function and enhanced performance

Abstract: Covalent double functionalization of GO is an effective approach to tune the properties of graphene-like materials. The first step is the ring-opening reaction of epoxides by amines, and the second step is the nucleophilic addition reaction of hydroxyl groups to α,β-unsaturated carbonyl compounds. The benefits of doubly functionalized GO are to possess multifunctions and many functions, confirmed by measuring proton conductivity and redox performance. The proton conductivity can be granted by introducing sulfonic acid functional groups on GO, while the redox property can be improved by introducing quinone molecules. The current study evidence that double functionalization efficiently works in the design of multifunctional GO for specific applications, such as electrolyte membranes for fuel cells and electrode materials for SCs.

5.1. Introduction

GO and its derivatives have attracted considerable interest from the scientific and industrial communities due to their excellent electrical,[1] mechanical properties,[2] and potential for large-scale production. Therefore, their applications have been actively investigated for transistors,[3] transparent electrodes,[4] sensors,[5–7] polymer composites,[8–10] ultrastrong materials,[11] electrocatalysts,[12–14] and energy storage devices.[15,16] GO has reactive oxygenated functional groups such as epoxy and hydroxyl groups at the basal plane and carboxylic acid and carbonyl groups at the edge.[17] Basal plane functionalization is more desirable to introduce as many functions as possible; therefore, nucleophilic addition to epoxide[18] and that of hydroxyl groups[19] have been investigated. Utilizing the epoxide and hydroxyl of GO in a stepwise manner is the concept of covalent double functionalization.[20] The covalent double functionalization allows the attachment of target molecules through different reactions. In addition, the bonds between GO and the molecules are more stable than noncovalent conjugates.[21–23]

Previous researches evidenced that double functionalization of GO can introduce various functional groups, but targeted applications have not been shown. In this work, we focused on the covalent double functionalization of GO to tune the electrochemical properties, and

applied for electrode materials. To this end, two different organic molecules with specific functions were introduced on GO using a stepwise covalent double functionalization; the first step consists of the ring-opening reaction of epoxide groups of GO with an amino compound, and the second step is the nucleophilic addition of hydroxyl groups on GO to an α,β-unsaturated carbonyl compounds. The advantageous feature of the strategy was confirmed by measuring proton conductivity and capacitance for SCs.

5.2. Results and discussion

Initially, GO was functionalized by simple organic molecules to optimize the double functionalization conditions. The first step consists of the reaction of propylamine with the epoxide groups of GO,[24–26] allowing to introduce the first functionality and to generate more hydroxyl groups, which subsequently reacted with α,β-unsaturated carbonyl compounds such as methylvinyl ketone (**a**), 1,4-benzoquinone (**b**) and 1,4-naphthoquinone (**c**) (Figure 1).[20] The prepared materials were characterized by XPS, FT-IR, and CV.

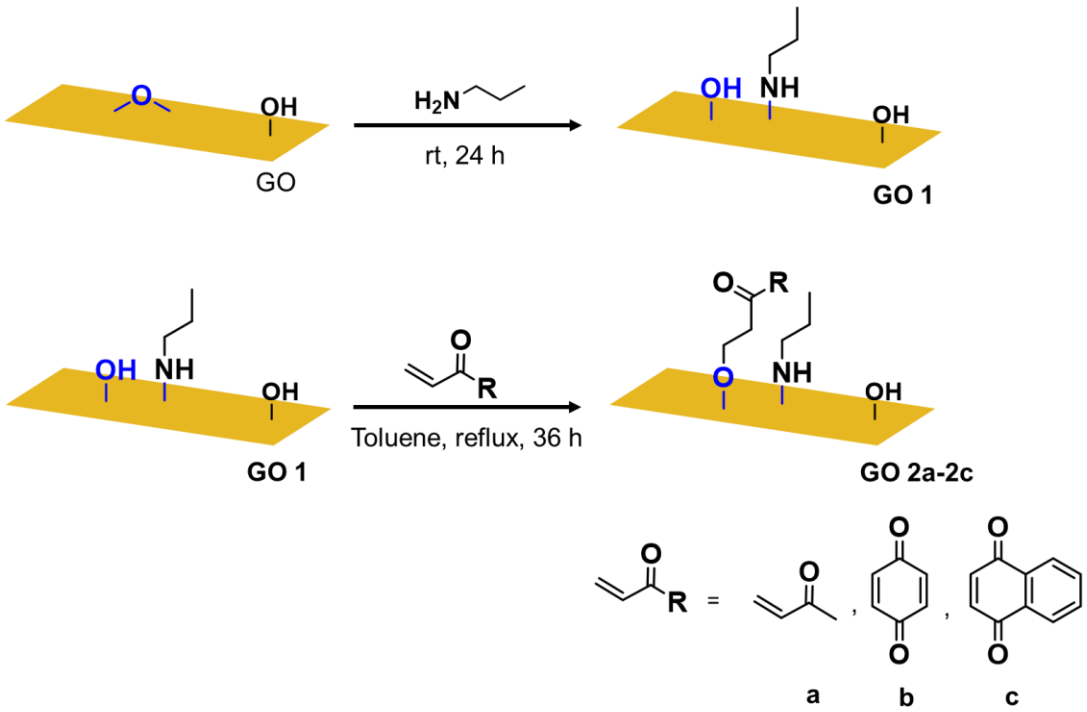

Figure 1: Synthesis of **GO1**, **GO 2a**, **GO 2b**, and **GO 2c**: for simplicity only one hydroxyl group derivatized in **GO 2 (a-c)**

The wide scan XPS spectra of propyl amine functionalized GO (**GO 1)**, and **GO 2a-2c** contains carbon, oxygen and nitrogen (Figure 2 i-iv). The presence of nitrogen atom in the spectra of **GO 1** confirmed the grafting of propylamine on the surface. The detail percentage of each element is listed in Table 1. The high-resolution XPS analysis of N 1s peak in **GO 1**, and **GO 2a-2c** appeared at 399.5 eV, attributed to the new N−C bond, thus confirming the epoxide opening (Figure 3 a-d).[27]

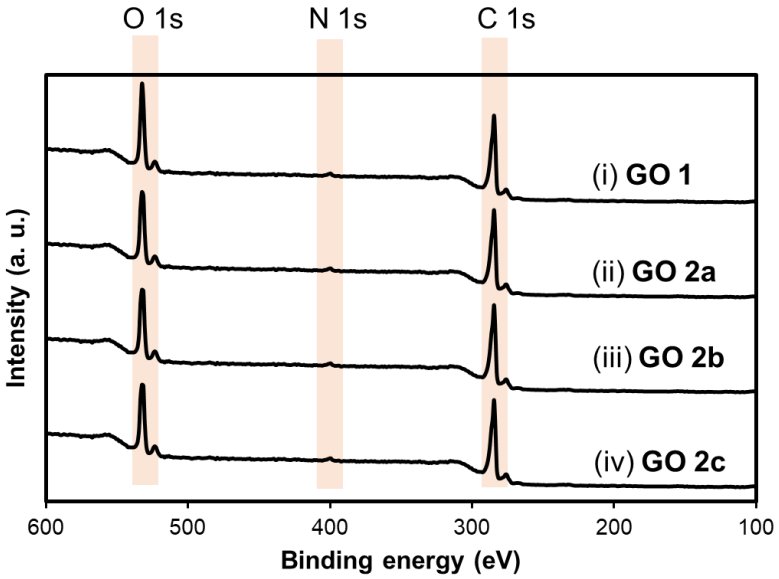

Figure 2: Wide scan XPS spectra of (i) **GO 1**, (ii) **GO 2a**, (iii) **GO 2b**, and (iv) **GO 2c**

Table 1: Quantitative comparison of detected element from the wide scan XPS spectra of **GO 1**, **GO 2a**, **GO 2b**, and **GO 2c**

Sample	**Element at.%**		
	C	**O**	**N**
GO 1	74.4	24.3	1.1
GO 2a	70.7	27.1	1.3
GO 2b	70.7	27.9	1.2
GO 2c	70.5	28.1	1.2

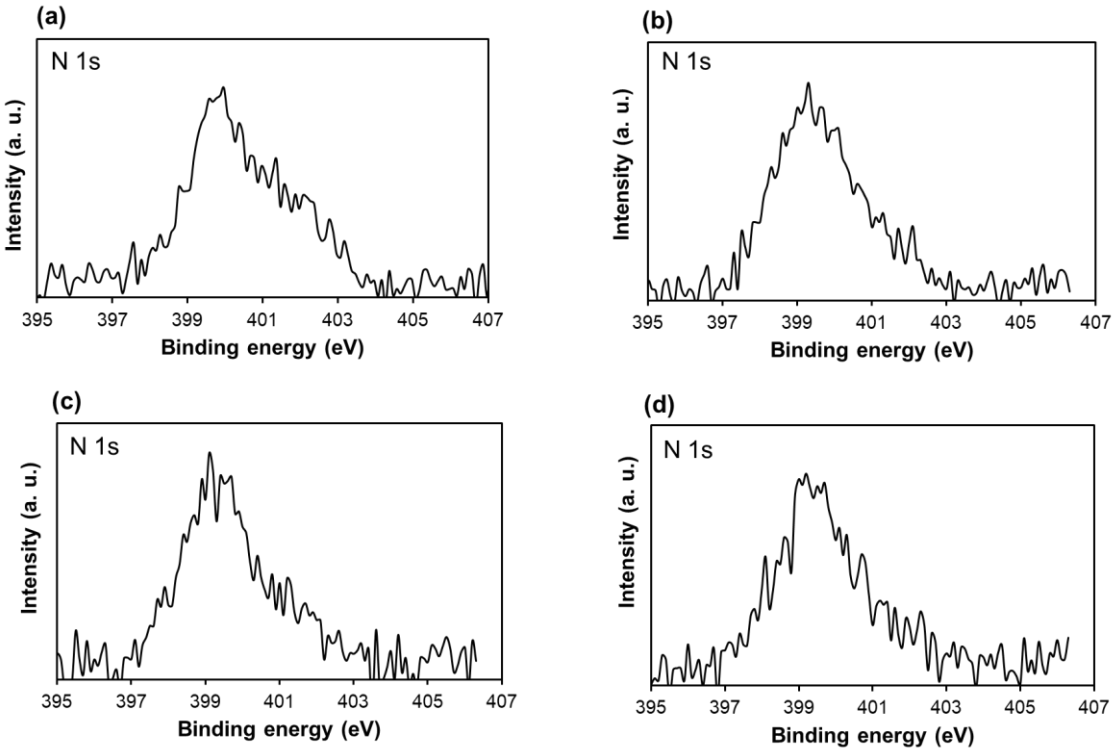

Figure 3: High-resolution N 1s XPS spectra of (a) **GO 1**, (b) **GO 2a**, (c) **GO 2b**, and (d) **GO 2c**

The synthesis of **GO 2a-2c** was confirmed from the high resolution C 1s XPS analysis. The XPS spectra of **GO 2a-2c** showed that the peak related to C=O group was increased due to the introduction of quinone molecules (Figure 4a (ii-iv)). The ratio of C=O bond in the **GO 1** changed from 4.1% to 5.2%, 6.1% and 5.9% in **GO 2a**, **GO 2b**, and **GO 2c** respectively (Figure 4b).[20,28] These changes could be explained by the grafting of α,β-unsaturated carbonyl compounds on GO. The surface functional groups of **GO 1**, and **GO 2a-2c** were further confirmed by FT-IR analysis. A peak at 1250 cm^{-1} was attributed to C-N bond, which confirmed the chemical modification of **GO 1** (Figure 4ci). The intensity of the C-OH peaks (1380 cm^{-1}) is decreased in **GO 2a-2c** as compared to **GO 1**, suggest the utilization of hydroxyl groups in the second step. A peak at 1726 cm^{-1} is detected in the FT-IR spectra of **GO 2a-2c**, assigned to the C=O group, related to the attachment of quinone molecules. These

all changes confirm the attachment of α,β-unsaturated carbonyl compounds **a**, **b**, and **c** in the second step (Figure 4c (ii-iv)).[29,30]

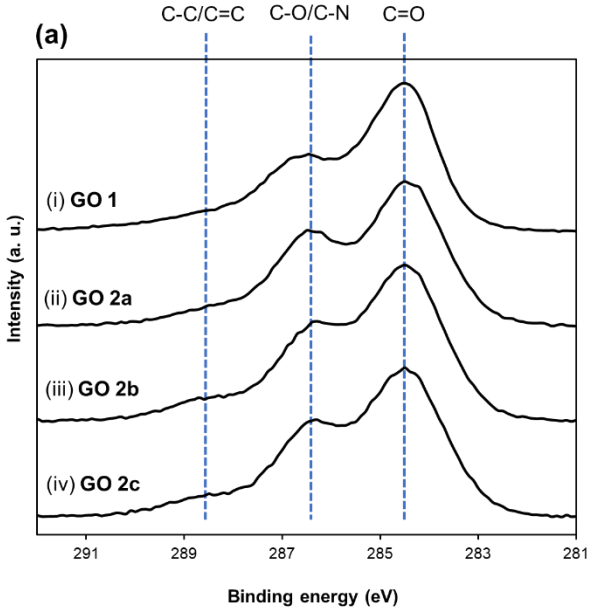

(b)

Samples	C-C	C-O	C=O
GO1	53.9%	41.9%	4.1%
GO 2a	58.3%	36.0%	5.2%
GO 2b	57.5%	36.3%	6.1%
GO 2c	58.2%	35.7%	5.9%

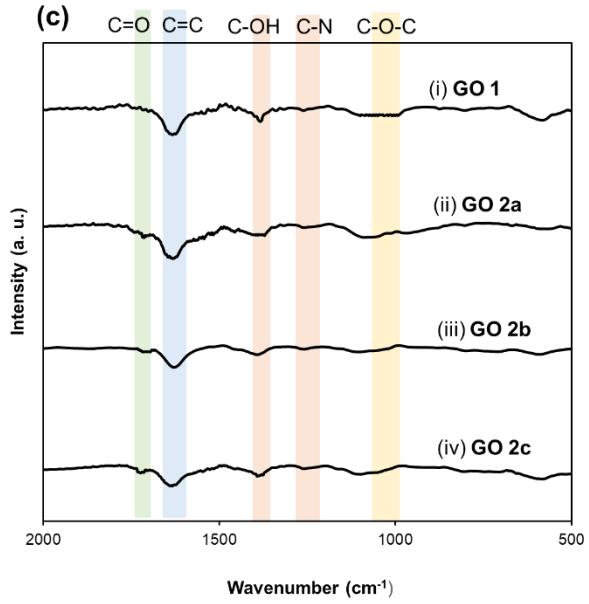

Figure 4: (a) High-resolution C 1s XPS spectra of (i) **GO 1**, (ii) **GO 2a**, (iii) **GO 2b**, and (iv) **GO 2c**,[31,32] (b) table for the quantitative analysis of high resolution C 1s XPS spectra of **GO 1**, **GO 2a**, **GO 2b**, and **GO 2c**, (c) FT-IR analysis of (i) **GO 1**, (ii) **GO 2a**, (iii) **GO 2b**, and (iv) **GO 2c**

To further confirm the double functionalization by Michael reaction, CV measurement was performed (Figure 5). CV is sensitive to the redox-active molecules.[33] The CV curve of **GO 2a** showed no redox peaks, while the CV curve of the **GO 2b**, and **GO 2c** showed the expected redox peaks. The redox peaks for **GO 2b**, and **GO 2c** appeared at different potentials. The redox potential of redox-active molecule changes with change in the molecular structure.

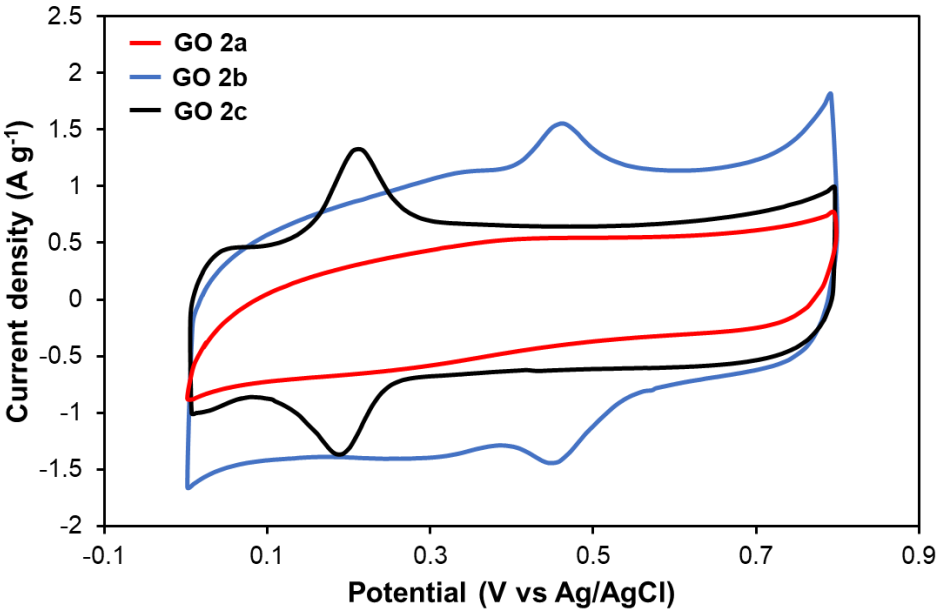

Figure 5: CV study of **GO 2a**, **GO 2b**, and **GO 2c**

5.2.1. Functionalization of GO for proton conductivity

Next, the role of double functionalized GO was investigated in the proton conductivity. Thus, the proton conductivity of the GO was improved by tuning the surface functional groups. For this purpose, sulfanilic acid was grafted on GO through epoxide group (**GO 3**), followed by the attachment of 1,4-benzoquinone (BQ) molecules (**GO 4**). Sulfanilic acid act as proton conducting material which are previously reported.[34] For comparison, aniline was functionalized on GO (**GO 5**), followed by the attachment of BQ (**GO 6**) (Figure 6).

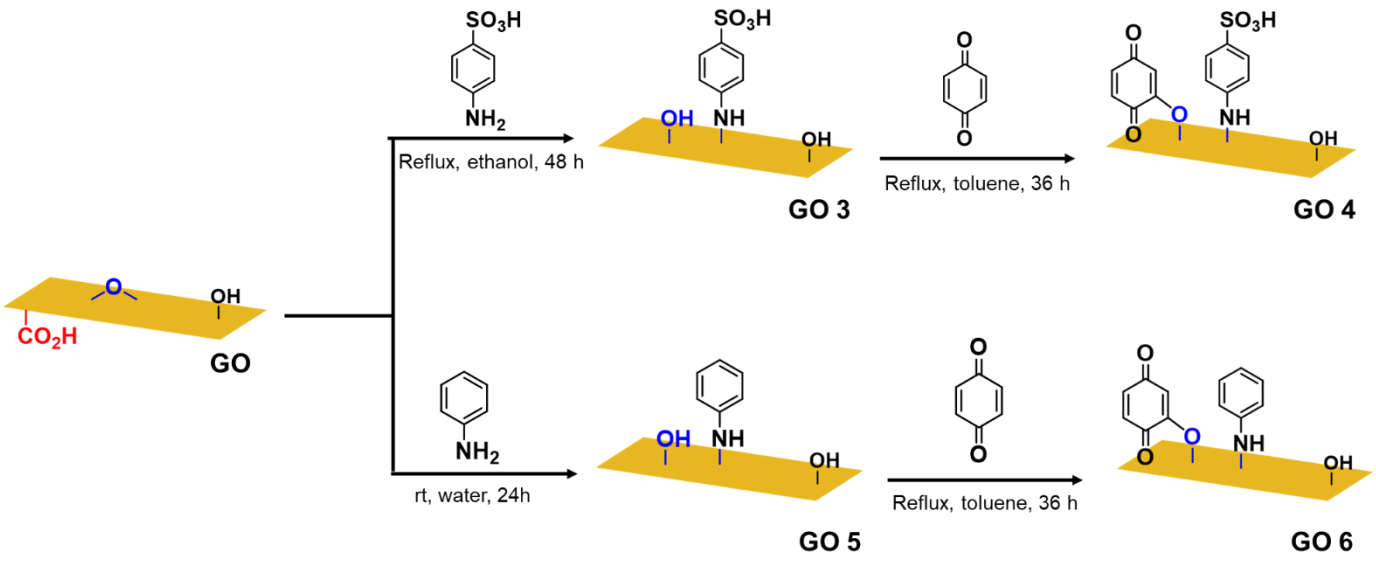

Figure 6: Synthesis of **GO 3**, **GO 4**, **GO 5**, and **GO 6**: (for simplicity only one hydroxyl group derivatized in **GO 4** and **GO 6)**

The synthesis of the materials was confirmed by XPS analysis. In the first step **GO 3** and **GO 5** was prepared through ring opening rection of epoxides. The wide scan XPS spectra of **GO 3** showed the presence of carbon, oxygen, nitrogen and sulfur, while the XPS spectra of **GO 5** contains carbon, oxygen and nitrogen (Figure 7). The presence of sulfur and nitrogen in **GO 3**, and **GO 5** confirmed the first step. The detail percentage of each element is given in Table 2. The high-resolution S 2p spectra of **GO 3**, and **GO 4** was appeared at 168.0 eV, attributed to the sulfonic group, thus confirm the presence of sulfanilic acid (Figure 8a and 8b). The high-resolution N 1s peak of **GO 3**, and **GO 5** was appeared at 399.5 eV, attributed to the new N−C bond, thus confirming the epoxide opening (Figure 8c and 8e). The same peaks (high-resolution N 1s) were also observed in the XPS spectra of **GO 4**, and **GO 6** (Figure 8d and 8f).

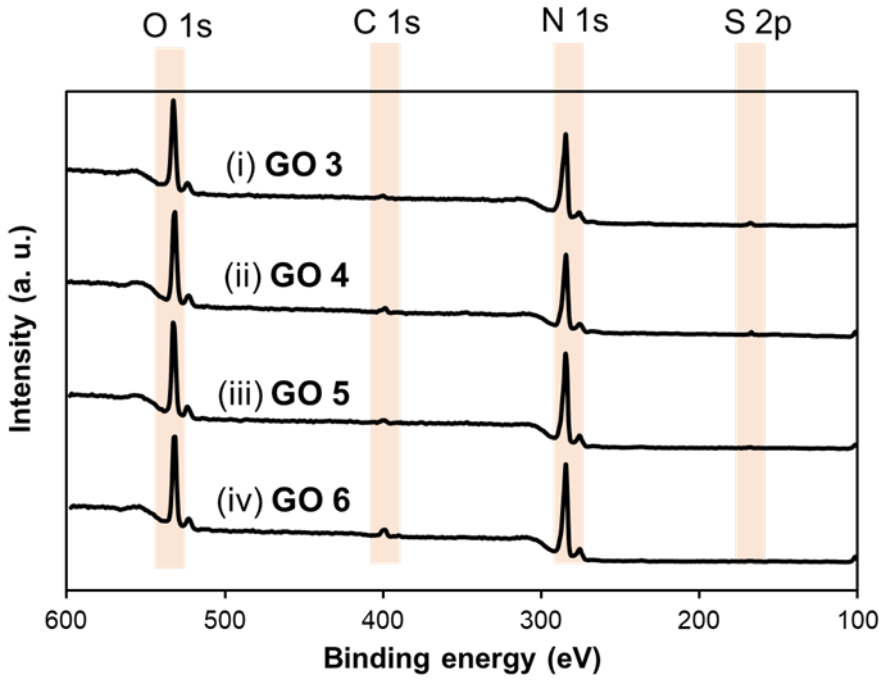

Figure 7: Wide scan XPS spectra of (i) **GO 3**, (ii) **GO 4**, (iii) **GO 5**, and (iv) **GO 6**

Table 2: Quantitative comparison of detected element from the wide scan XPS spectra of **GO 3**, **GO 4**, **GO 5**, and **GO 6**

Sample	**at.% (Element)**			
	C	O	N	S
GO 3	71.3	25.5	1.1	1.0
GO 4	71.9	25.3	1.2	1.0
GO 5	73.6	25.0	1.2	--
GO 6	73.8	24.2	1.2	--

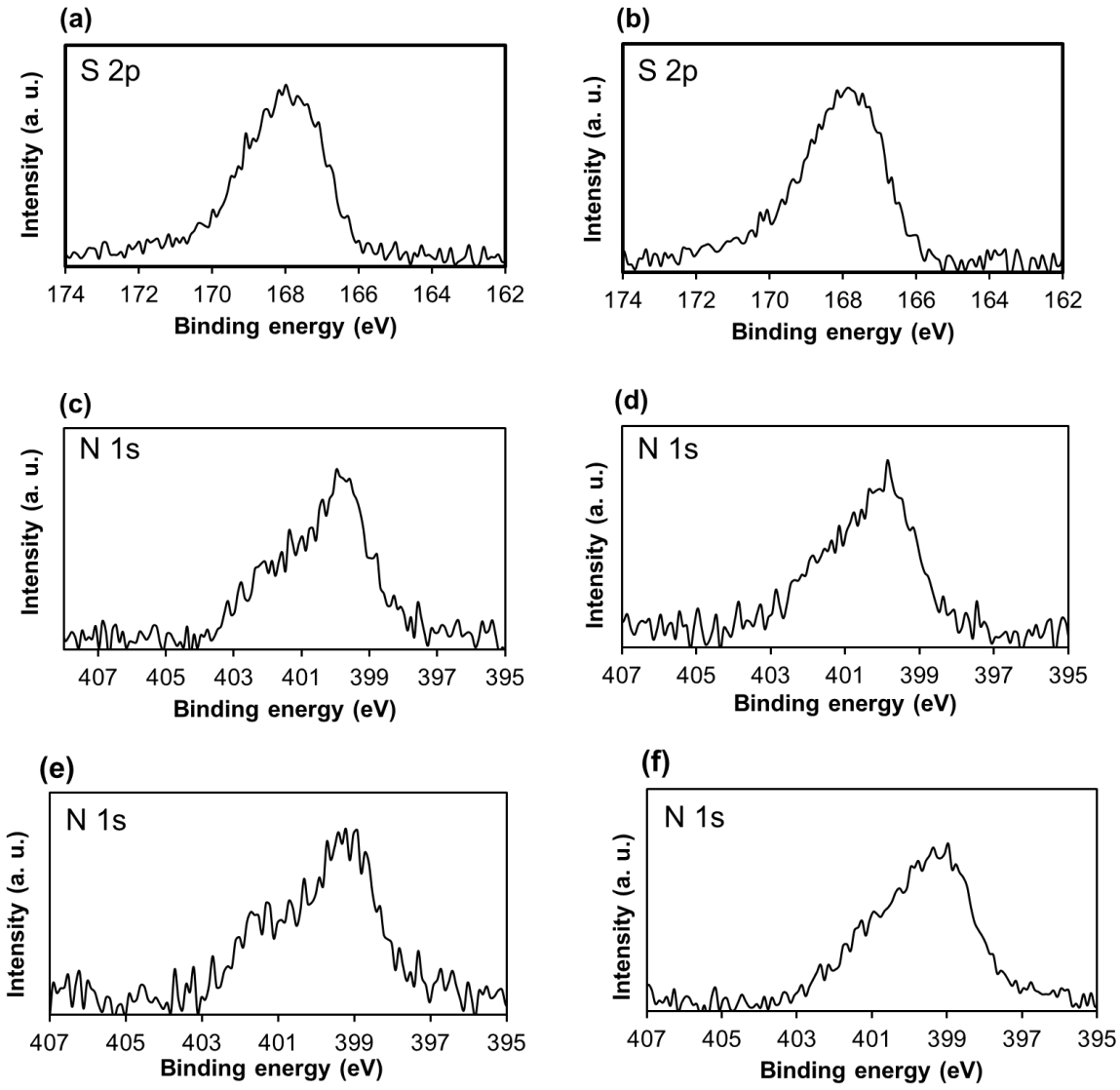

Figure 8: High-resolution S 2p XPS spectra of (a) **GO 3** and (b) **GO 4**, N 1s XPS spectra of (c) **GO 3**, (d) **GO 4**, (e) **GO 5**, and (f) **GO 6**

The second step was confirmed by the high-resolution C1s XPS spectra (Figure 9). The number of C=O group was increased in **GO 4**, and **GO 6**, due to the introduction of quinone molecules. The ratio of C=O bond was 4.5%, and 5.1% in **GO 3**, and **GO 5** respectively. The

number of C=O group was increased in **GO 4**, and **GO 6** to 6.0%, and 6.1% respectively (Table 3). Thus, confirming the grafting of BQ molecules.

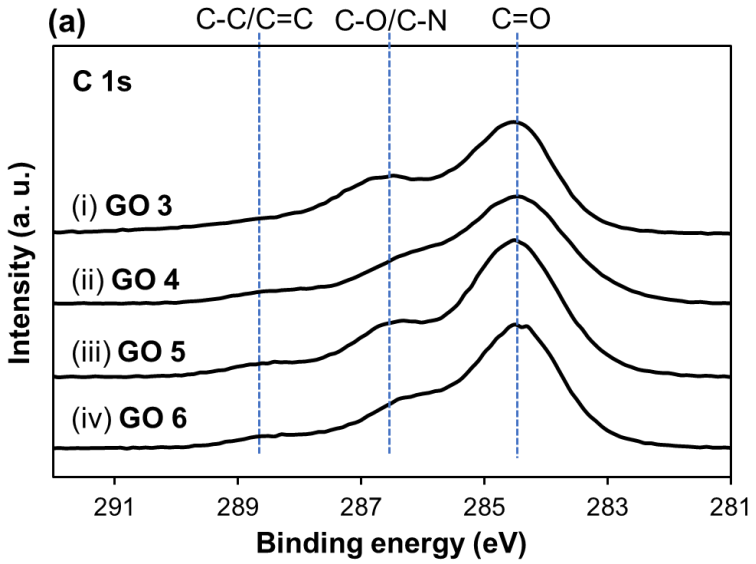

Figure 9: High-resolution C 1s XPS spectra of (i) **GO 3**, (ii) **GO 4**, (iii) **GO 5**, and (iii) **GO 6**

Table 3: Detail quantitative analysis of high-resolution C 1s XPS spectra of **GO 3**, **GO 4**, **GO 5**, and **GO 6**

Samples	C-C	C-O	C=O
GO 3	53.9%	41.4%	4.5%
GO 4	54.7%	40.1%	6.0%
GO 5	72.0%	22.8%	5.1%
GO 6	72.9%	21.7%	6.1%

The proton conductivity was evaluated by electrochemical impedance spectroscopy. The measurement was performed in two electrode system. The Sample electrode was sandwich between the two stainless steel spacer and assembled (Figure 10). The proton conductivity of

each sample was analyzed in terms of an equivalent circuit consisting of resistors and capacitors (Figure 11). The Nyquist plot of **GO 4**, and **GO 6** showed three types of resistance such as R, R_1 and R_2 (Figure 12a and 12b). The resistors and capacitors values were obtained after fitting in equivalent circuit (Table 4). The proton conductivity was calculated from the R values given by the electrical circuit and considering the pellet thickness and surface area. The R value for **GO 4** was 7.0 ohm (inset in Figure 12a), while the R value for **GO 6** was 509.4 ohm (inset in Figure 12b). The proton conductivity of **GO 4**, and **GO 6** was 7 x 10^{-3} S cm^{-1} and 6 x 10^{-5} S cm^{-1} respectively. These results indicate that **GO 4** showed 100 times high proton conductivity, which may be due to the fast ion transportation, facilitating by sulfonic acid functional group.[35] Furthermore, the proton conductivity of **GO 3** was also measured. The R value of **GO 3** was 11.0 ohm (Figure 13). The proton conductivity of **GO 3** was lower (4 x 10^{-3} S cm^{-1}) than **GO 4**, suggesting the usefulness of covalent double functionalization method.

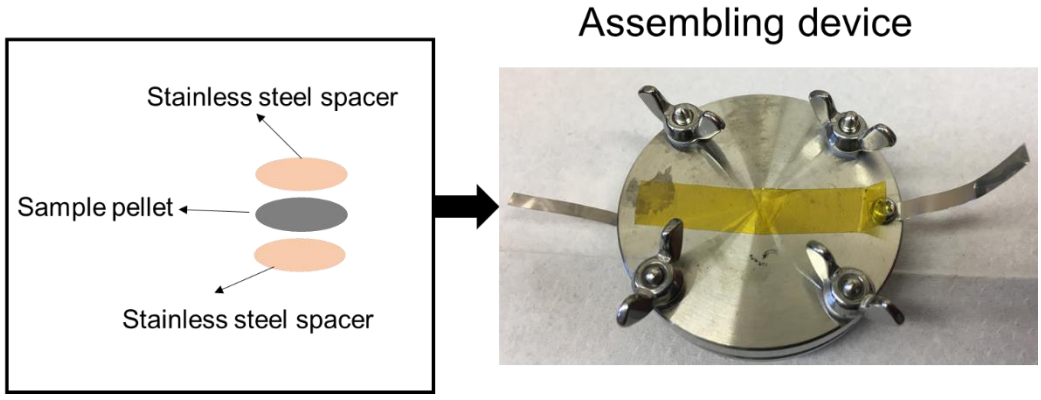

Figure 10: Electrode fabrication for proton conductivity

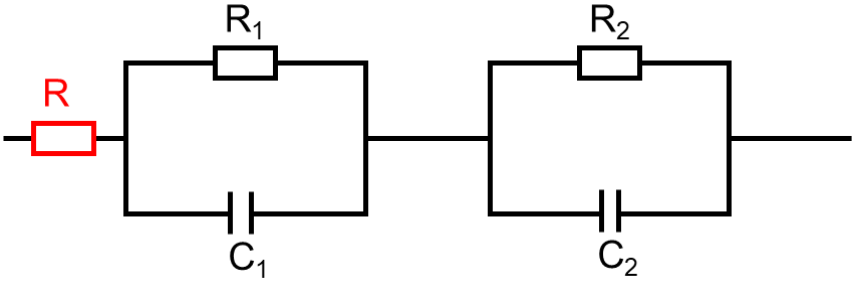

Figure 11: The equivalent circuit model for **GO 4**, and **GO 6**

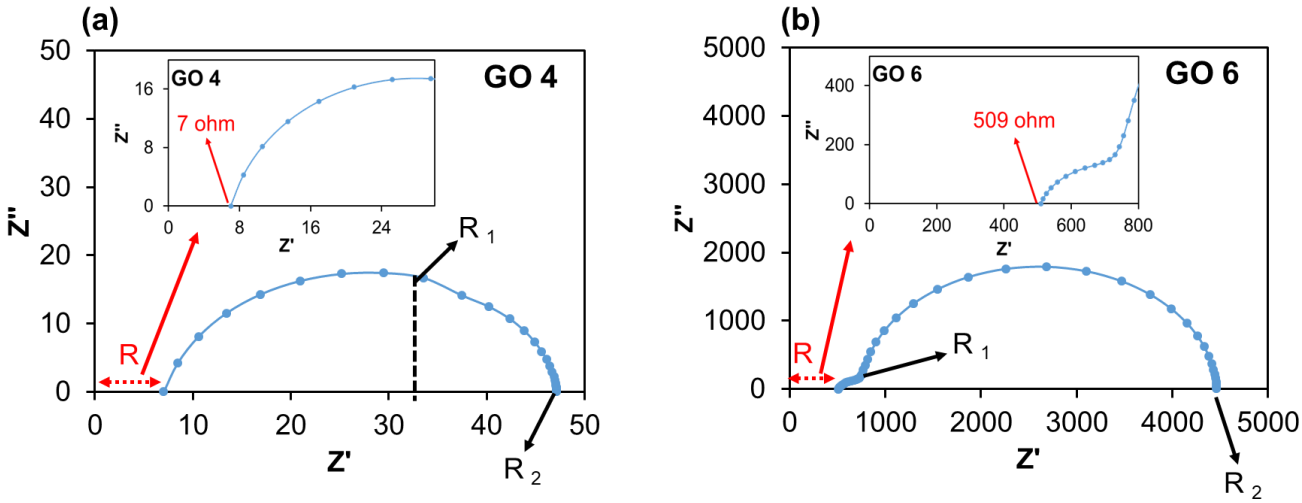

Figure 12: Impedance spectra of (a) **GO 4**, and (b) **GO 6**

Table 4: The resistors and capacitors value of **GO 4**, and **GO 6**, after fitting in equivalent circuit

Parameters	GO 4	GO 6
R_{sol}	7	506.3
R_1	26.7	246.4
C_1	5.2×10^{-8}	2.7×10^{-9}
R_2	14.2	3712.3
C_2	6.6×10^{-8}	1.3×10^{-8}

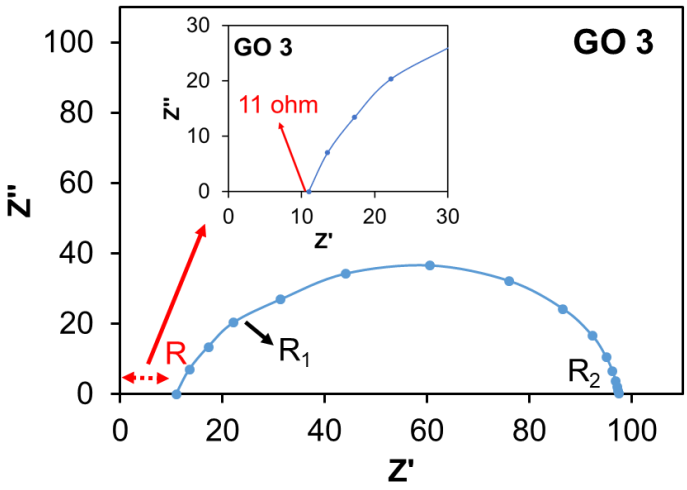

Figure 13: Impedance spectra of **GO 3**.

5.2.2. Functionalization of GO for SCs

Graphene has been widely investigated as electrode material due to its large surface area,[36] and excellent electrical conductivity,[37] and mechanical properties.[38] Organic-based electrode materials consist of carbon-based scaffolds and immobilized redox-active materials. In this context, we introduced 2-amino naphthoquinone (ANQ) and BQ molecules on GO, to develop high performance SCs. **GO 7**, and **GO 8** was prepared through covalent mono functionalization method (Figure 14a), while **GO 9** was prepared through covalent double functionalization method (Figure 14b). The prepared materials were confirmed by XPS, and CV studies.

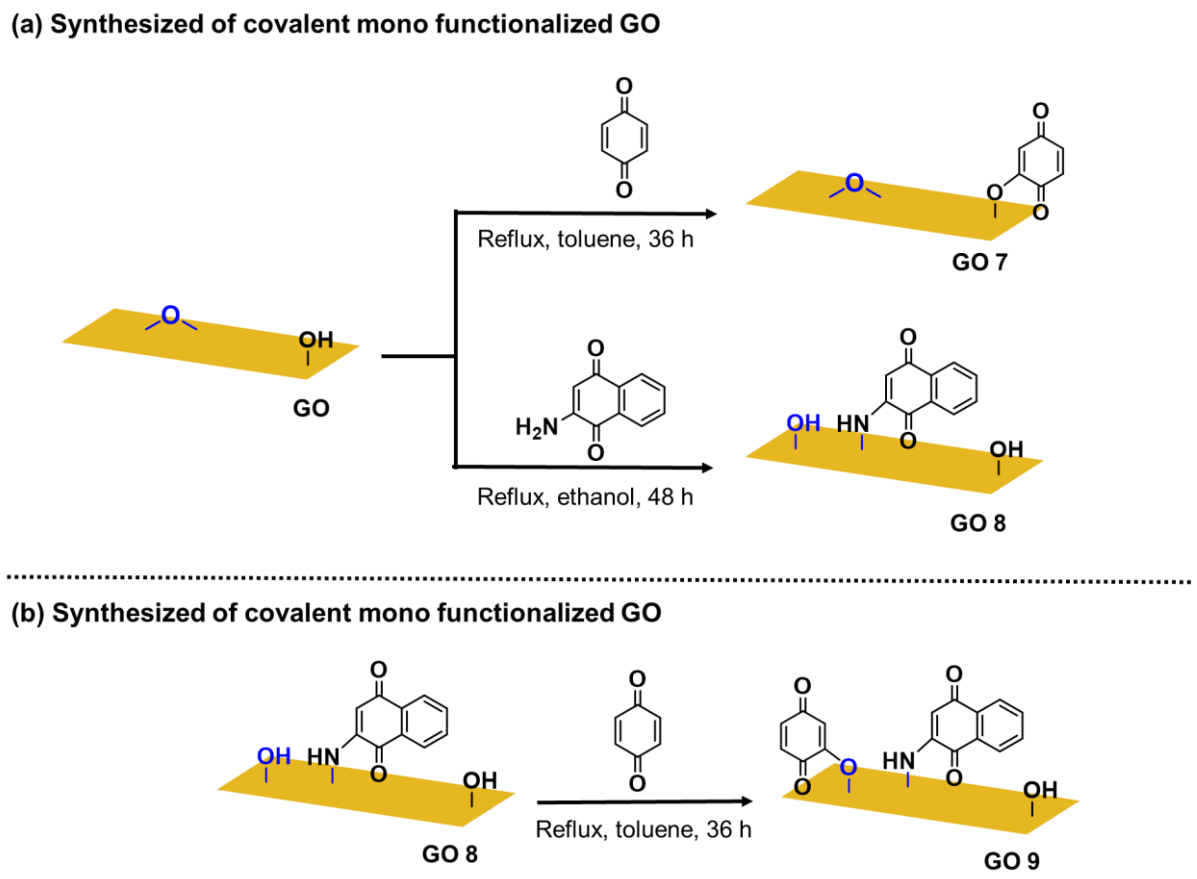

Figure 14: Synthesis of (a) covalent mono-functionalized GO **(GO 7**, and **GO 8)** and (b) covalent double-functionalized GO **(GO 9)**: for simplicity only one hydroxyl group derivatized in **GO 9**).

The XPS spectra of **GO 8** contains carbon, oxygen and nitrogen (Figure 15 ii). The presence of nitrogen atom in the spectra of **GO 8** confirming the functionalization of ANQ molecules on GO. The detail percentage of each element is given in Table 5. The high-resolution N 1s XPS spectra of **GO 8**, and **GO 9** showed peak at 399.5 eV, attributed to the new N−C bond, thus confirming the epoxide opening (Figure 16a and 16b).

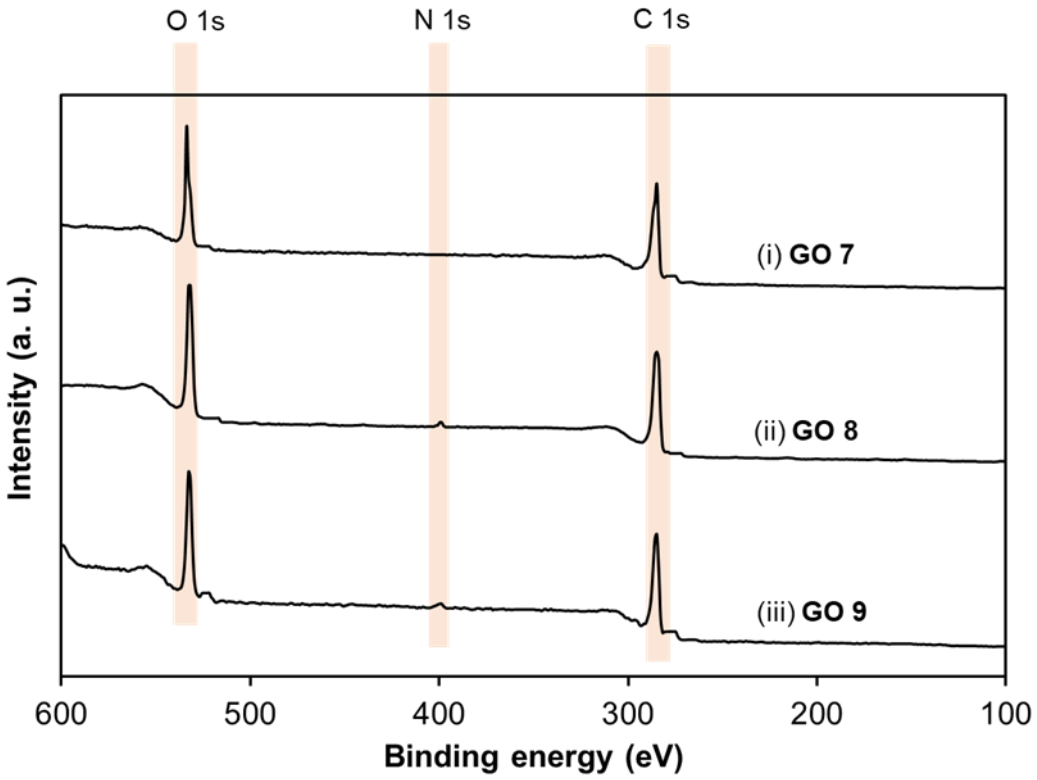

Figure 15: Wide scan XPS spectra of (i) **GO 7**, (ii) **GO 8**, and (iii) **GO 9**

Table 5: Quantitative comparison of detected element from the wide scan XPS spectra of **GO 7**, **GO 8**, and **GO 9**

Sample	**Element at.%**		
	C	O	N
GO 7	73.3	26.7	--
GO 8	72.4	26.2	1.2
GO 9	71.6	26.8	1.5

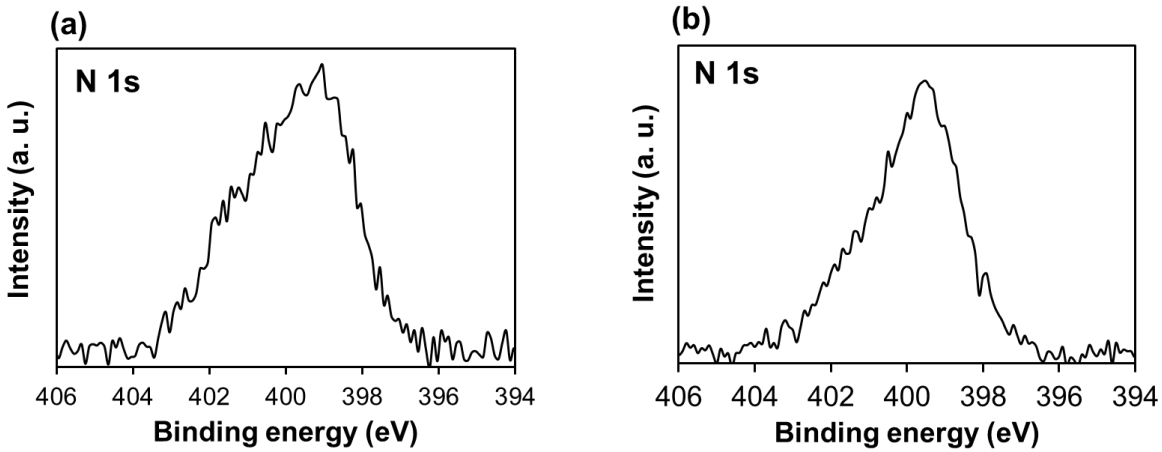

Figure 16: High-resolution N 1s XPS spectra of (a) **GO 8**, and (b) **GO 9**

The high-resolution C 1s XPS spectra showed that **GO 8** still contains large number of hydroxyl groups (Figure 17aii). The spectra of **GO 9** showed that the peak related to hydroxyl group was decreased while the peak of C=O group was increased due to the introduction of more quinone molecules (Figure 17aiii). The area of the C−C, C-OH and C=O peaks in the detailed analysis of the C1s spectrum of **GO 9** was changed from 43.9%, 50.9%, and 3.4% to 44.6%, 47.3%, and 8.0 %, respectively, compared with **GO 8** (Table 6). These changes could be explained by the grafting of BQ molecules onto GO.

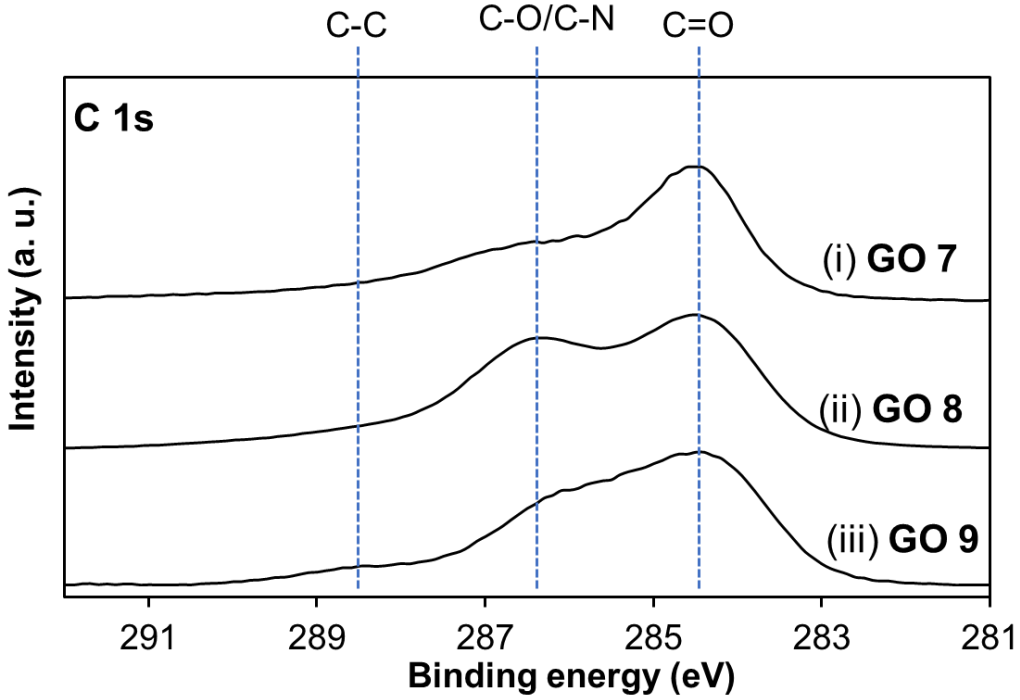

Figure 17: (a) High-resolution C 1s XPS spectra of (i) **GO 7**, (ii) **GO 8**, and (iii) **GO 9**

Table 6: Detail quantitative analysis of high-resolution C 1s XPS spectra of **GO 7**, **GO 8**, and **GO 9**

Samples	C-C	C-OH	C=O
GO 7	50.3%	45.1%	4.4%
GO 8	43.9%	50.9%	3.4%
GO 9	44.6%	47.3%	8.0%

5.2.3. Electrochemical performance as a SCs

The electrochemical behavior of **GO 7**, **GO 8**, and **GO 9** were evaluated by CV analysis. **GO 7** showed an oxidation peak at 0.53 V and a reduction peak at 0.51 V (Figure 18ai), while **GO 8** has an oxidation peak at 0.15 V and a reduction peak at 0.12 V (Figure 18aii). The redox peaks for **GO 7**, and **GO 8** appeared at different potential, due to different

molecular structure. Similar redox peaks were observed in **GO 9**, such as oxidation peaks at 0.17 V and 0.54 V, and reduction peaks at 0.10 V and 0.50 V, confirms the double functionalization of GO (Figure 18aiii). Furthermore, the CV curve suggests that **GO 9** has higher electrochemical performances than **GO 7**, and **GO 8**. This enhanced performance is likely due to the introduction of more quinone molecules, confirming again the advantage of the covalent double functionalization method. When the CV curves of **GO 9** were acquired using different scan rates, all the curves maintained their shape, indicating a stable super-capacitive behavior of **GO 9** (Figure 18b). Next, the rate capabilities of **GO 7**, **GO 8**, and **GO 9** were measured at different current densities (1 A g^{-1}, 3 A g^{-1}, 5 A g^{-1}, 10 A g^{-1}, 20 A g^{-1} and 30 A g^{-1}). The specific capacitance of **GO 7**, and **GO 8** was 154 F g^{-1} and 100 F g^{-1}, respectively, at a current density of 1 A g^{-1}, which is decreased to 100 F g^{-1} and 82 F g^{-1} at 30 A g^{-1} (Figure 18cii and 18ci). The capacitance of **GO 9** initially decreased before becoming stable (Figure 18ciii). The specific capacitance of **GO 9** was 254 F g^{-1} at a current density of 1 A g^{-1}, which decreased to 185 F g^{-1} at a current density of 30 A g^{-1} (Figure 18ciii). **GO 9** showed high specific capacitance even at high current density which may be due to the introduction of more quinone molecules on GO surface, which allows fast transportation of ions. These specific capacitances of each sample were calculated after five cycles. Finally, the cycling stability of **GO 7**, **GO 8**, and **GO 9** was evaluated at a current density of 20 A g^{-1}. **GO 7**, and **GO 8** displayed a capacitance of 71 F g^{-1} and 57 F g^{-1}, respectively, with a capacitance retention of 71% and 69% after 1000 cycles (Figure 18dii and 18di). **GO 9** showed a specific capacitance of 153 F g^{-1} with a capacitance retention of 85 % after 1000 cycles (Figure 18diii). These results suggest that a high number of charge/discharge cycles, **GO 9** still maintains its high capacitance as compared to **GO 7**, and **GO 8**.

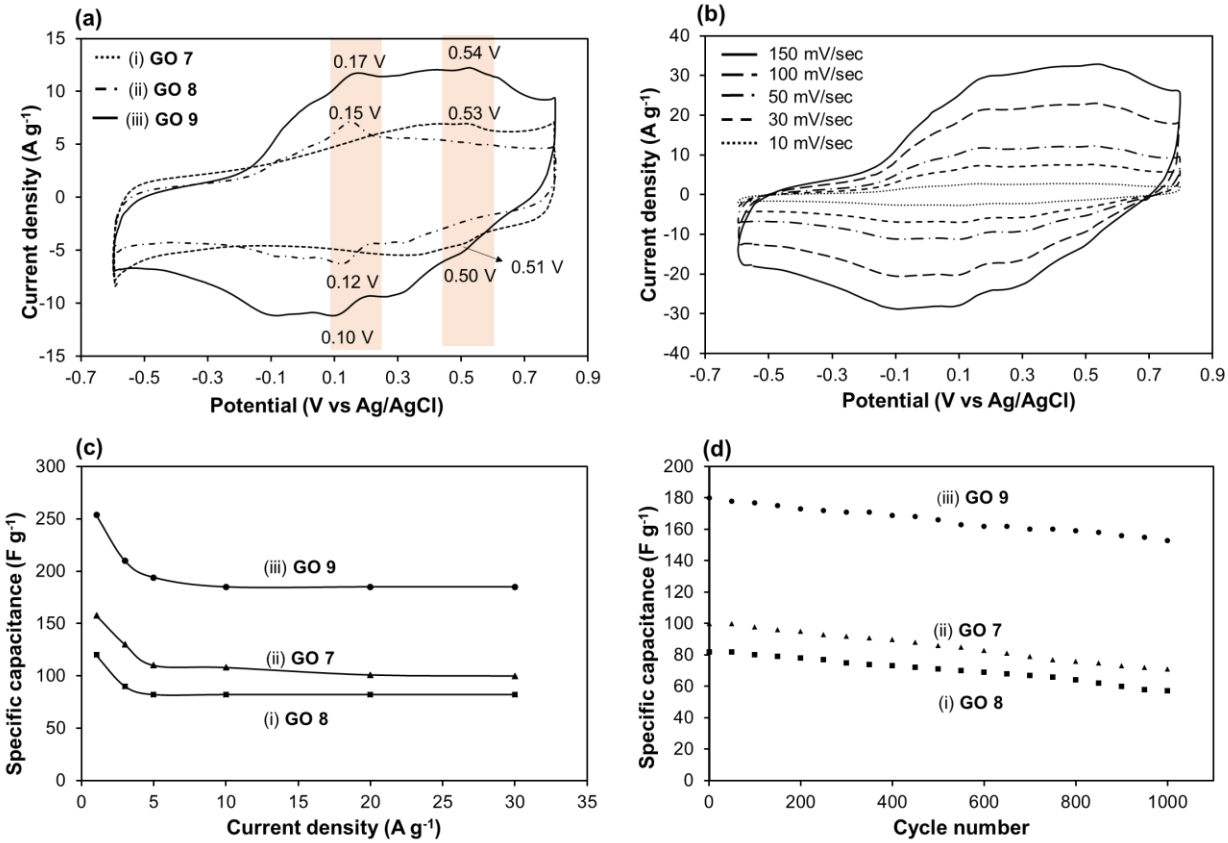

Figure 18: Electrochemical evaluation in three-electrode system at a scan rate of 50 mV s^{-1}: (a) CV profile of (i) **GO 7**, (ii) **GO 8**, and (iii) **GO 9**, (b) **GO 9** at different scan rates, (c) specific capacitance of (i) **GO 8**, (ii) **GO 7**, and (iii) **GO 9** as a function of current density, (d) cycling stability of (i) **GO 8**, (ii) **GO 7**, and (iii) **GO 9** at a current density of 20 A g^{-1}.

The electrochemical performance of **GO 9** was also compared with **GO 2b** (functionalization of GO by propylamine, followed by the attachment of BQ). The CV curve showed that **GO 9** demonstrated high electrochemical performance than **GO 2b** (Figure 19). The galvanostatic charge/discharge behavior of **GO 7**, **GO 8**, and **GO 9** was measured at a current density of 1 A g^{-1}. **GO 9** showed stable behavior than **GO 7**, and **GO 8** (Figure 20a). Figure 20b showed the galvanostatic curve of **GO 9** at different current densities.

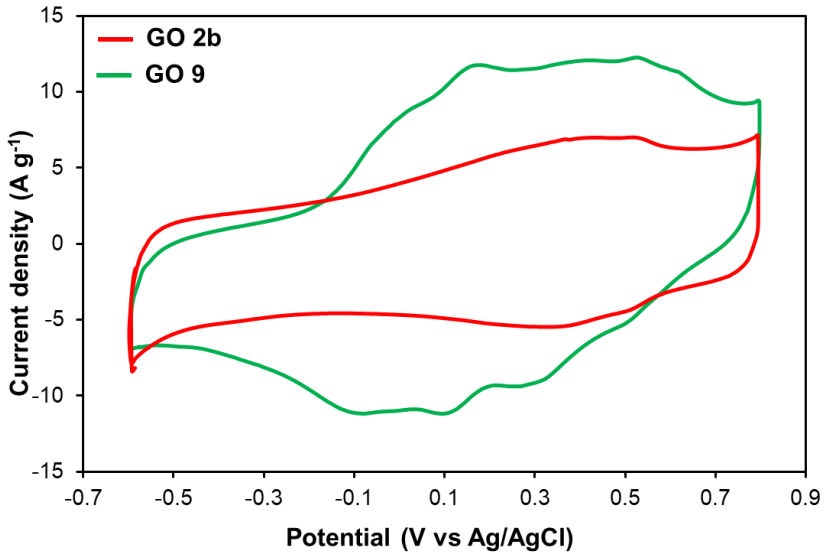

Figure 19: Electrochemical evaluation in three-electrode system: CV profile of **GO 2b**, and **GO 9** at a scan rate of 50 mV s^{-1}

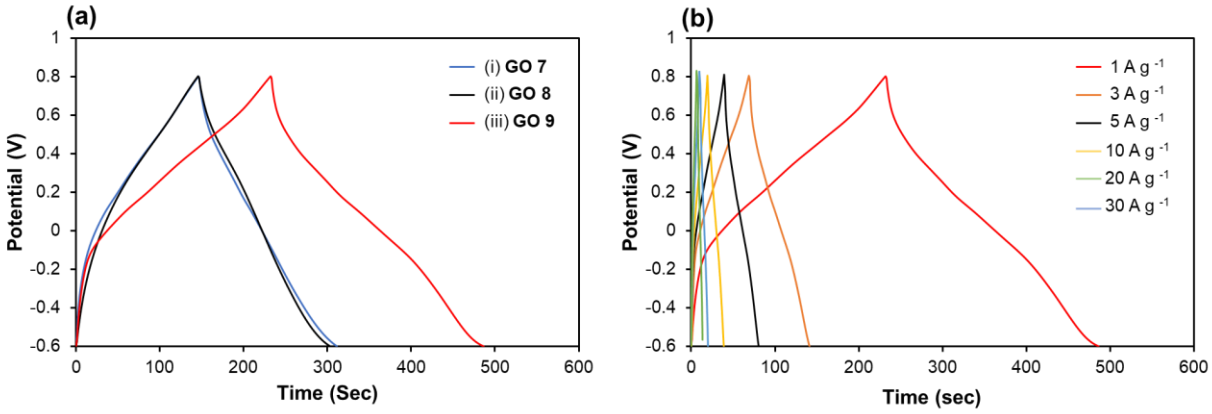

Figure 20: (a) Galvanostatic charge discharge curve of (i) **GO 7**, (ii) **GO 8**, and (i) **GO 9** at a current density of 1 A g^{-1} (b) **GO 9** at different current density

5.3. Conclusion

In summary, a series of organic molecules were introduced onto the surface of GO by using a covalent double functionalization method. In first step, the aminated compounds were reacted with the epoxide groups of GO. The monofunctionalized GO, containing more OH groups compared to pristine GO, was then modified with α,β-unsaturated carbonyl compounds. The prepared materials were applied as electrode materials for proton conductivity and SCs. The proton conductivity of GO was improved by attaching sulfanilic acid, followed by the introduction of BQ molecules. The SC performance was improved by introducing two redox-active molecules onto GO through the same covalent double functionalization approach. This strategy could be exploited further to prepare multifunctional GO conjugates with potential applications in many fields.

5.4. Experimental section

5.4.1. Chemicals and materials

Natural graphite fakes (99.8%) were obtained from Alfa Aesar.1,4 benzoquinone, methyl vinylketone, propylamine and aniline was obtained from Tokyo chemical industry Co., Ltd. Toluene was obtained from Kanto chemical co. ink. Potassium permanganate ($KMnO_4$), sulfuric acid (H_2SO_4, 96%), ethanol, sodium azide, acetic acid, tetrahydrofuran, 1,4-naphthoquinone and sulfanilic acid were obtained from Wako Co., Ltd and used as received.

5.4.2. Synthesis of 2-amino-1,4-naphthoquinone

A round-bottom flask equipped with a magnetic stir-bar was charged with 1,4-naphthoquinone (2.37 g, 15 mmol, 1.0 equiv.) and H_2O/THF (1/4, 50 mL). To the mixture, a solution of sodium azide (2.93 g, 45 mmol, 3.0 equiv.) and acetic acid (3 mL) in distilled water (8 mL) was added and stirred at room temperature. After 7 h, the reaction was concentrated in vacuo and dissolved in ethyl acetate. The resulting solution was washed with 1 M NaOH, extracted with ethyl acetate, and washed with saturated NaCl. The organic layers were dried over $MgSO_4$ and the solvent was removed in vacuo. The crude residue was

purified by silica gel column chromatography (hexane/ethyl acetate = 1/2) to give 2.3 g (89%) as a brown solid.[39]

5.4.3. Synthesis of GO

Graphite powder (100 g) was dispersed into concentrated H_2SO_4 (2.5 L). After cooling the mixture in an ice bath, $KMnO_4$ (300 g) was added and reaction mixture was kept below 55 °C. The mixture was stirred at 35 °C for 2 h to complete the oxidation process. Next, deionized water (5 L) was added slowly and temperature was kept below 50 °C with continuous stirring, then followed by the addition of H_2O_2 (30% aq., 250 mL) into the mixture. Finally, the brown crude graphite oxide was purified by performing 10 times centrifugation, and GO is prepared. Concentration of GO was measured by drying the GO dispersion under vacuum at 50 °C.

5.4.4. General procedure for the synthesis of GO 1, and GO 5

In a typical procedure, amine (1 mL) was added dropwise to the suspension of GO (250 mg L^{-1}, 400 mL) under vigorous stirring in a flask. The resulting mixture was allowed to stir for 24 h at room temperature, then filtered and thoroughly washed with ethanol and water several times. The obtained solid was freeze-dried for two days.

5.4.5. General procedure for the synthesis of GO 2 (a-c), GO 4, GO 6, GO 7, and GO 9

To a dispersion of GO (40 mg) in toluene (5 mL), a solution of α,β-unsaturated carbonyl compounds (300 mg) in toluene (10 mL) was added. The mixture was refluxed for 36 h at 112 °C with constant stirring. After completion of reaction the mixture was filtered and washed with water and toluene several times respectively. The sample was then dried under vacuum for two days at 50 °C.

5.4.6. Synthesis of GO 3, and GO 8

In a typical procedure, amine (300 mg) was dissolved in 30 mL ethanol and then added to GO aqueous dispersion (10 mL, 10 mg mL^{-1}, 100 mg). The mixture was sonicated for 1 h to get a homogeneous dispersion. The dispersion was refluxed for 48 h and purified by centrifugation and washing (ethanol and then water, 3 times each). The product was finally freeze dried for two days.

5.4.7. Instruments and measurements

The functional groups on the surface of GO were recorded by FT-IR (SHIMADZU IR Tracer 100), Using KBr analysis. The elemental compositions were determined by XPS. The XPS was carried out on a JPS-9030 with a pass energy of 20 eV.

The electrochemical behavior of prepared samples was measured using three electrode system. In the three-electrode system, the platinum foil and Ag/AgCl electrode were used as the counter electrode and reference electrode, respectively. The working electrode was fabricated by mixing electrode material (4 mg) and carbon black (0.7 mg) in 0.4 mL Nafione solution, which is sonicated for I h to make fine dispersion. Then 3 µL of above suspension using a pipet gun was dropped onto the glassy carbon electrode (3 mm) and completely dried at 50 °C for 1 h under vacuum. The electrochemical performance was measured in a potential range of -0.6-0.8 V, with a scan rate of 50 mVs^{-1}. All electrochemical experiments were performed in 0.5 M H_2SO_4 aqueous electrolyte. The specific capacitance of the SCs (C (F/g)) was calculated from the discharge curve according to the following formula:

$$C = \frac{I \, X \, \Delta t}{m \, X \, \Delta V} \qquad \ldots\ldots\ldots\ldots\ldots\ldots \quad 1$$

where I is the constant current in discharging, m is the mass of active material on working electrode, Δt is the discharge time, and ΔV is the voltage change during discharge.

For proton conductivity the sample was pressed into 10 mm diameter pellets. The thickness of the pellet for **GO 4**, and **GO 6** was 0.414 mm 0.25 mm respectively. The Sample electrode was sandwich between the two stainless steel spacer and assembled.[40] The electrochemical impedance test was conducted at a frequency range of 1000 kHz to 1 Hz at 0 V with an AC perturbation of 10 mV. The proton conductivity was measured by following by equation:

$$\sigma = \frac{L}{Z \, .A} \qquad \ldots\ldots\ldots\ldots\ldots\ldots \quad 2$$

where L is the thickness of the electrode, Z is impedance value and A is the electrode surface area.

5.5. References

1. J.-H. Lee, S.-J. Park and J.-W. Choi, *Nanomaterials*, 2019, **9**, 297.
2. D. G. Papageorgiou, I. A. Kinloch and R. J. Young, *Prog. Mater. Sci.*, 2017, **90**, 75–127.
3. B. Zhan, C. Li, J. Yang, G. Jenkins, W. Huang and X. Dong, *Small*, 2014, **10**, 4042–4065.
4. S. Pang, Y. Hernandez, X. Feng and K. Müllen, *Adv. Mater.*, 2011, **23**, 2779–2795.
5. H. Huang, S. Su, N. Wu, H. Wan, S. Wan, H. Bi and L. Sun, *Front Chem.*, 2019, **7**, 399.
6. W. Yuan and G. Shi, *J. Mater. Chem. A*, 2013, **1**, 10078–10091.
7. M. Hernaez, *Sensors*, 2020, 20, 3196.
8. T. Kuilla, S. Bhadra, D. Yao, N. H. Kim, S. Bose and J. H. Lee, Prog. *Polym. Sci.*, 2010, **35**, 1350–1375.
9. C. Wang, Y. Yang, R. Li, D. Wu, Y. Qin and Y. Kong, *Chem. Commun.*, 2020, **56**, 4003–4006.
10. D. Majumdar, *Innovative Energ. Res.*, 2016, **5**, 1–9.
11. Z. Xu, H. Sun, X. Zhao and C. Gao, *Adv. Mater.*, 2013, **25**, 188–193.
12. V. Mazánek, J. Luxa, S. Matějková, J. Kučera, D. Sedmidubský, M. Pumera and Z. Sofer, *ACS Nano*, 2019, **13**, 1574–1582.
13. D. Higgins, P. Zamani, A. Yu and Z. Chen, *Energy Environ. Sci.*, 2016, **9**, 357–390.
14. D. Geng, N. Ding, T. S. A. Hor, Z. Liu, X. Sun and Y. Zong, *J. Mater. Chem. A*, 2015, **3**, 1795–1810.
15. R. Khan, R. Nakagawa, B. Campeon and Y. Nishina, *ACS Appl. Mater. Interfaces*, 2020, **12**, 12736–12742.
16. Z. J, Y. D, Y. Z, Y. Q and Z. H, *Small*, 2014, **10**, 3480–3498.
17. D. R. Dreyer, S. Park, C. W. Bielawski and R. S. Ruoff, *Chem. Soc. Rev.*, 2010, **39**, 228–240.
18. B. Xue, J. Zhu, N. Liu and Y. Li, *Catal Commun.*, 2015, **64**, 105–109.

19. I. A. Vacchi, S. Guo, J. Raya, A. Bianco and C. Ménard-Moyon, *Eur. J. Chem.*, 2020, **26**, 6591-6598.
20. S. Guo, Y. Nishina, A. Bianco and C. Ménard-Moyon, *Angew. Chem. Int. Ed.*, 2020, **132**, 1558–1563.
21. J. Park, M. Yan, *Acc. Chem. Res.* 2013, **46**, 181-189.
22. J. M. Englert, C. Dotzer, G. Yang, M. Schmid, C. Papp, J. M. Gottfried, H.-P. Steinrück, E. Spiecker, F. Hauke, A. Hirsch, *Nat. Chem.* 2011, **3**, 279-286.
23. R. Khan, Y. Nishina, *Nanoscale,* 2021, **13**, 36-50.
24. J. Yan, G. Chen, J. Cao, W. Yang, B. Xie, M. Yang, *New Carbon Mater.* 2012, **27**, 370-376.
25. F. Zhou, H. N. Tien, Q. Dong, W. L. Xu, H. Li, S. Li, M. Yu, *J. Membr. Sci.* 2019, **573**, 184-191.
26. F. Samadaei, M. Salami-Kalajahi, H. Roghani-Mamaqani, M. Banaei, *RSC Adv.* 2015, **5**, 71835-71843.
27. Y. Ding, F. Zhang, J. Xu, Y. Miao, Y. Yang, X. Liu and B. Xu, *RSC Adv.*, 2017, **7**, 28754–28762.
28. Z. Liu, L. Wang, G. Ma, Y. Yuan, H. Jia and W. Fei, *J. Mater. Chem. A.*, 2020, **8**, 18933–18944.
29. X. Wang, J. Wu, L. Zhou, X. Wei and W. Wang, *J. Eng. Tribol.*, 2018, **232**, 1428-1436.
30. F. Zhou, H. N. Tien, Q. Dong, W. L. Xu, H. Li, S. Li and M. Yu, *J. Membr. Sci.*, 2019, **573**, 184–191.
31. L. Chen, Z. Xu, J. Li, B. Zhou, M. Shan, Y. Li, L. Liu, B. Li, J. Niu, *RSC Adv.* 2014, **4**, 1025-1031.
32. F. Han, S. Yang, W. Jing, K. Jiang, Z. Jiang, H. Liu, L. Li, *Opt. Express*, 2014, **22**, 11436-11445.
33. Q. Chen, J. Sun, P. Li, I. Hod, P. Z. Moghadam, Z. S. Kean, R. Q. Snurr, J. T. Hupp, O. K. Farha, J. F. Stoddart, *J. Am. Chem. Soc.* 2016, **138,** 14242-14245.

34. C. Yin, J. Li, Y. Zhou, H. Zhang, P. Fang and C. He, *ACS Appl. Mater. Interfaces*, 2018, **10**, 14026–14035.
35. A. Khabibullin, S. D. Minteer and I. Zharov, *J. Mater. Chem. A.*, 2014, **2**, 12761–12769.
36. V. H. Luan, H. N. Tien, L. T. Hoa, N. T. M. Hien, E.-S. Oh, J. Chung, E. J. Kim, W. M. Choi, B.-S. Kong and S. H. Hur, *J. Mater. Chem. A.*, 2012, **1**, 208–211.
37. H. Murata, Y. Nakajima, N. Saitoh, N. Yoshizawa, T. Suemasu and K. Toko, *Sci Rep.*, 2019, **9**, 1–5.
38. L. Liu, J. Zhang, J. Zhao and F. Liu, *Nanoscale*, 2012, **4**, 5910–5916.
39. E. S. Inks, B. J. Josey, S. R. Jesinkey, C. J. Chou, *ACS Chem. Biol.*, 2012, **7**, 331-339.
40. T. Ando, S. Yubuchi, A. Sakuda, A. Hayashi, M. Tatsumisago, *Electrochemistry* 2019, **87**, 289-293.

Chapter: 6

Final conclusion

In conclusion, the manuscripts report the research conducted during my doctor course at Okayama University.

They all detail robust functionalization features of graphene and applications for energy storage systems.

- The third chapter presents the functionalization of graphene through onium bonding and applications for energy devices (Figure 1a).
- The fourth chapter shows the covalent functionalization of conductive polymers on GO through cross linker for SCs applications (Figure 1b).
- Chapter five presents stepwise covalent double functionalization of GO with organic molecules to tune the electrochemical properties (proton conductivity and SCs) (Figure 1c).

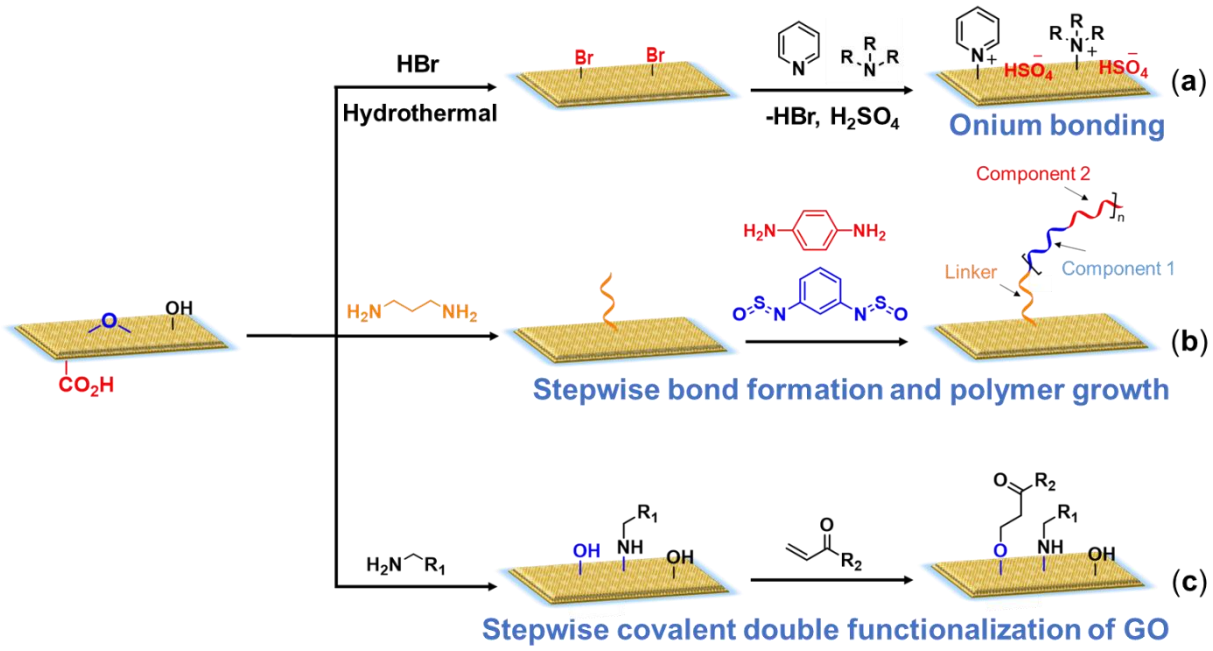

Figure 1: Robust functionalization of graphene for energy storage systems

(**Robust functionalization of graphene for Advanced energy devices**)

Efficient and selective methods for graphene functionalization are needed because they allow tuning of graphene surface and electronic properties. To date, graphene has been functionalized using ionic bonds, non-covalent interactions, and covalent bonds. Covalent bonds are durable and can adequately reflect the function of the molecules introduced. However, strict and severe reaction conditions are required for their formation. Non-covalent and ionic interaction are weak; molecule dissociation occurs readily (Table 1). As a result, onium bond was formed. Onium bond is simple, and strong like covalent bond.

Table 1: Comparison and functionalization method of graphene (The detail comparison and references is given in chapter 3)

Method	Advantages	Disadvantage
Covalent bond	Strong	Severe reaction conditions
Noncovalent bond	Mild, simple	Fragile, limited to hydrophobic molecules
Ionic bond	Mild, simple	Fragile, limited to hydrophilic molecules
Onium bond	Strong, simple	

New concept for graphene functionalization using halogenated graphene has been developed, in which brominated graphene is successfully functionalized by heteroatom-containing molecules to form onium bonds, such as pyridinium or ammonium. The counter ion, bromide, is replaced with other anions, such as sulfate, by treating with sulfuric acid, while retaining the molecules, which demonstrates durable properties of onium bonding (Figure 2A).

To emphasize the advantages of this strategy for graphene functionalization, the performance for energy-related applications, such as biofuel cells, SCs, and LIBs, is evaluated after introducing redox-active moieties onto graphene through onium bonding.

SCs properties based on the use of onium bonding were found very promising. The cycling stability of the fabricated symmetric cells was evaluated, with the capacitance of onium composite maintained without any noticeable fading after 10,000 cycles (Figure 2B). Furthermore, the retention was 100% after 10,000 cycles. For comparison, the cycling stability of the mixed sample (non-covalent composite) was measured, showed a capacitance retention of 67% after 3000 cycles (Figure 2B). This decrease in capacity was due to the dissociation of redox-active molecules from the graphene surface after a certain time in the aqueous electrolyte. In contrast, the onium bond between IQD and graphene was strong and stable in the aqueous electrolyte. These results were among the best values reported for small conjugated carbonyl compounds functionalized on carbon materials (Table 2).

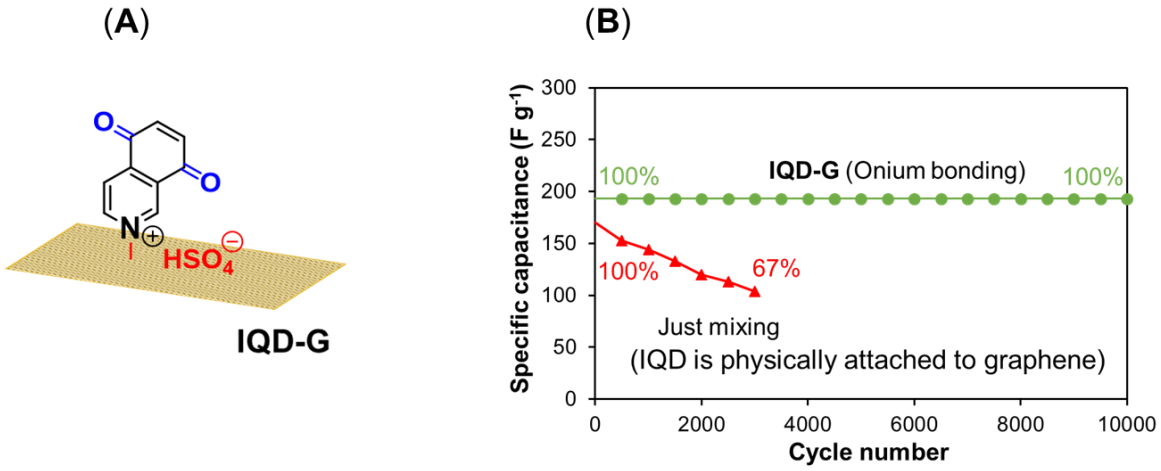

Figure 2: (A) Preparation of Onium–Graphene Hybrid, (B) cycling stability of onium hybrid and just mixing samples (physical interaction) at a current density of 10 A g^{-1} in SCs device.

Table 2: Comparison of this work with the published data for quinone-containing carbon-based electrodes (All references is given in chapter 3)

Electrode material	Electrolyte	Retention (%) (cycle number)	Current density/scan rate	Ref.
TBHQ@gr	1 M H_2SO_4	92 (800)	1 A g^{-1}	[38]
AQ@CFs	1 M H_2SO_4	89 (5000)	20 A g^{-1}	[39]
AQ@gr	1 M HCl	77 (10 000)	10 A g^{-1}	[40]
AT@AC	1 M H_2SO_4	90 (1000)	200 mA g^{-1}	[41]
HQ@gr	1 M H_2SO_4	86 (10 000)	10 A g^{-1}	[42]
PQ@OLC	1 M H_2SO_4	90 (10 000)	200 mV s^{-1}	[43]
NQ@OLC	1 M H_2SO_4	92 (10 000)	50 mV s^{-1}	[44]
dgPQ@AC	1M KOH	80 (1000)	2 A g^{-1}	[45]
HQ@AC	1 M H_2SO_4/HQ	65 (4000)	4.42 mA cm^{-2}	[46]
Catechol/AC	1 M H_2SO_4	75 (10 000)	7.5 A g^{-1}	[47]
BPA/gr.	1 M H_2SO_4	90 (4000)	1 A g^{-1}	[48]
AQ/gr	1 M H_2SO_4	97 (2000)	10 A g^{-1}	[49]
RGO/AQDS	1 M H_2SO_4	82 (10,000)	1 A g^{-1}	[50]
THAQ/RGO	1 M H_2SO_4	97 (10,000)	1 A g^{-1}	[51]
IQD-G	0.5 M Na_2SO_4	100 (10,000)	20 Ag^{-1}	This work

Breakthroughs

- **My research is quite original,** because new concept for graphene functionalization using brominated graphene has been developed, in which brominated graphene is successfully functionalized by heteroatom-containing molecules to form onium bonds, such as pyridinium or ammonium. Onium bond is simple and strong and can be prepared without the addition of any acid or catalyst.
- Several research groups functionalized graphene through covalent bond, non-covalent bond and ionic bonds. Covalent bond requires strict and severe reaction conditions while ionic bond and non-covalent bonds are weak, molecular dissociation occur readily. The onium bond is alternative for these interactions because onium bond is simple and strong.

(**Grafting conductive polymers on GO through cross linker: A stepwise**

Various graphene-polymer composites were synthesized through non-covalent and covalent interaction, and high capacitive performances were achieved. Non- covalent interaction between graphene and polymer enduring the volumetric changes during charging-discharging cycles, hence constrains the cycling stability. Covalent interaction is strong, but previously reported method used harsh reaction conditions, and also the polymer structure was disrupting after few hundred cycles. As a result, a covalently cross-linked graphene–polymer composite was formed.

A three-step reaction furnished a composite of graphene and a conductive polymer. In the first step, GO was modified with a diamine, which acted as a linker for polymer attachment. In the second step, an initiating site was attached to the free amine of the linker. Finally, a polymer was grown from the initiation site, and GO was reduced during polymer growth (Figure 3). The method does not require any catalyst, acid, or reducing agent, furnishing the graphene–polymer composite in a straightforward procedure. The electrical properties of the composite were evaluated to determine its suitability as an electrode material for a SCs. The covalent cross-linked polymer-graphene composite demonstrated good cycling stability than non-crosslinked graphene–polymer mixture. The capacitance retention

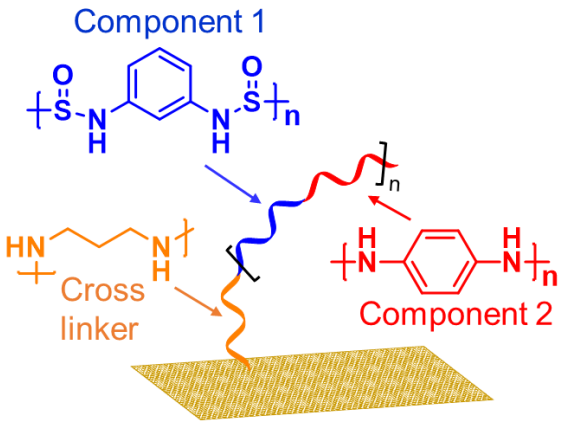

Figure 3: Schematic representation of **GO 3** (polymer-graphene)

of the covalent cross-linked polymer was 98% after 1000 cycles as compared to the 63% the non-crosslinked graphene-polymer mixture (Figure 4). These results were among the best values reported for polymer-graphene composites with respect to cycling stability (Table 3).

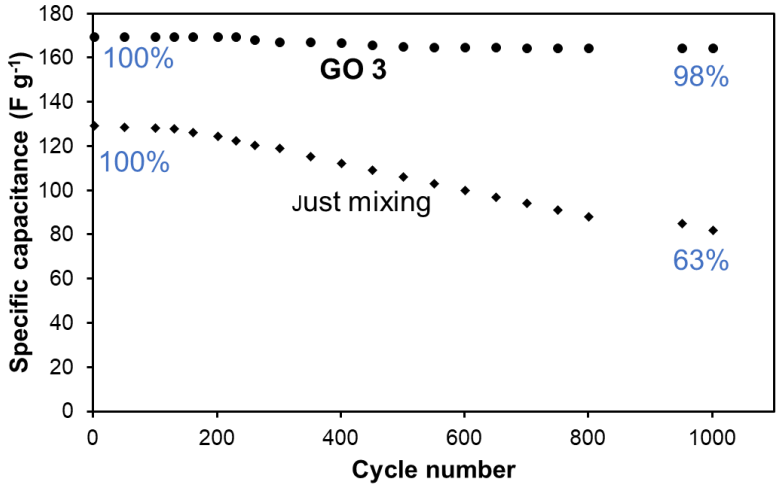

Figure 4: Cycling stability of **GO 3** and just mixing samples at a current density of 10 A g^{-1}, in SCs device

Table 3: Comparison of SCs performance of this work with published data in three-electrode systems measurement (All references is given in chapter 4)

Material	Cycle number	Capacity retention	Measurement conditions	References
PANI-G	1500	90%	10 A g^{-1}	[35]
PANI-G	1000	91%	2 A g^{-1}	[36]
PANI-G	1500	80%	0.5 A g^{-1}	[37]
PANI-G	200	96%	3 A g^{-1}	[38]
PANI-G	1000	85%	0.5 A g^{-1}	[39]
Ppy-G	1000	92%	1 A g^{-1}	[40]
Ppy-G	200	93%	5 A g^{-1}	[41]
Ppy-G	1500	71%	50 mV s^{-1}	[42]
PEDOT-G	1000	88%	0.3 A g^{-1}	[43]
PEDOT-G	2000	87%	0.5 A g^{-1}	[44]
Ppy-G	500	90%	100 mVs^{-1}	[45]
Ppy-G	1000	91%	1 A g^{-1}	[46]
GO 3	1000	98%	10 A g^{-1}	This work

Breakthrough

- **My research is quite original,** because multi-components polymer was grafted on graphene using a three-step reaction, involving a cross-linker, initiator, and monomer. The polymer-graphene hybrids showed good electrochemical stability. The covalent cross-linked polymer-graphene composite demonstrated a high capacitance and good cycling stability than non-crosslinked graphene–polymer mixture. The capacitance retention of the covalent cross-linked polymer was 98% after 1000 cycles as compared to the 63% the non-crosslinked graphene-polymer mixture.
- The polymer-graphene composite was synthesized without the addition of any acid or catalyst.
- Previously reported methods attached polymer to graphene either through non-covalent bond or by covalent bond without using cross linker. The electrochemical

stability of those polymer-graphene composites as a SCs is less stable as compared to this work (Table 3).

- Secondly, most of the previously reported methods used oxidative polymerization method to introduce polymer on graphene which require harsh reaction conditions (using strong acid). While in this research the polymer-graphene composite was obtained by simple mixing and heating.

(**Covalent double functionalization of GO with organic molecules**)

Previous researches evidenced that double functionalization of GO can introduce various functional groups, but targeted applications have not been shown. In this work, we focused on the covalent double functionalization of GO to tune the electrochemical properties, and applied for electrode materials. To this end, two different organic molecules with specific functions were introduced on GO using a stepwise covalent double functionalization; the first step consists of the ring-opening reaction of epoxide groups of GO with an amino compound, and the second step is the nucleophilic addition of hydroxyl groups on GO to an α,β-unsaturated carbonyl compounds. The advantageous feature of the strategy was confirmed by measuring proton conductivity and capacitance for SCs.

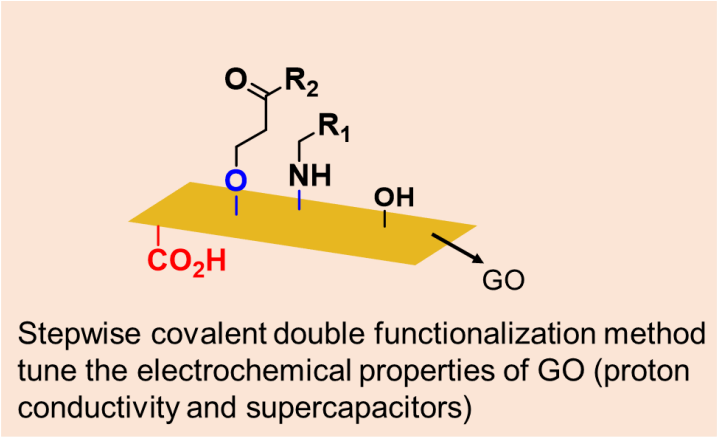

Figure 5: Schematic representation of covalent double functionalization of GO

Proton conductivity measurement

The role of covalent double functionalized GO was investigated in the proton conductivity. Thus, the proton conductivity of the GO was improved by tuning the surface functional groups. For this purpose, sulfanilic acid was grafted on GO through epoxide group (**GO 3**), followed by the attachment of BQ molecules (**GO 4**). Sulfanilic acid act as proton conducting material which are previously reported. For comparison, aniline was functionalized on GO (**GO 5**) followed by the attachment of BQ (**GO 6**) (Figure 6). The prepared materials were confirmed by XPS analysis.

The proton conductivity was evaluated by electrochemical impedance spectroscopy. The Nyquist plot of **GO 4** and **GO 6** showed three types of resistance such as R, R_1 and R_2 (Figure 7a and 7b). The proton conductivity was calculated from the R values given by the electrical circuit and considering the pellet thickness and surface area. The R value for **GO 4** was 7.0 ohm (inset in Figure 7a), while the R value for **GO 6** was 509.4 ohm (inset in Figure 7b). The proton conductivity of **GO 4**, and **GO 6** was 7 x 10^{-3} S cm^{-1} and 6 x 10^{-5} S cm^{-1} respectively. These results indicate that **GO 4** showed good proton conductivity, which may be due to the fast ion transportation, facilitating by sulfonic acid functional group.

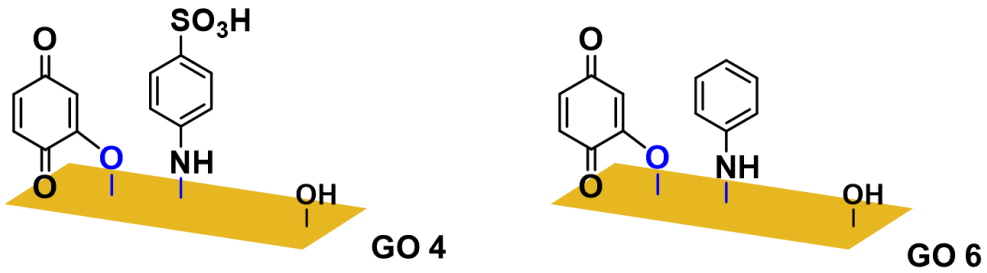

Figure 6: Synthesis of **GO 4**, and **GO 6**

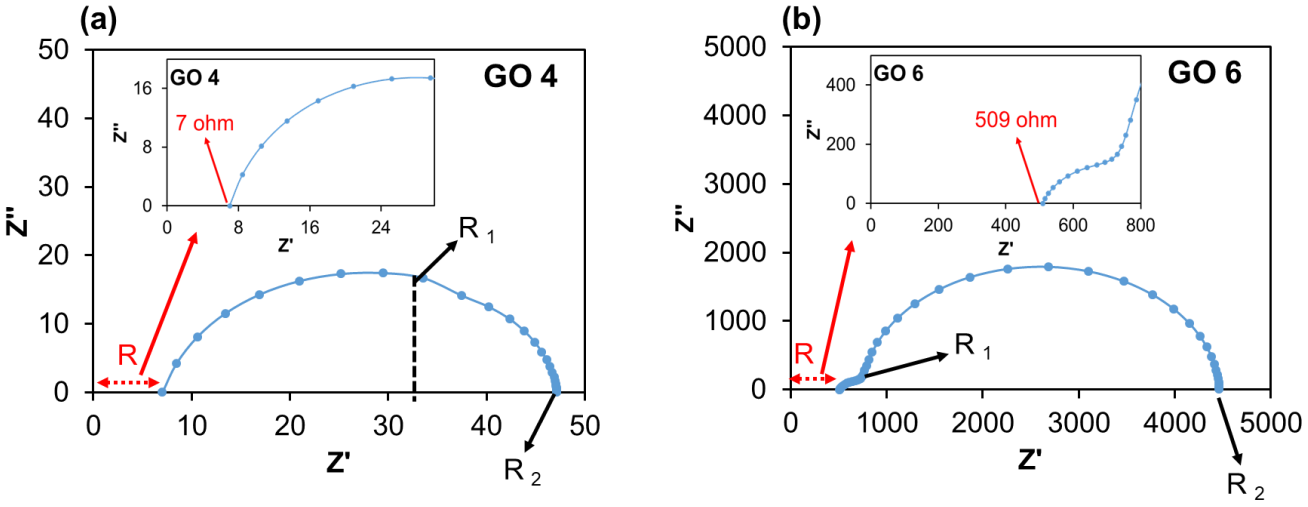

Figure 7: Impedance spectra of (a) **GO 4**, and (b) **GO 6**

Supercapacitor performance measurement

For the SCs performance evaluation two redox-active moieties such as 2-amino naphthoquinone (ANQ) and BQ molecules were introduced on GO. **GO 7**, and **GO 8** was prepared through covalent mono-functionalization method**,** while **GO 9** was prepared through covalent double-functionalization method (Figure 8). The specific capacitance of **GO 7**, and **GO 8** was 100 F g^{-1} and 82 F g^{-1} respectively, at a current density of 30 A g^{-1}, which is 63% and 68% of its capacitance at 1 A g^{-1}. The specific capacitance of **GO 9** reached 185 F g^{-1} at a current density of 30 A g^{-1}, which is approximately 73 % of its capacitance at 1 A g^{-1} (254 F g^{-1}) (Figure 9). The high electrochemical performance is attributed to the introduction of more quinone molecules.

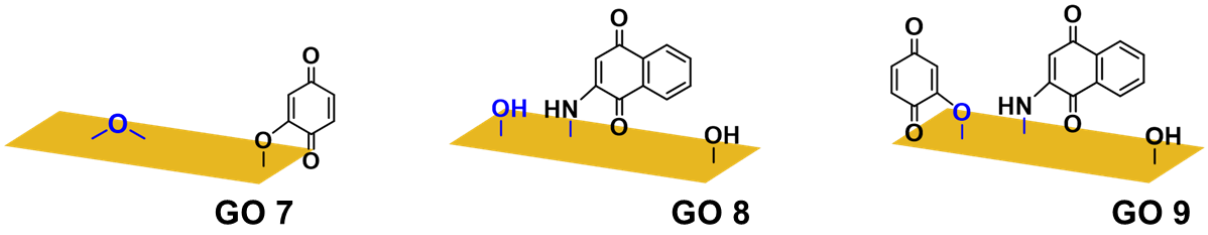

Figure 8: Synthesis of **GO 7**, **GO 8**, and **GO 9**

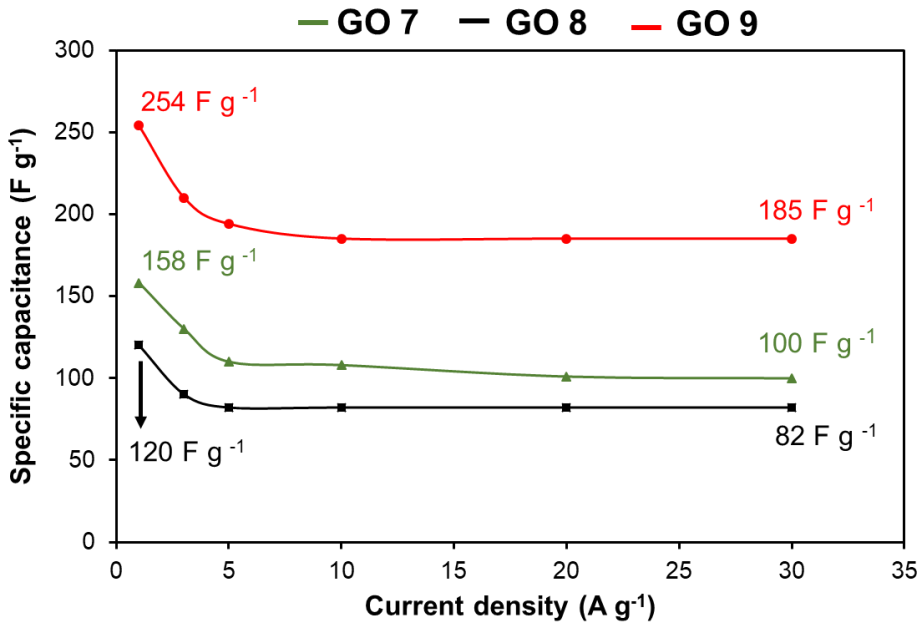

Figure 9: Specific capacitance of **GO 7**, **GO 8**, and **GO 9** as a function of current density.

Breakthroughs

- **My research is quite original,** because stepwise covalent double functionalization of graphene was performed and showed their advantages for proton conductivity and SCs. The proton conductivity was improved by tuning the surface functional group of GO. Proton conductivity was improved from 6 x 10^{-5} S cm^{-1} to 7 x 10^{-3} S cm^{-1} by replacing aniline with sulfanilic acid. Similarly, the SCs performance of double-functionalized GO was high than the mono-functionalized GO. The specific capacitance of mono-functionalized GO was up to 158 F g^{-1}at a current density of 1 A g^{-1}. The specific capacitance of double functionalized GO was 254 F g^{-1} at a current density of 1 A g^{-1}. These results suggest that step wise covalent double functionalization of GO is efficient way to enhance the electrochemical performance.
- Previous researches evidenced that double functionalization of GO can introduce various functional groups, but targeted applications have not been shown. In this work, we focused on the covalent double functionalization of GO to tune the

electrochemical properties. The advantageous feature of the strategy was confirmed by measuring proton conductivity and capacitance for SCs.

Future prospective

The covalently bonded composites prevent the dissolution of small redox-active molecules, stabilize the polymer structure, and shows better electrochemical stability than non-covalently bonded ones. The literature survey reveals that comprehensive research has not been done on the covalent functionalization of graphene-based materials for SCs and LIBs applications, despite the development of various types of organic transformations in recent years. Only a few traditional reactions have been employed for the functionalization of graphene (Figure 10). Interestingly, there reported quite a limited number of papers on the covalent functionalization of classic carbons, such as carbon black, ketjen black, and activated carbon; most of the studies focused on the functionalization of novel nanocarbons, such as graphene and CNTs. Therefore, further investigation is needed combining traditional and latest chemical transformations and classical carbons and nanocarbons for developing advanced electrochemical electrode materials.

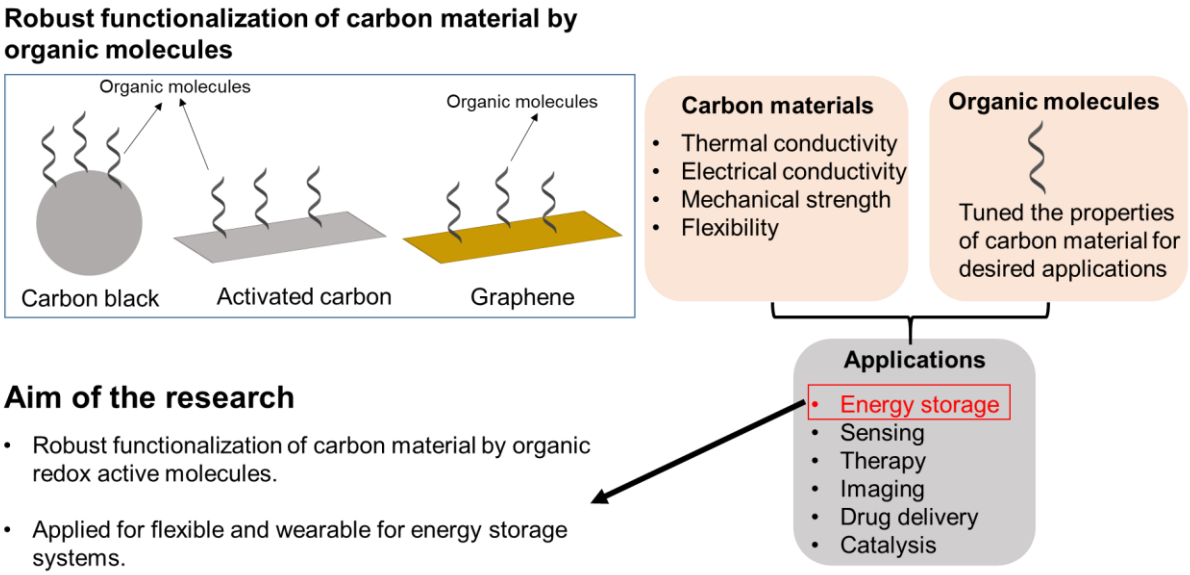

Figure 10: Strategy and future research plan

List of abbreviation:

Full name	Abbreviation
Graphene oxide	GO
Reduced graphene oxide	RGO
Supercapacitors	SCs
Electrical double-layer capacitors	EDLCs
Lithium-ion batteries	LIBs
single-walled carbon nanotubes	SWCNT
multi-walled carbon nanotubes	MWCNT
chemical vapor deposition	CVD
silicon carbide	SiC
Fourier transform infrared	FT-IR
X-ray photoelectron spectroscopy	XPS
thermogravimetric analysis	TGA
Scanning electron microscopy	SEM
Atomic force microscopy	AFM
polypyrrole	Ppy
Polyaniline	PANI
Phenylenediamine	PD
Poly(phenylenediamine)	PPD
Amino-anthraquinone	AAQ
Anthraquinone	AQ
2-amino-3-chloro-1,4-naphthoquinone	ACNQ
3-chloro-1,4-naphthoquinone	CNQ
2-aminopyrene-3,4,9,10-tetraone	PYT
Thiourea	TU
Adenine	AD
Benzobisoxazole	BBO
Benzoxazole	BO
Poly(3,4-ethylene dioxythiophene)	PEDOT
1,3-bis(2-benzimidazolyl)-5-aminobenzene	BOA
Polyorthoaminophenol	PAP
N,N′-bissulphinyl-m-benzenediamine-p-phenylenediamine	SAB
Thiourea-formaldehyde	TF
2,2,6,6-tetramethylpiperidin-1-oxyl	TEMPO

Tetrahydroxybenzoquinone	THBQ
Nitroxide	NO
Naphthalenediimide diamine	NDIDA
N,*N*′-diamino-1,4,5,8-naphthalenetetracarboxylic bisimide	DNTCB
Polysulfur	PS
Poly(2,2,6,6-tetramethylpiperidinyloxy-4-ylmethacrylate	PTMA
pyridine	Py
diisopropylamine	iPr_2NH
trimethylamine	Et_3N
isoquinolinedione	IQD
Energy-dispersive X-ray	EDS
Open-circuit voltage	OCV
cyclic voltammogram	CV
Phosphate buffer saline	PBS
Flavin adenine dinucleotide-glucose dehydrogenase	FAD-GDH
Hydrobromic acid	HBr
[bis(trifluoroacetoxy)iodo] benzene	PIFA
N-methylpyrrolidone	NMP
Polyvinylidene difluoride	PVDF
2-amino naphthoquinone	ANQ
1,4-benzoquinone	BQ

List of publications

1. A simple and robust functionalization of graphene for advanced energy devices,
   Rizwan Khan, Ryo Nakagawa, Benoit Campeon and Yuta Nishina,
   ACS Appl. Mater. Interfaces, 2020, 12, 12736-12742.

2. Grafting conductive polymers on graphene oxide through cross-linker: a stepwise approach,
   Rizwan Khan, Yuta Nishina**,**
   j. Mater. Chem. A, 2020, 8, 13718-13724.

3. Covalent functionalization of carbon materials with redox-active organic molecules for energy storage, *(Review paper)*
   Rizwan Khan, Yuta Nishina,
   Nanoscale, 2021,13, 36-50.

This thesis is dedicated to my parents

For their endless love, support and encouragement

ACKNOWLEDGEMENT

All praises to Almighty Allah and His blessing for the completion of this study.

First and Foremost, I would like to express my sincere gratitude to my advisor Prof. Yuta Nishina for the continuous support of my Ph.D. study and research. His guidance helped me in all the time of research. His insightful feedback pushed me to sharpen my thinking and brought my work to a higher level.

I wish to express my deepest gratitude to my dear friend Dr. Sohail Ahmad, who introduced me to prof. Yuta Nishina and creating this thesis opportunity.

I would like to express my gratitude to Okayama University for giving me the opportunity to complete this study.

I thank my laboratory members for their support and cooperation: Dr. Obata. Dr. Komoda, Dr. Nakano, Dr. Azuma, Dr. Matsumura, Dr. Benoit, Dr. Sohail, Dr. Nizami, Mrs. Nusrat, Mr. Cheng, Mr. Zhou, Ms. Hori, Mr. Fuji, Mr. Nakagawa, Mr. Takeda, Mr. Miyagawa, Mr. Kubo, Mr. Iguchi, Ms. Shibahara, Mr. Kaji, Mr. Takahashi, Mrs. Tamagawa, Mrs. Ohkubo, Dr. Uchida, and Mr.Tomita,

My sincere thank goes to Dr. Benoit, Mrs. Ohkubo, Dr. Azuma, Ms. Hori, Mr. Fuji, Mr. Nakagawa, and Dr. Komoda for all of his help and assistance.

I wish to shows my gratitude to my master supervisor Dr. Maria Sadia for their encouragement and support during my master study.

I would like to thank to my brothers: Taimor Khan, Uzair Khan, and Mansoor Khan. It would not be possible to write this thesis without their support.

Last but not the least, I would like to thank to my mother, the most important person of my life. She has been the source of inspiration and gave me strength in difficult times. She continually provides their moral, spiritual, and emotional support. Thank you for everything.